UC Davis

UC Davis Electronic Theses and Dissertations

Title

Dermal Granulopoiesis

Permalink

https://escholarship.org/uc/item/15h1j7v2

ISBN

9798193262152

Author

Cirves, Evan Patrick

Publication Date

2026-09-08

Peer reviewed|Thesis/dissertation

eScholarship.org Powered by the California Digital Library
University of California

Dermal Granulopoiesis

By

EVAN P. CIRVES
DISSERTATION

Submitted in partial satisfaction of the requirements for the degree of

DOCTOR OF PHILOSOPHY

in

Biomedical Engineering

in the

OFFICE OF GRADUATE STUDIES

of the

UNIVERSITY OF CALIFORNIA

DAVIS

Approved:

_____
Steven C. George, Chair

_____
Anthony Passerini

_____
Aidan Gilchrist

Committee in Charge

2026

Abstract

Local dermal granulopoiesis constitutes a highly coordinated, tissue-specific immune response wherein peripheral skin inflammation directly signals to hematopoietic stem and progenitor cells (HSPCs) to drive emergency neutrophil production at the site of infection. Mouse studies have observed this process and its necessity for host survival but have not thus far offered any therapeutic potential from these findings. Here we first developed a hydrogel delivery platform for transplanting HSPCs directly to the sites of dermal wounds in mice, demonstrating the potential of these hydrogels to promote local granulopoiesis and wound healing. Despite this successfully developed application, traditional *in vivo* models have only observed this phenomenon in murine models, and interspecies variations in immune biology have made it difficult to determine whether this process occurs in human models as well. Here we deploy a microphysiological system modeling the skin that is capable of supporting immune cell trafficking and local differentiation of HSPCs. We found that within the skin microphysiological system, both neutrophils and HSPCs trafficked to artificially stimulated skin infection in a predictable and repeatable manner. Critically, neutrophils migrated into the dermis while HSPCs remain localized to the vascular niche where they are capable of producing neutrophil-like phagocytes capable of bacterial clearance from wounds. Ultimately these studies provide mechanistic insight into localized regulation of dermal granulopoiesis in humans, and demonstrate a viable biomaterial strategy for harnessing this phenomenon therapeutically to treat severe wounds.

Acknowledgements

I first would like to thank Dr. George and all the members of the George Lab for their support and guidance over the years while pursuing my PhD. I could not have done the work I have without their guidance, training, and constructive criticism. I especially owe great thanks to Evelyn Zarate-Sanchez for her peer insight into my project and having the chance to work together on closely related projects. I would also like to thank my committee members—Dr. Passerini and Dr. Gilchrist— for their critical feedback, advice, and time given to my project. I am grateful to the UC Davis Department of Biomedical Engineering for the collaborative environment they provided that connected me with other biomedical engineers. Finally, I would like to thank my friends—old and newly made at UC Davis—and family for their unwavering support during this difficult and laborious time.

Table of Contents

1 Chapter 1: General Introduction 1

2 Chapter 2: *Ex Vivo* Neutrophil Granulopoiesis in Gelatin Methacrylate (GelMA) Hydrogels 4

2.1 Introduction 4

2.2 Materials & Methods 8

2.3 Results 16

2.3.1 GelMA Hydrogel Mechanical Properties Determine HSPC Survival and Cell-Matrix Interactions 16

2.3.2 Culture in GelMA Hydrogels Increases Granulopoiesis and Neutrophil Differentiation in Comparison to Cells Cultured in Suspension 18

2.3.3 Neutrophils Originated from GelMA Encapsulated HSPCs Exhibit Equivalent or Higher Levels of Activation and Function in Comparison to Culture in Suspension Conditions 24

2.3.4 GelMA Hydrogels Provide a Synthetic Niche for Neutrophil Transplantation 28

2.4 Discussion 34

2.5 Conclusion 41

2.6 Supplemental Materials 42

3 Chapter 3: An Integrated Microphysiological Model of Human Bone Marrow and Skin 47

3.1 Introduction 47

3.2 Materials & Methods 50

3.3 Results 59

3.3.1 Single Multi-Organ MPS Platform 59

3.3.2 Bone Marrow Microenvironment MPS 61

3.3.3 Skin Microenvironment MPS 65

3.3.4 SM-MPS Response to Inflammation 69

3.3.5 Progenitor Response in the SM-MPS 71

Discussion 74

3.4 Conclusion 79

3.5 Supplemental Materials 81

4 Chapter 4: Recruitment and Local Granulopoiesis of HSPCs in a 3D Skin Model 83

4.1 Introduction 83

4.2 Materials & Methods 87

4.3 Results 93
4.3.1 Skin-on-a-Chip (SC) Platform 93
4.3.2 Skin-on-a-Chip response to simulated inflammation 96
4.3.3 PMN and HSPC attachment and migration dynamics 99
4.3.4 The SDF-1/CXCR4 axis in cell binding and retention 102
4.3.5 Anti-bacterial response of HSPC-derived granulocytes in SC 104
4.4 Discussion 108
4.5 Conclusion 113
4.6 Supplemental Materials 114
5 Chapter 5: Future Directions 116
6 Appendix 120
6.1 Glossary 120
6.2 References Cited 122

1 Chapter 1: General Introduction

Antibiotic-resistant bacterial infections pose a grave threat to global healthcare, summing in an estimated over 1 million deaths every year[1]. For instance, MRSA, or methicillin resistant *Staphylococcus aureus,* represents over 125,000 hospitalizations annually[2]. As antibiotic resistance of bacteria rises globally, new and unconventional methods are necessitated to face this global health threat. Thus, new models and therapies need to be developed to generate better understanding of the immune system to fight these infections.

The first line of defense of the human immune system against bacterial pathogens is the polymorphonuclear neutrophil (PMN)[3,4]. These are short-lived immune cells of the adaptive immune system with a half-life of around ~12 hours[5,6]. PMNs are generated by hematopoietic stem and progenitor cells in the bone marrow and produce on average 10^{11} cells per day[7]. The traditional paradigm thus far has been that PMNs directly combat infection by moving from circulation into the wound bed to clear infection through multiple anti-bacterial mechanisms such as NETosis[8,9], reactive oxygen species (ROS) production[10], and phagocytosis[11].

Though PMN recruitment to wound beds is crucial to wound healing and bacterial clearance, certain patient populations are more at-risk for negative outcomes due to acute neutropenia. Persons receiving chemotherapy treatment for diseases such as acute myeloid leukemia are depleted of HSPCs and are prone to develop severe and fatal infections[12]. One therapy for these patients is being infused with donor leukocytes, though these treatments require multiple infusions and still lead to an increased propensity to systematic reinfection[13]. This rationale applies to several other patients

receiving chemotherapy. Other at-risk patient populations include diabetics which have directly observed to have lower neutrophil counts[14].

Though HSPCs produce a steady number of PMNs in circulation, there are two major ways HSPCs regulate output of these PMNs as effector cells. The first and most well-studied method is emergency granulopoiesis. Emergency granulopoiesis is an adaptive immune response in which HSPCs residing in the bone marrow produce two to ten-fold more PMNs in circulation depending on the severity of septic signals detected (i.e., TLR2 agonists)[15–18]. With more PMNs in circulation, more are available to traffic to and clear sites of infection. Emergency granulopoiesis also increases not only more PMNs in circulation, but also immature neutrophils and CD34+ HSPCs[19].

In a less-known manner, HSPCs are capable of more directly fighting infection at the site of inflammation through a process known as local granulopoiesis (or extramedullary granulopoiesis)[20–22]. This is the process in which HPSCs that circulate in blood naturally translocate to wound sites and set up a local granulopoietic niche that generates functional PMNs within the wound rather on relying on PMNs to traffic to the wound from circulation. Local granulopoiesis has been shown to account for over 25% of PMNs found in the site of skin infection in mouse models. Inoculation of murine wound-beds with *S. aureus* resulted in a two-fold increase in systems PMN circulation—indicative of the emergency granulopoiesis mechanism acting as expected. However, PMNs at the site of infection also increased ten-fold in the same study[20]. In fact, HSPC recruitment to murine wound beds has been shown to be critical to survival when PMN recruitment was impaired[22]. TLR2 agonism is a critical component of HSPC myelopoiesis in local dermal wounds. For example, HSPCs can be activated *via* TLR2

to increase proliferation rate and cause rapid myeloid differentiation both *in vivo* and *in vitro*[23,24].

However, studies thus far studying local granulopoiesis have only been attempted in animal models[20–22]. This of course makes logical sense due to the difficulties of observing this phenomenon directly in humans, let alone testing the hypothesis ethically. Thus, *ex vivo* models of human skin are necessary for discerning any mechanistic insight of HSPCs dynamics in human systems. Microphysiological systems (MPSs) provide an experimental platform to recapitulate the 3D biology of the skin.

We hypothesize that dermal local granulopoiesis occurs in humans as well as mice. We developed a 3D MPS of skin to model the dynamics of PMN and HSPC binding to human skin, as well as offer some mechanistic insight into the recruitment and retention of these immune cells in the skin niche over time. Through these studies, we hope to better understand the role of HSPCs in dermal wound healing while also offering new mechanisms to leverage in future therapies aiming to treat infectious wounds.

2 Chapter 2: *Ex Vivo* Neutrophil Granulopoiesis in Gelatin Methacrylate (GelMA) Hydrogels

Adapted from: "Neutrophil Granulopoiesis Optimized Through Ex Vivo Expansion of Hematopoietic Progenitors in Engineered 3D Gelatin Methacrylate Hydrogels" by Evan Cirves et al. published in Advanced Healthcare Materials. February 2024

2.1 Introduction

Polymorphonuclear leukocytes (PMNs)—commonly known as neutrophils—are the most abundant white blood cells in circulation and crucial in the innate immune response against pathogens[3,4]. They are the first line of defense in combating skin infections and are necessary removing bacteria to initiate the process of tissue healing. PMNs are continuously produced by hematopoietic stem and progenitor cells (HSPCs) in the bone marrow and subsequently released into circulation to surveil tissue. In the event of a dermal wound and acute infection, HSPCs migrate out of their niche in the bone marrow and undergo emergency granulopoiesis which increases PMN production and their availability in circulation[25,26]. Human patient populations that suffer from acute neutropenia—such as those receiving chemotherapy treatment for acute myeloid leukemia (AML)—are depleted of HSPCs and are prone to develop severe and often fatal infections[12]. These patients are typically infused with donor leukocytes, but such treatments require multiple infusions with an increased probability of systematic reinfection[13]. *Ex vivo*-produced PMNs derived from HSPC cultures represent a potential source of autologous cells for infusion or delivery to sites of infection[27]. This approach, however, has not been used clinically due to the high cost of inefficient expansion of

CD34+ HSPCs in suspension cultures within a bioreactor, and a lack of criteria for determining the potency of myeloid expansion for any given donor HSPCs[28]; furthermore, bolus injection of purified allogenic or donor PMNs directly into chronic wounds results in a high rate of cell apoptosis and ineffective antibacterial functionality that limits the therapeutic efficacy of infusion[29–32].

In addition to emergency granulopoiesis–which HSPCs produce PMNs in the bone marrow in much greater quantities—HSPCs can leave the bone marrow niche and enter circulation to eventually migrate toward infected wounds where they locally proliferate and differentiate into mature PMNs following toll-like receptor 2 (TLR2) mediated recognition of *Staphylococcus aureus* (*S. aureus*)[20,21]. Local granulopoiesis accounts for up to 30% of PMNs in a dermal site of infection in murine models, making them crucial for survival in mouse models of methicillin-resistant *S. aureus* (MRSA) infection[20]. Inducing an acute *S. aureus* infection in a full-thickness skin wound resulted in a twofold increase in PMNs in circulation and a tenfold increase in PMN recruitment to the infected wound[20]. HSPC trafficking and local myeloid granulopoiesis at the site of MRSA infections is a critical host immune mechanism for circumvention of impaired PMN recruitment mediated virulence factor alpha-toxin[22]. This discovery motivates the development of local HSPC administration as an immune therapy to combat intractable infections in patients with impaired PMN tissue recruitment—or insufficient vascular perfusion and antibacterial function like those found in diabetic wounds[33]. The current challenge to overcome in exploiting local granulopoiesis is in the design of a bone marrow mimetic niche; this niche must facilitate cell-matrix and cell-cell signaling *via* paracrine growth factors (e.g., stem cell factor [SCF], granulocyte colony-stimulating

factor [G-CSF], FMS-like tyrosine kinase 3 [flt3]) and interleukins that promote terminal PMN differentiation of CD34+ HSPCs.

A limitation of engineered cell therapies is the vehicle used for delivery since bolus injection can lead to cell apoptosis and low therapeutic efficacy. The strategy to encapsulate HSPCs in a hydrogel-based biomimetic matrix provides for the maintenance of myeloid progenitors and sustained, localized release of PMNs within the site of inflammation. HSPCs and other stem-like progenitors are preserved longer within collagen hydrogels versus suspension culture; this is especially critical in the case of granulopoiesis that requires maintenance of the self-renewal properties of HSPCs[34]. Further tuning of biochemical properties of a substrate can dictate the extent of HSPC function by adjusting the substrate's storage modulus and porosity to mimic the *in vivo* bone marrow environment that preserves stem-like populations. For example, previous studies focused on the co-culture of HSPCs and mesenchymal stem cells (MSCs) in gelatin methacrylate (GelMA)[35]. Results showed the production of lineage-positive (Lin+) PMN progenitors while maintaining stem populations. However, these studies did not quantify the efficiency of PMN expansion or maturation into functional phagocytes.

In these current studies, GelMA hydrogels—with prescribed stiffness to simulate the bone marrow niche—were produced to optimize the efficacy of HSPC granulopoiesis and local generation of functional PMNs. PMNs produced in these hydrogels were compared with those grown in suspension cultures to define both methods capacity for antibacterial function in both *in vitro* and *in vivo* mouse studies. Previously established C57BL/6 mouse lines including enhanced green fluorescent protein-lysozyme M (EGFP-LysM) and MRP8-FFLUC were leveraged to quantify

myeloid differentiation and expansion[36]. This established a potential approach to deliver functional PMNs *in vivo.*

2.2 Materials & Methods

Generation of Transgenic Mice Approval: EGFP-lysozyme M (LysM) knock-in mice (EGFP-LysM-mice[36]) were kindly gifted by Dr. Thomas Graf (Center for Genomic Regulation, Spain). To generate the MRP8 FFLuc line, the following mice strains were obtained from the Jackson Laboratories (Bar Harbor, Maine) and cross-bred at the University of California, Davis: avis: B6.Cg-Tg(S100A8-cre,-EGFP)1Ilw/J (Jax Strain #02 1614)[37] and STOCK Gt(ROSA)26Sortm1(Luc)Kael/J (Jax Strain #03 4320)[38]. To identify and select offspring mice expressing the firefly luciferase reporter, mice were subcutaneously administered 250 mg/kg of d-Luciferin (Cat# 122799, Perkin Elmer)[39] and imaged in an IVIS Spectrum (Perkin Elmer). All animal experiments were approved by the Institutional Animal Care and Use Committee (IACUC) of the University of California at Davis and were performed following the guidelines of the Animal Welfare Act and the Health Research Extension Act.

HSPC Isolation and In Vitro *Culture:* Murine bone marrow was harvested from hind legs of 8 week or older EGFP-LysM knock-in mice. After CO_2-induced euthanasia, femurs, fibulas, and tibias were aseptically collected and ground in EasySep Buffer (STEMCELL Cat# 20144) and finally filtered through a 70 µm cell strainer. Stem cells were negatively isolated using the EasySep Mouse Hematopoietic Progenitor Cells Isolation Kit (STEMCELL Cat# 19856A); Cells were further isolated using the EasySep Mouse CD117 (cKIT) Positive Selection Kit (STEMCELL Cat# 18757). Cells were resuspended at 1E6 cells/mL in HSPC expansion media consisting of STEMSPAN SFEM II (STEMCELL), recombinant murine stem cell factor (0.1 µg/mL, SCF, STEMCELL), recombinant murine Flt3-ligand (0.1 µg/mL, STEMCELL), recombinant

murine granulocyte colony-stimulating factor (0.01 µg/mL, G-CSF, STEMCELL), recombinant murine interleukin 3 (0.01 µg/mL, IL-3, STEMCELL), and recombinant murine interleukin 6 (0.01 µg/mL, IL-6, STEMCELL). HSPCs were cultured in 48-well suspension culture plates with 1 mL of HSPC expansion media per well. Each well was initially seeded with 2E5 HSPCs in suspension or encapsulated in GelMA, incubated at 37 °C, 5% CO_2, and fed every 2 days.

GelMA Gel Production and Mechanical Properties Characterization: GelMA gels were produced as previously described[40]. Briefly, Gelatin methacryloyl (GelMA; 300 bloom, MilliporeSigma) was dissolved at 20% (w/v) in complete media with 0.6% (w/v) 2-Hydroxy-4'-(2-hydroxyethoxy)-2-methylpropriophenone (Irgacure 2959) with agitation at 80 °C for 15 minutes. The 20% GelMA was then diluted in complete media to yield 5% GelMA or 10% GelMA solution containing 0.3% Irgacure. HSPCs were encapsulated in the different GelMA solutions to a final concentration of 5E6 cells/mL. The final solution was dispensed (40 µL) into 6mm x 1mm high molds and exposed to 17 mW/cm^2 ultraviolet (EV, 320-500 nm) light for 1 minute before culture using an Omnicure S2000 Spot UV Curing System (Excelitas Technologies, Waltham, MA).

The mechanical and physical properties of GelMA gels were analyzed as previously described[41]. The storage modulus of 8 mm diameter x 2mm height gels was analyzed using a Discovery HR-2 hybrid stress-controlled rheometer. The constructs were placed between 8 mm parallel plates (axial force set at 0.2 Newtons) and were strained from a range of 0.001-5% with a frequency of 1 Hz. The values of storage modulus (G') were obtained from the linear viscoelastic region. Volumetric swelling ratio (Q) was calculated by the following equation as previously described:

$$Q = \frac{\frac{W_S - W_D}{\rho_W} + \frac{W_D}{\rho_P}}{\frac{W_D}{\rho_P}} \quad (1)$$

where ρ_W is the density of water and ρ_P is the density of polymer (1.35 g/mL)[41,42]. Mesh size of the crosslinked polymers in the constructs was estimated using swelling and storage modulus as previously described[41–43]. The molecular weight between crosslinks (M_C) was then determined by the following equation:

$$M_C = \frac{C_P RT}{G'} \quad (2)$$

where C_P is the polymer concentration, R is the gas constant, and T is the temperature. Mesh size (ξ) was then calculated as follows:

$$\xi = Q^{\frac{1}{3}} \left(\frac{2M_C}{M_r}\right)^{\frac{1}{2}} C_n^{\frac{1}{2}} \quad (3)$$

where the molecular weight of the repeating unit M_r (91.19 g/mol), the amino acid bond length l (4.28 Å), and Flory's characteristic ratio C_n for GelMA (8.8785) as previously described[43].

To obtain the hydrogel swelling ratio, the wet weight (WS) of the constructs was recorded, the constructs were frozen at -80 °C overnight, lyophilized for 48 hours, and then weighed again to obtain the dry weight (WD).

HSPC Viability and Morphology Assessment: To visualize cell morphology, cell-laden GelMA constructs were collected after 1 day of culture and fixed with 4% paraformaldehyde at 4 °C overnight, washed twice with PBS, and permeabilized with Triton-X 100 (0.05%) for 5 minutes at room temperature. Cell actin cytoskeleton was stained with Alexa Fluor 488 Phalloidin solution (Thermo Fisher; 1:40 in PBS). Cell nuclei were stained with DAPI (Thermo Fisher; 1:500 in PBS). Gels were imaged using

confocal microscopy (Leica TCS SP8). Cell viability was analyzed by a live/dead assay (LIVE/DEAD Viability/Cytotoxic Kit) per the manufacturer's protocol (Thermo Fisher) in which samples are simultaneously stained with green-fluorescent ethidium homodimer-1 to indicate loss of plasma membrane integrity. Fluorescent images were taken using confocal microscopy (Leica TCS SP8). The percentage of living cells and shape descriptors were quantified through image analysis in ImageJ. For quantification of DNA level and caspase 3/7 activity, constructs were collected, sonicated, and lysed in a passive lysis buffer (Promega). Total DNA content was determined using a PicoGreen Quant-iT DNA Assay Kit (Invitrogen). Cell apoptosis was measured using Caspase-Glo 3/7 assay (Promega). For both assays, a BioTek Synergy HTX Multi-mode Microplate Reader (Agilent) was used.

RT-qPCR: Samples were collected in 0.3 mL of TRIzol Reagent (Invitrogen) and homogenized using an ultrasonic processor. RNA was isolated following the manufacturer's instructions. Following RNA isolation, 800 ng of RNA was reverse transcribed with the QuantiTect Reverse Transcription Kit (QIAGEN) and normalized to a final concentration of 12 ng/mL. RT-qPCR was performed using the Taqman PCR Master Mix (QIAGEN) on a QuantStudio 6 system (Applied Biosystems). Mice-specific primers for GAPDH (Mm99999912_g1), MMP14 (Mm00485054_m1), and MMP8 (Mm00439509_m1) were purchased from Thermo Fisher Scientific. Critical threshold values (C_t) were quantified for each gene. The ΔC_t was quantified by subtracting the samples' Ct value of the housekeeping gene, *GAPDH*. The $\Delta\Delta C_t$ was quantified by subtracting the average ΔC_t of the suspension cells on Day 7. The relative expression values for each gene of interest are presented at $2^{-\Delta\Delta Ct}$.

GelMA Culture Confocal Imaging: Gels were cultured for 7 days before being fixed in Fixation Buffer (Biolegend) for 1h. Gels were then incubated in 5 mg/mL DAPI for 30 minutes before being washed twice with and imaged on an Olympus FV3000 confocal microscope with 60x objective. The EasySep Mouse CD117 (cKIT) Positive Selection Kit (STEMCELL Cat# 18757) that was used on day 0 to isolate HSPCs contained a PE-CD117 antibody used in the isolation process, and this antibody conjugate was preserved over 7 days and the fixation process as seen in confocal images.

HSPC Phenotypic Characterization: Cell-laden gels were cultured for 7 days before being collected individually. Hydrogels were fragmented using a scalpel and incubated in collagenase type IV (1000 Units/mL, Gibco) at 37 °C for 20 minutes. Escaped and suspension cells were harvested by gently pipetting and transferring to a new tube. This process was repeated with EasySep Buffer to detach over 90% of cells. After centrifugation and washing with EasySep Buffer, cells were labeled with a panel of antibodies for 30 minutes: CD117-PE (Biolegend Cat# 105808, 1:100), CD11b-Alexa Fluor 700 (Biolegend Cat# 101222, 1:1000), SCA-1-APC (Biolegend Cat# 108112, 1:1000), Ly6C-APC/Fire750 (Biolegend Cat# 128046, 1:100), Ly6G-PE/Cy7 (Biolegend Cat# 127618, 1:100), and fixable viability dye eFluor506 (Thermo Fisher Cat#: 65-0866-14, 1:1000). Flow cytometry was performed using the Attune NxT Acoustic Focusing Flow Cytometer (Thermo Fisher). Compensation controls, unstained samples, and fluorescence-minus-one controls were used to gate cell populations.

CD11b Upregulation Assay: Cells were isolated as described earlier, with encapsulated and escaped cells combined from hydrogel wells. Cells from three GelMA wells were pooled and divided into three tubes for stimulation. This process was serially

repeated using 15 wells for N = 5 replicates. Suspension cells were similarly pooled. After centrifugation, cells were resuspended in HBSS +/+ and 0.1% human serum albumin containing phorbol 12-myristate 13-acetate (PMA, 10 ng/mL). Cells were labeled with CD11b-Brilliant Violet 711 (Biolegend Cat# 101242, 1:1000), and Zombie Yellow Fixable Viability dye (Biolegend Cat# 423103, 1:100). Tubes were incubated for 20 minutes at 37 °C, followed by treatment with Fixation Buffer (Biolegend). Cells were washed with EasySep Buffer twice before flow cytometry was performed using the Attune NxT Acoustic Focusing Flow Cytometer (Thermo Fisher).

ROS Activity: Cells were isolated with encapsulated and escaped cells combined from hydrogel wells. After centrifugation, cells were resuspended in tubes with HBSS +/+ and placed on a 37 °C hotplate to warm for 45 minutes. Depending on condition, tubes were treated with 10 ng/mL PMA and labeled with CD11b-Brilliant Violet 711 (Biolegend Cat# 101242, 1:1000), Dihydrorhodamine 123 (Thermo Fisher Cat# D23806, 10μM), and Zombie Yellow Fixable Viability dye (Biolegend Cat# 423103, 1:1000). Tubes were incubated at 37 °C for another 20 minutes before the reaction was extinguished by placing on ice for 10 minutes. Cells were spun down and resuspended in EasySep buffer and measure using the Attune NxT Acoustic Focusing Flow Cytometer (Thermo Fisher).

NETosis Assay: Calls from individual 9 cultures were isolated at day 7 and pooled. 1E5 cells/mL were seeded into a 96 well plate in HBSS +/+ in the presence of *P. aeruginosa* (1E8 CFU), PMA, or vehicle control. Plates were then incubated for 12 hours at 37 °C, stained with 20 μL of 5 μM SYTOX Orange, and incubated at room

temperature for 15 minutes. Plates were then imaged on the IVIS Spectrum for SYTOX orange to measure NET output.

Phagocytosis Assay: N=3 cultures of cells were isolated at 1E6 cells/mL for each condition of GelMA, suspension, or bone marrow cells. Phagocytosis was induced using a pHrodo *S. aureus* BioParticle Phagocytosis kit using the kit's protocol. pHrodo MFI was measured on EGFP+ cells using the AttuneNxT Flow Cytometer.

Luciferase Activity Quantification and In Vivo *Cell Transplantation:* On day 7, hydrogel constructs with encapsulated PMN derived from HSPC of MRP8-FFLuc mice were sub-dermally implanted into recipient C57Bl6/J mice. >20 minutes prior to surgery, mice intraperitoneally received 0.03 mg/mL Buprenex. Dorsal area of each mouse was shaven and aseptically sterilized with gauze in povidone-iodine and gauze in 70% isopropanol. An intradermal pouch was created using surgical scissors into which hydrogel constructs were transplanted. The pouch was stitched and mice were monitored for recovery. Mice received a daily subcutaneous dose of 250 mg/kg of d-Luciferin 5 min prior to imaging in an IVIS Spectrum to quantify MRP8-luciferase activity *in vivo*. As a proof of concept of therapeutic application, a sample size of N = 1 was used in this experiment for each of the groups. All animal experiments were approved by the Institutional Animal Care and Use Committee (IACUC) of the University of California at Davis and were performed following the guidelines of the Animal Welfare Act and the Health Research Extension Act.

Statistical Analysis: Data in this section are presented as a means ± standard deviation unless otherwise stated, and all data points are included in each graph. Normality was tested through the Shapiro-Wilk test ($\alpha = 0.05$). Statistical analyses were

done using one-way ANOVA with post-hoc Tukey test, two-way ANOVA with Tukey's multiple comparisons test, or unpaired t-test when necessary. For data following a non-normal distribution, Kruskal-Wallis test was used. $P < 0.05$ was considered significant. Statistical significance was indicated in each graph as * ($p < 0.05$), ** ($p < 0.01$), *** ($p < 0.001$), **** ($p < 0.0001$).

Ethics Approval Statement: Animal studies were approved by the Institutional Animal Care and Use Committee (IACUC) at the University of California, Davis under protocol codes 19922 and 21790.

2.3 Results

2.3.1 GelMA Hydrogel Mechanical Properties Determine HSPC Survival and Cell-Matrix Interactions

During emergency granulopoiesis, *de novo* expansion of PMNs by HSPC progenitors occurs in the bone marrow niche which provides a rapid increase in the number of mature PMNSs released into circulation to meet the demand at recruitment sites for infection events. To mimic the mechanical properties of the perivascular and endosteal regions where HSPCs undergo granulopoiesis, we cultures HSPCs in GelMA over a range of stiffnesses[44]. Three GelMA concentrations (5%, 10%, and 20%) were selected to produce gels with a Young's moduli ranging from 0.25 to 24.7 kPa. While 5% GelMA produced hydrogels with the lowest storage modulus, they also exhibited the highest swelling ratio and porosity in comparison to 10% and 20% (Figure 2-1).

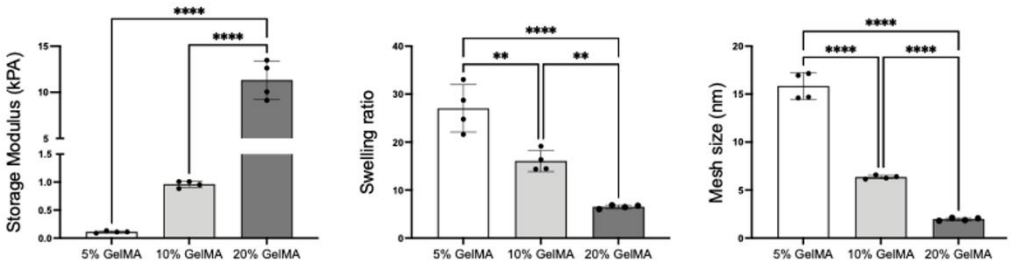


Figure 2-1. Storage modulus, swelling ratio, and mesh size of either 5%, 10%, or 20% GelMA hydrogels after production. N = 4.

To explore the effects of the physical properties of hydrogels on cell survival, HSPCs were encapsulated in GelMA and maintained in culture. Following 1 day of encapsulation, we observed greater DNA content for cells in 5% GelMA gels compared to cells in 10% and 20% gels (Figure 2-2, left). We evaluated the relationship between

DNA content and cell apoptosis by assessing caspase 3/7 activity, which revealed higher apoptosis as the density of GelMA increased (Figure 2-2, right).

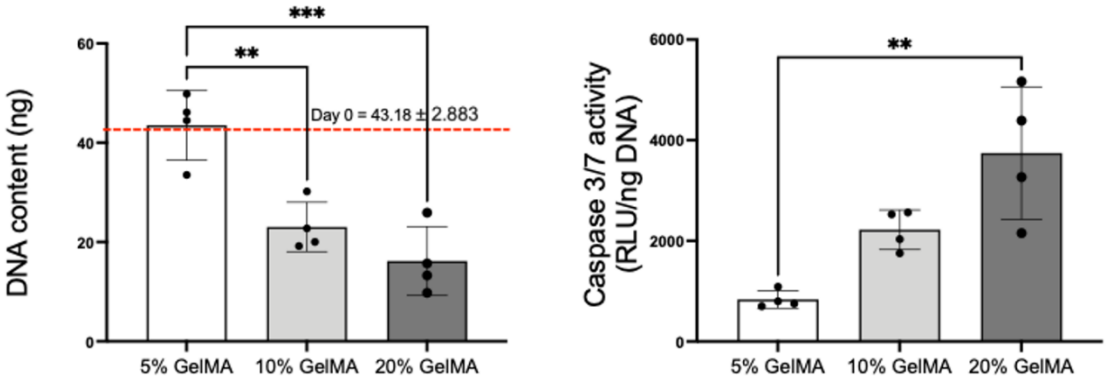


Figure 2-2. DNA content and caspase 3/7 activity in HSPC-laden GelMA hydrogels 24h after cell encapsulation. N = 4.

In addition to DNA and caspase 3/7 activity, live/dead staining confirmed a higher frequency of cell mortality in the 10% and 20% GelMA gels in comparison to the 5% gels; nearly all cells in the 5% case were viable (~ 95%) (Figure 2-3, Supplementary Figure 2-1).

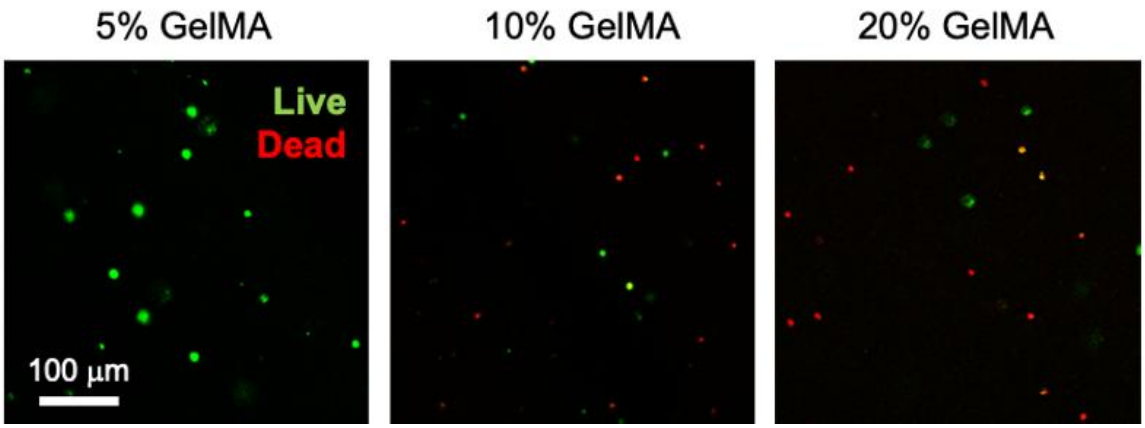


Figure 2-3. LIVE/DEAD (living cells in green, dead cells in red) characterization of encapsulated HSPCs 24h after hydrogel production.

Cell morphology was also by staining F-actin on encapsulated HSPC cytoskeletons. While cells encapsulated in 5% GelMA frequently exhibited a polarized

morphology with multiple pseudopods, cells in 10% and 20% GelMA were comparatively smaller and remained spherical (Figure 2-4, Supplementary Figure 2-2). This suggests there are increased cell-matrix interactions occurring in 5% gels.

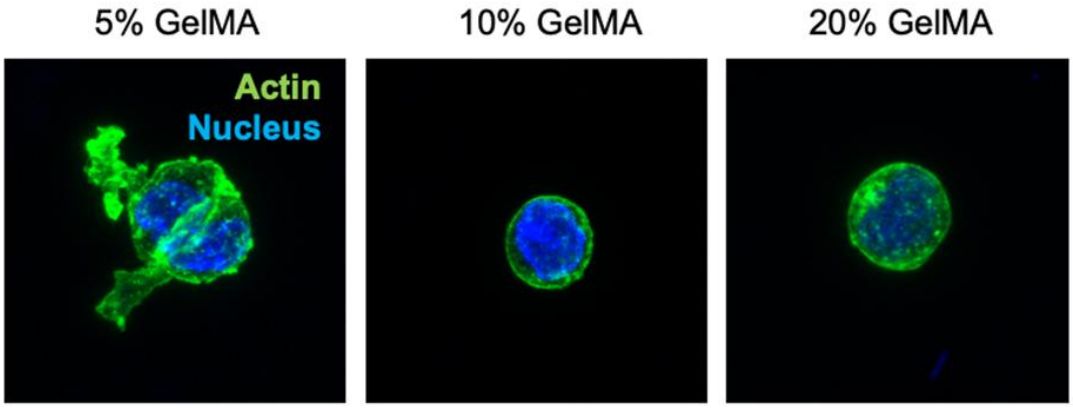


Figure 2-4. Fluorescent imaging of HSPC actin cytoskeleton in the different GelMA gels 24 h after production.

To confirm that the observed differences were due to GelMA crosslinking, a control experiment was conducted to evaluate the effect of UV treatment on HSPC suspensions after 3 days of culture, revealing no difference in cell viability or oxidative stress (Supplementary Figure 2-3).

2.3.2 Culture in GelMA Hydrogels Increases Granulopoiesis and Neutrophil Differentiation in Comparison to Cells Cultured in Suspension

Previous reports have confirmed the key role of hydrogel mechanics in HSPCs maintenance and differentiation, but the role of the 3D microenvironment in HSPC granulopoiesis remains unexplored[35]. To evaluate the effects of 3D GelMA culture on HSPC granulopoiesis in comparison to equal numbers seeded in suspension culture, HSPCs were isolated form the bone marrow of LysM-EGFP mice and encapsulated in 5% GelMA; They were maintained in culture for 3 days in myeloid differentiate media

supplemented with G-CSF, SCF, IL-3, IL-6, and Flt-3. LysM-EGFP mice possess the enhanced green fluorescent protein (EGFP) inserted in the lysozyme M (LysM) promoter region, thereby facilitating the quantification of mature PMNs that express the highest levels of LysM-EGFP. In addition, HSPC differentiation was assessed by identifying undifferentiated HSPCs (LSK+) and granulocyte-monocyte progenitors (GMPs) that express low levels of LysM-EGFP (Figure 2-5)[45].

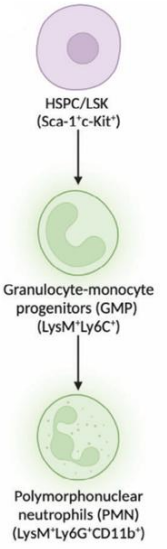


Figure 2-5. LysM-EGFP cells were stained with Sca-1+ c-KIT+ to determine undifferentiated HSPCs (LSK cells), with Ly6C+ to determine granulocyte-monocyte progenitors (GMPs), and with Ly6G+CD11b+ to assess the polymorphonuclear neutrophil populations (PMNs).

After 3 days of *in vitro* culture, equivalent numbers of viable cells were observed in suspension and GelMA gels, but there were significantly more GMPs and PMNs detected in dissolved gels (Figure 2-6).

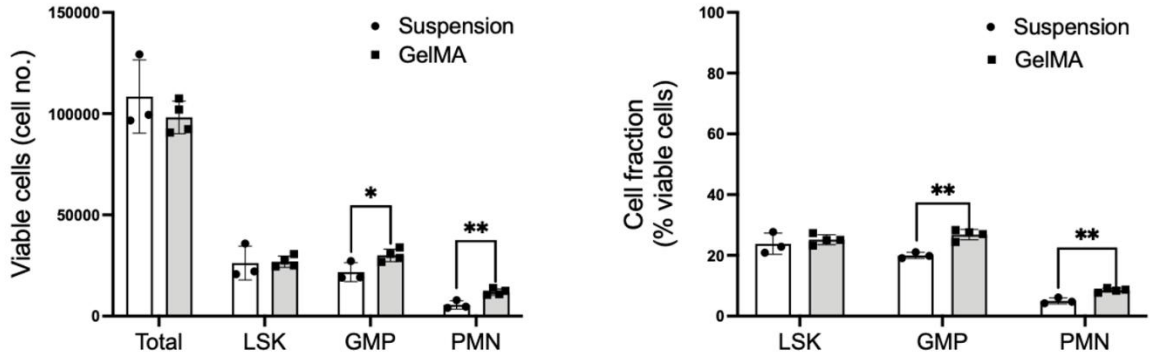


Figure 2-6. After 72 h of *in vitro* culture in either suspension or 5% GelMA gels, cells were isolated and the total number of viable cells was determined through FACS. The fractions of LSK, GMP, and PMN populations were also determined. N = 3 – 4.

We determined the expansion of GMPs and PMNs per input HSPC—in regard to fold-number-expanded—encapsulated in GelMA was significantly higher than HSPCs grown in suspension, although the total fold expansion was similar in both conditions. We conclude that there is enhanced differentiation and expansion of PMNs derived from HSPCs cultured in 3D gels as opposed to culture in suspension (Figure 2-7).

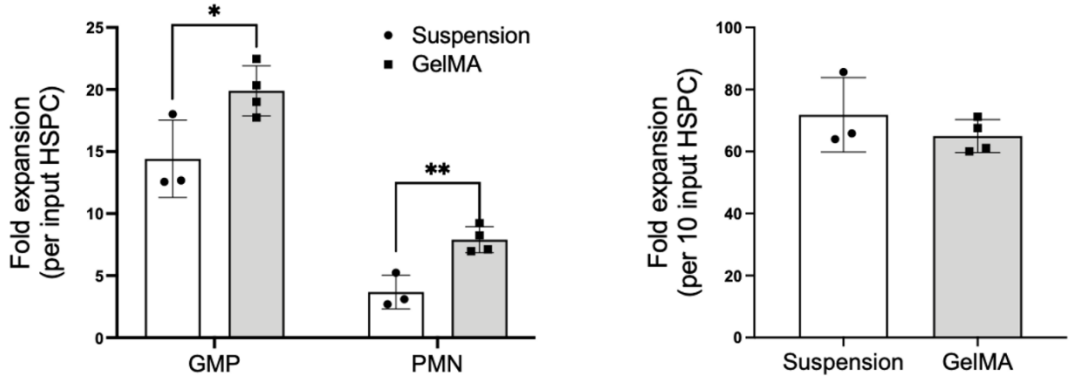


Figure 2-7. Myeloid expansion per input HPSC towards GMP or PMN phenotypes (left). The total fold-expansion of all cells detected per input HSPC was also determined after culturing. N = 3 in suspension and N = 4 in GelMA. * Denotes significance ($p < 0.05$); ** Denotes significance ($p < 0.01$).

HSPCs and PMNs express metalloproteases and catabolic enzymes that degrade collagen and other ECM components[46,47]. We hypothesized that this process

facilitates the escape of PMNs from their porous 3D GelMA microenvironment where they remain viable in suspension (Figure 2-8).

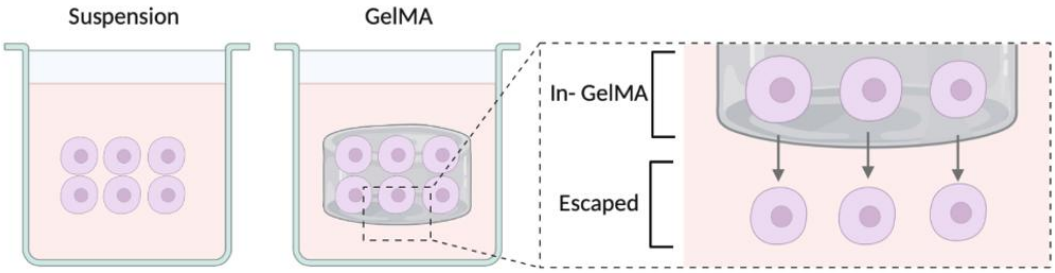


Figure 2-8. Graphical representation of analyzed cell populations defining the cells that remained encapsulated in GelMA gels (in-GelMA) *versus* cells that escaped the hydrogel (escaped).

To analyze the phenotype of cell populations that escaped from GelMA, HSPCs were cultured in either suspension or GelMA for 7 days in differentiation media. We observed equivalent fractions of viable LSK, GMP, and PMN populations were detected between suspension and GelMA cultured HSPCs (Figure 2-9).

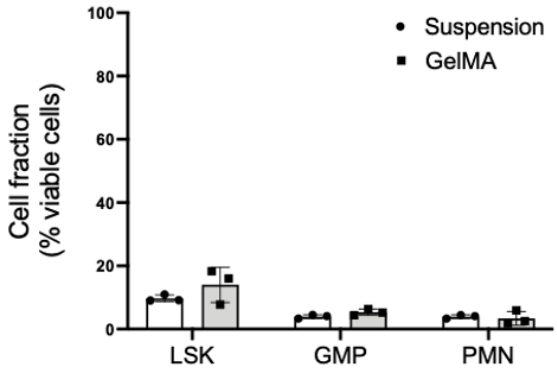


Figure 2-9. Percentage of LSK, GMP, and PMN cells in suspension or GelMA after 7 days. N = 3.

In the GelMA group, ~ 40% of total cells escaped from intact 3D gels (Figure 2-10).

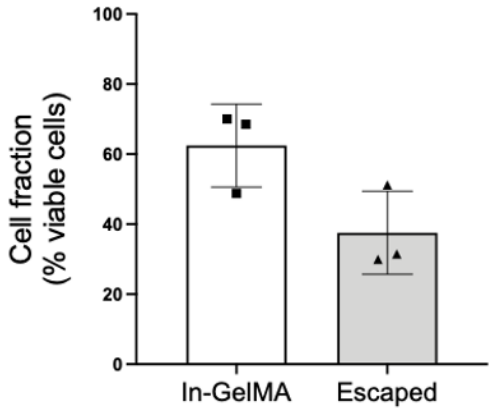


Figure 2-10. Percentage of cells that remained inside the GelMA hydrogels *versus* cells that escaped the 3D matrix after 7 days. N = 3.

To further investigate the mechanism of HSPC escape from GelMA gels, matrix metalloprotease (MMP) 8 and 14 gene expressions were analyzed on day 7. Cells encapsulated in GelMA expressed significantly higher levels of MMP14 compared to those that have escaped (Supplementary Figure 2-4). Since MMP14 activity is broad-acting collagenous and required for proper neutrophil migration and transendothelial migration, this data is consistent by showing how encapsulated cells exhibit increased capacity to degrade the GelMA matrix. In contrast, MMP8 expression was varied, and significant differences in expression between encapsulated and escaped cells were not detected (Supplementary Figure 2-5). While LSK cells constituted the highest fraction of cells that remained in the gels, GMPs represented the highest fraction which escaped (Figure 2-11).

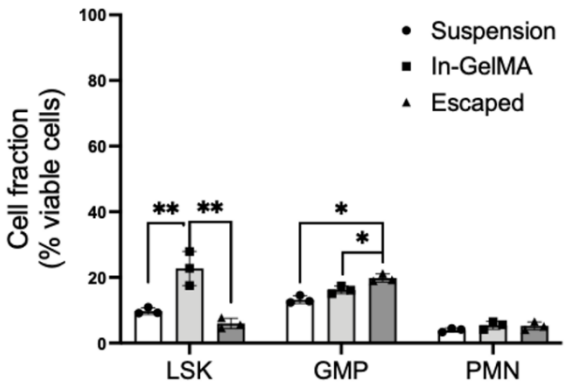


Figure 2-11. Percentage of LSK, GMP, and PMN cells in suspension, in-GelMA, and escaped after 7 days of differentiation in culture. N = 3. * Denotes significance ($p < 0.05$); ** Denotes significance ($p < 0.01$).

Moreover, the mean fluorescence intensity of LysM-EGFP$^+$ cells was higher in cells remaining in gels and those that escaped (Figure 2-12), whereas all cells cultured in suspension had lower intensity (Supplementary Figure 2-6).

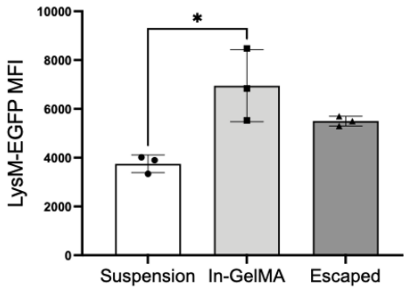


Figure 2-12. Median Fluorescence Intensity (MFI) of LysM-EGFP$^+$ cells after 7 days of differentiation in culture. N = 3. * Denotes significance ($p < 0.05$).

Thus, we conclude that LSK cells self-renew more leading to greater expansion of mature PMNs capable of migration out of GelMA compared to suspension-grown cells.

2.3.3 Neutrophils Originated from GelMA Encapsulated HSPCs Exhibit Equivalent or Higher Levels of Activation and Function in Comparison to Culture in Suspension Conditions

A hallmark of antimicrobial and inflammatory activity of PMNs is their capacity to produce superoxide radicals, i.e., reactive oxygen species (ROS), due to the NADPH oxidase complex (Figure 2-13)[10].

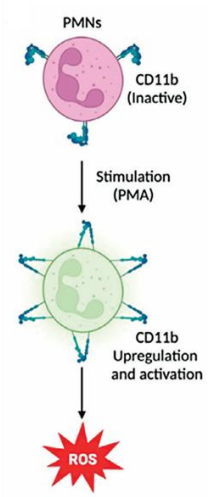


Figure 2-13. Schematic showing inactivated neutrophils responding to PMA and subsequently upregulating and activating CD11b and increasing ROS production.

To assess PMN activation in GelMA *versus* suspension after 7 days of culture, ROS production was quantified through activation of NADPH-oxidase in response to the addition of the secretagogue phorbol myristate acetate (PMA, 10 ng/mL). As a positive control, PMNs freshly isolated from mouse bone marrow were also assessed. PMNs expanded in GelMA generated equivalent levels of ROS as compared to those produced in suspension both at baseline and with PMA stimulation (Figure 2-14).

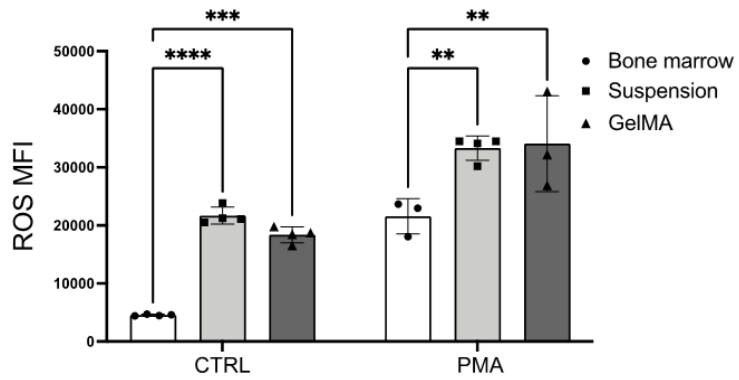


Figure 2-14. Reactive oxygen species (ROS) Median Fluorescence Intensity (MFI) of CD11b+ neutrophils extracted from bone marrow (C57BL/6J mice) or cultured *in vitro* for 7 days in either suspension or GelMA, when exposed to no stimulus (CTRL) or to 10 ng/mL PMA. N = 3-4. ** Denotes significance ($p < 0.01$); *** Denotes significance ($p < 0.001$); **** Denotes significance ($p < 0.0001$)

By comparison, naïve PMNs isolated from bone marrow exhibited exceptionally low baseline levels and lower stimulated ROS production. We conclude that *ex vivo* PMN expansion in the 3D microenvironment effectively produced mature PMNs that are capable of ROS production at levels on par with those cultured in suspension.

CD11b is upregulated to the plasma membrane in response to degranulating stimuli, where it regulates leukocyte adhesion and extravasation (Figure 2-13)[48]. To further assess PMN maturation and functionality, we quantified the relative surface expression of CD11b on bone marrow PMNs compared with cells expanded in suspension or GelMA gels. In response to PMA stimulation, cells encapsulated in GelMA or isolated from bone marrow upregulated ~ 100% more CD11b compared with suspension (Figure 2-15).

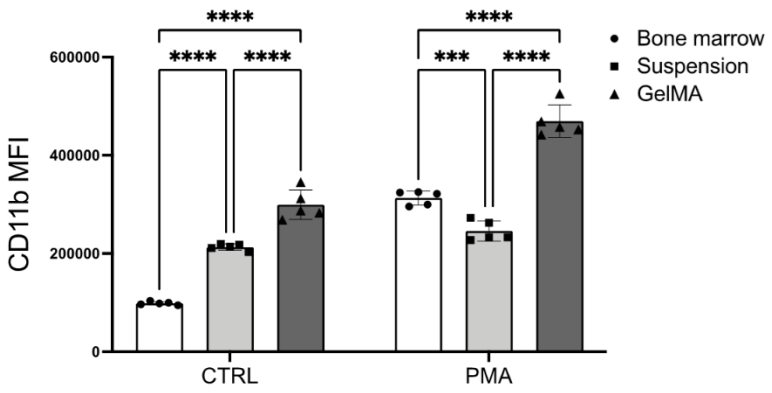


Figure 2-15. CD11b MFI in CD11b+/LysM+ neutrophils extracted from bone marrow (LysM-EGFP mice) or cultured *in vitro* for 7 days in either suspension or GelMA. N = 5. *** Denotes significance ($p < 0.001$); **** Denotes significance ($p < 0.0001$)

Thus, PMNs expanded from HSPCs in GelMA and those isolated from bone marrow exhibited a greater capacity to degranulate and upregulate membrane CD11b receptors in response to ionophore-mediate calcium flux.

To further examine the microbial functions of PMNs differentiated in GelMA, neutrophil extracellular trap (NET) formation and phagocytosis of *S. aureus* were measured (Figure 2-16).

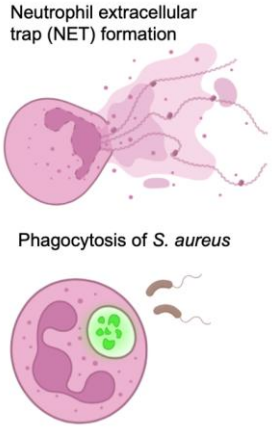


Figure 2-16. Schematic defining the biological responses: NET formation and phagocytosis.

PMNs cultured in GelMA showed equivalent levels of NETosis following exposure to the gram-negative bacteria *Pseudomonas aeruginosa* compared with bone marrow isolated cells (Figure 2-17).

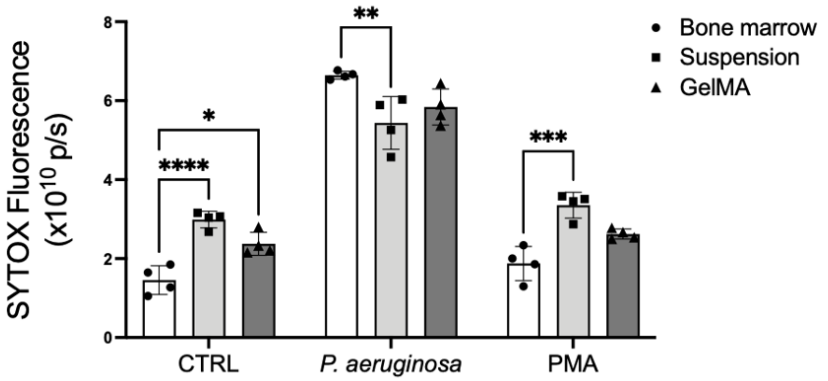


Figure 2-17. Average fluorescence of SYTOX Orange as an analog for NETosis. Cells were expanded in culture for 7 days before analysis. N = 4. * Denotes significance ($p < 0.05$); ** Denotes significance ($p < 0.01$); *** Denotes significance ($p < 0.001$); **** Denotes significance ($p < 0.0001$)

In contrast, PMNs expanded in suspension scored a higher baseline level but generated a smaller increase in NETosis compared to bone marrow or GelMA. We next tested the capacity for phagocytosis of gram-positive bacteria *S. aureus*-coated bioparticles. PMNs expanded in GelMA gels or suspension registered increased phagocytic capacity compared with those extracted from bone marrow (Figure 2-18).

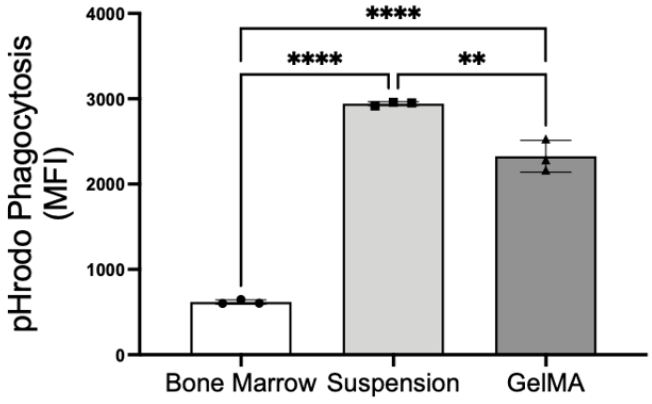


Figure 2-18. Average fluorescence of pH-reactive *S. aureus* bioparticles phagocytosed by EGFP+ cells and measured *via* Attune NxT flow cytometer. Cells were expanded for 7 days in culture before analysis. N = 3. ** Denotes significance ($p < 0.01$); ****Denotes significance ($p < 0.0001$)

Taken together, phenotypic analysis of effector functions indicates that HSPC expansion in GelMA or suspension produced more mature PMNs with a greater capacity for antibacterial activation than those from bone marrow.

2.3.4 GelMA Hydrogels Provide a Synthetic Niche for Neutrophil Transplantation

After characterizing the survival, expansion, and activation potential of PMNs derived from HSPCs encapsulated in GelMA, we assess the potential of 5% GelMA as a 3D niche for the delivery of HSPCs and expanded PMNs *in vivo*. HSPCs extracted from MRP8-FFLUC mice, which possess firefly luciferase (FFLUC) inserted in the myeloid-related protein 8 promoter region, were used to image and quantify PMN expansion. We first confirmed that the MRP8-FFLUC luciferase signal correlated directly with PMN numbers (Supplementary Figure 2-7). We quantified myeloid differentiation and expansion of PMNs from HSPCs encapsulated in 5% GelMA hydrogels compared with those maintained in suspension culture in either non-supplemented basal media (CTRL) or differentiation (DIFF) media. After HSPC isolation, luciferase activity indicative of mature PMNs was not observed in HSPCs seeded either in suspension of 5% GelMA hydrogels (Figure 2-19), confirming that naïve HSPCs do not express the FFLUC gene product.

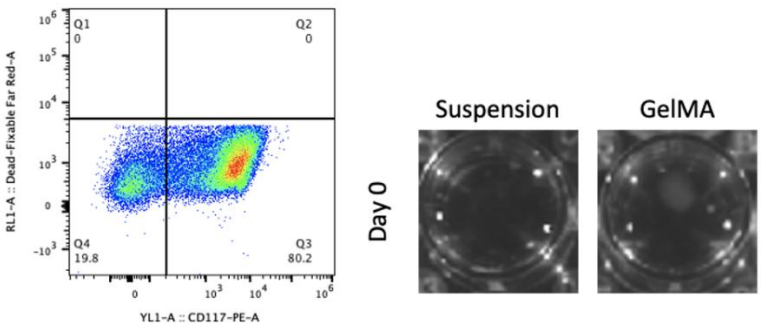


Figure 2-19. (left) Confirmation of > 80% of CD117+ HSPCs after cell isolation from the bone marrow of MRP8-FFLUC mice. (right) Luciferase activity at day 0 after isolation in cells in suspension or encapsulated in 5% GelMA gels.

Following 3 days of *in vitro* culture, luciferase activity was present in cells in suspension and those encapsulated in GelMA gels cultured in DIFF media, revealing the capacity to initiate granulopoiesis. After 7 days of culture, luciferase activity levels between the suspension and the GelMA groups cultured in DIFF media were not significantly different. But GelMA typically exhibited focal sites of higher expansion activity. In contrast, when cultured in CTRL media, luciferase activity was only detected in the GelMA group (Figure 2-20).

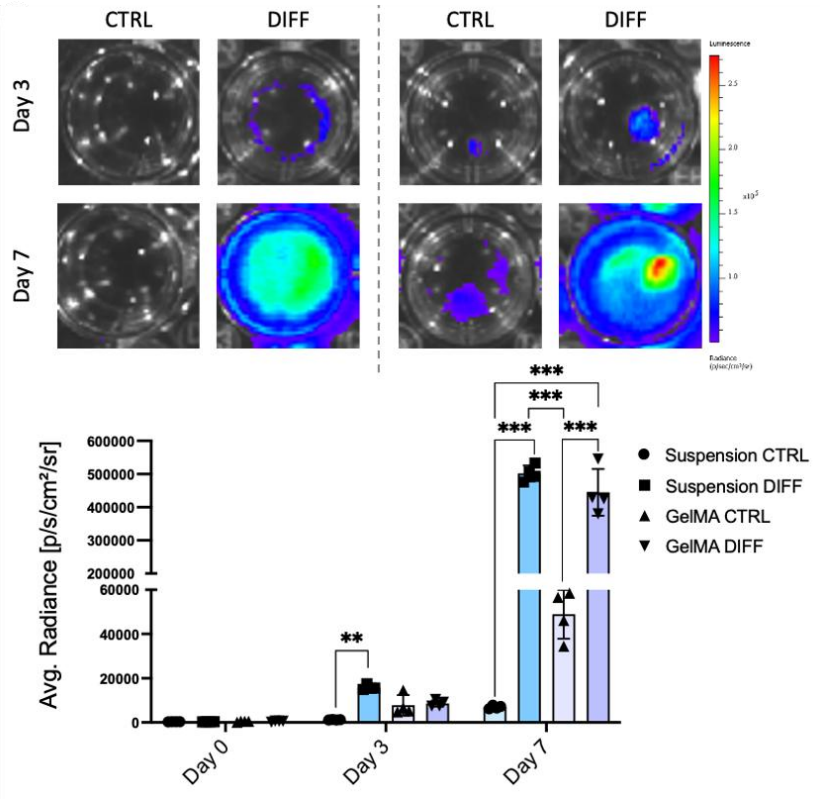


Figure 2-20. Luciferase activity after 3 days of *in vitro* culture in cells cultured in suspension or encapsulated in GelMA gels and maintained in basal (CTRL) or differentiation (DIFF) media. Below is quantification with N = 4. **Denotes significance ($p < 0.01$); ***Denotes significance ($p < 0.001$).

Cell populations cultured in suspension or GelMA were analyzed by flow cytometry to assess the relationship between luciferase expression and HSPC differentiation. The quantity of LSK, GMP, and PMNs were significantly higher in the suspension and GelMA groups cultured in differentiation media in comparison to culture in CTRL media (Figure 2-21).

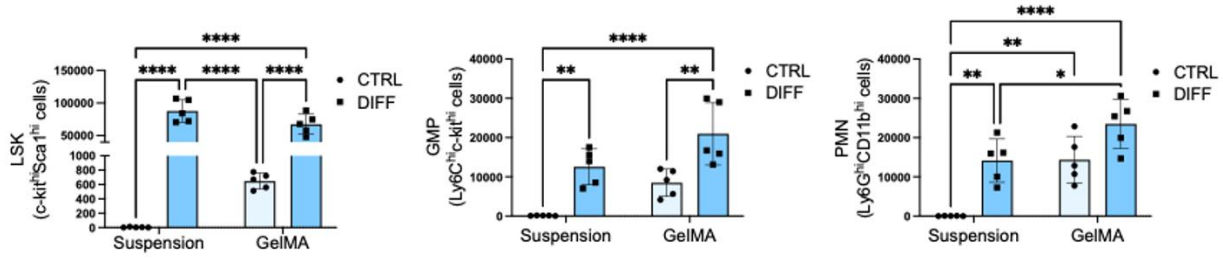


Figure 2-21. Phenotypic characterization of MRP8-FFLUC cell populations cultured in suspension or GelMA in maintenance (CTRL) or differentiation (DIFF) media. Number of LSKs (Sca-1+ckit+), GMPs (Ly6C+ckit+),

and PMNs (Ly6G+CD11b+) after 7 days of *in vitro* culture. N = 5. *Denotes significance ($p < 0.05$); **Denotes significance ($p < 0.01$); ****Denotes significance ($p < 0.0001$).

Consistent with the luciferase activity depicted in (Figure 2-20), we detected a significantly higher expansion efficiency of PMNs in the GelMA group in comparison to the suspension group when cultured in control conditions. We conclude that GelMA hydrogel cultures produce greater numbers of mature PMNs *versus* suspension cultures even when frequency of LSK and GMPs are present at similar numbers.

Finally, we explored the potential of GelMA hydrogels to serve as a synthetic niche for the transplantation of HSPC-derived PMNs *in vivo*. HSPCs isolated from MRP8-FFLUC mice were cultured in either suspension or encapsulated in 5% GelMA for 7 days in differentiation media conditions (Figure 2-22).

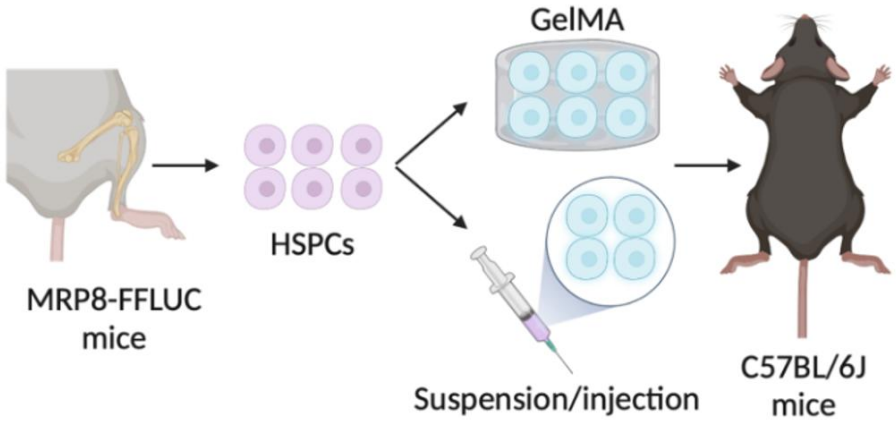


Figure 2-22. Transplantation of neutrophils expanded from MRP8-FFLUC HSPCs cultured in either suspension or GelMA gels into C57BL/6J mice. A schematic of experimental methods.

After confirming a similar level of luciferase activity (e.g., PMN and progenitor numbers) in the suspension and GelMA groups (Figure 2-23), the cells in suspension or cell-laden gels were transplanted into the flank of C57BL/6J mice and luciferase activity was monitored for 5 days.

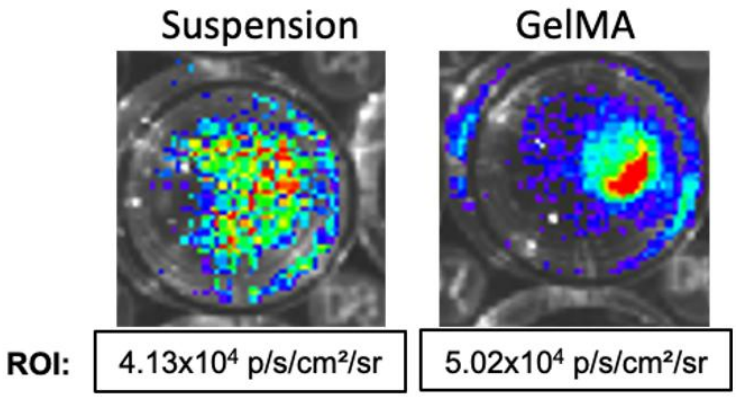


Figure 2-23. Luciferase activity in the suspension and GelMA groups after 7 days of *in vitro* culture.

Cells encapsulated in GelMA were able to survive following 5 days of implantation without loss of PMN phenotype as confirmed by luciferase activity (Figure 2-24).

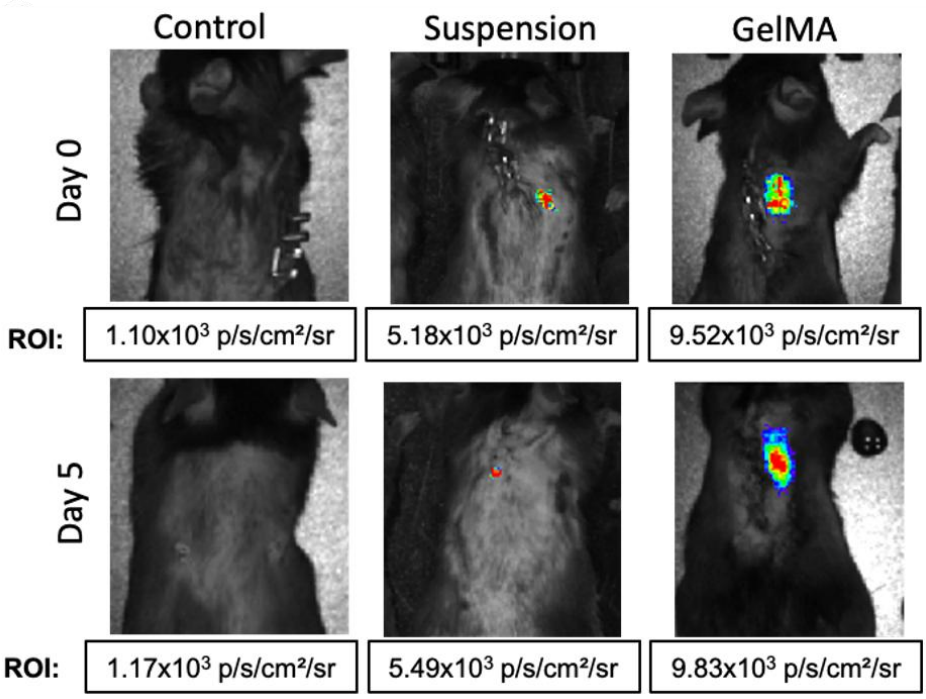


Figure 2-24. Luciferase activity of cells in suspension or GelMA at days 0 and 5 after transplantation into C57BL/6J mice.

Conversely, cells in suspension were less prevalent visually with a 40% reduction in signal detection at 5 days. Neutrophils in the GelMA gels also remained localized to

the implanted area, highlighting the potential of this system to precisely control sites of granulopoiesis after transplantation.

2.4 Discussion

We applied GelMA hydrogels as a 3D synthetic scaffold for encapsulation and maintenance of naïve HSPCs in 3D *in vitro* culture, as well as their ability to undergo granulopoiesis and expand into mature PMNs. Bone marrow-derived HSPCs from LysM-EGFP and MRP8-FFLUC reporter mice provided continuous readouts of the expansion efficiency and maturation of HSPCs into GMPs and PMNs. Encapsulated HSPCs exhibited 100% higher efficiency of LSK retention and granulocyte expansion and provided means to concentrate PMNs that retained the capacity to escape the hydrogel. These PMNs were functional based on their capacity to upregulate CD11b, undergo stimulated ROS production, produce NETs, and phagocytose bacteria. Finally, we demonstrated that this approach allows for *in vivo* implantation of HSPC-loaded gels and detects site-specific granulopoiesis, which is clinically relevant for the local production of PMNs at sites of acute and chronic infection.

Our design criteria were focused on engineering a 3D microenvironment that mimicked the fibrous nature and stiffness of the stem cell niche in the bone marrow. In this work, we chose GelMA as 3D matrix for HSPC cultivation due to its biocompatibility, tunable mechanical properties, the promotion of cell-substrate interactions, and degradability *via* cell-secreted enzymes. Previous reports revealed the storage modulus to be between 0.25 and 24.7 kPa, leading us to generate 5%, 10%, and 20% GelMA constructs with stiffnesses ranging from 0.2 kPa to 10 kPa[44]. The 5% gels, with a Young's modulus of ~ 0.2 kPa, exhibited the highest maintenance of HSPC survival 24 hours post-encapsulation. This stiffness and porosity correlated with increased DNA content, low activity of apoptotic markers, and increased cytoskeletal activity of HSPCs

within the microenvironment. Maintaining the self-renewal properties of naïve LSK populations is crucial for the most efficient generation of GMPs that fuel granulopoiesis. Like previous reports that used 4% GelMA gels for maintenance of LSK phenotype-cells during *in vitro* culture, FACS analysis revealed that ~ 10-20% of cells in gel cultures—one week after encapsulation— retained an LSK phenotype[35]. Confocal images after 7 days of culture also revealed CD117+ cells surrounded by numerous progenitors at various stages of differentiation evidenced by polymorphonuclear cells consistent with granulocyte development and EGFP+ reporter expression. Our goal in using a 3D crosslinked gelatin matrix was to provide a synthetic niche that maintains HSPC self-renewal and increase the quantity of GMPs and PMNs produced per input LSK compared to suspension cultures. Thus, we observed a ~ 20-fold expansion of GMPs in GelMA versus a ~ 15-fold expansion in suspension culture after 3 days, and a one-fold increase in PMNs produced compared to suspension cultures. Previous studies expanding human CD34+ HSPCs in a suspension bioreactor required 7 days to reach a 20-fold expansion of GMPs versus 3 days in our GelMA cultures[49]. These results also confirm previous 3D collagen substrate studies reporting that suspension culture of HSPCs yields fewer differentiated GMPs and PMNs than 3D microenvironments[34].

HSPC differentiation and PMN maturation were visualized using HSPCs harvested from LysM-EGFP reporter mice[36]. These reporter mice were previously used to demonstrate the phenomenon of extramedullary granulopoiesis in *S. aureus* infected wounds where they provide up to 20% of resident PMNs within 3 days[20]. The LysM-EGFP reporter was also useful in FACS studies to quantify HSPC differentiation to GMPs and PMNs. Utilizing this approach, we observed that LSK-seeded hydrogels

showed improved differentiation into GMPs, whereby day 3 gels produced ~ 8 PMNs per seeded HSPC compared to ~ 3 PMNs in suspension cultures. By day 7 of *in vitro* culture, the difference in expansion efficiency between the two groups diminishes compared to cultures on day 3. We believe this is a result of the limitation of nutrient availability and cell-cell contact inhibition that limits the rate of HSPC expansion at later times. The total cell expansion rate in suspension and GelMA conditions remained similar, indicating that the matrix provided a milieu that promoted granulocyte differentiation in response to inflammatory cytokines and growth factors. Extracellular matrices affect transport through the transient interactions of cytokines and growth factors with substrates that can hinder diffusion and advection[50,51]. With this in mind, encapsulated HSPCs and LSK progenitors within GelMA may receive fewer signals from soluble media factors that direct differentiation (paracrine signaling), though also receive increased cell-cell communication directed differentiation (autocrine signaling). Since PMNs secrete collagenases such as MMP14 that facilitates matrix remodeling, we investigated the phenotypic differences in cells that remained within and escaped the gels[52]. After one week of culture, ~ 40% of the total cells escaped the gels, confirming the GMP and PMN capacity to exit the GelMA matrix. LSK cells were predominantly found in the gel phase rather than escaping into the suspension. This observation may reflect the mechanism of PMN extravasation from human bone marrow, which PMNs are continuously recruited into circulation while maintaining HSPC populations. This is further evidenced by the observation of increased F-actin-mediated cytoskeletal activity and adhesion of HSPCs within the 5% GelMA. In future studies, we anticipate that this transport phenomenon could be leveraged to improve PMN

expansion produced in bioreactors where GMPs and PMNs can be continually expelled from GelMA while LSK and early progenitors remain encapsulated in their niche to maintain granulopoiesis. This motivates future work involving bioreactor-based manufacturing of *ex vivo* neutrophils and the generation of mathematical models that can predict the transport of egressed cells leaving 3D matrices for the optimization of the biomanufacturing process. GelMA cultures also generated PMNs expressing higher levels of lysozyme M, an antimicrobial effector molecule responsible for bacterial wall degradation, in EGFP+ cells compared to suspension conditions[53]. This leads us to believe that 3D culture conditions are more suited for greater phenotypic expression of lysozyme markers.

The oxidative burst capacity of neutrophils is a hallmark of the antimicrobial function of mature myeloid immune cells. After 7 days of GelMA culture, isolated CD11b+ cells responded to PMA stimulation of Protein Kinase-C by increasing ROS production to a greater degree than bone marrow cells. GelMA expanded PMNs expressed higher baseline ROS than bone marrow PMNs when unstimulated. This supports the contention that CD11b+ PMNs derived from HSPCs expanded in GelMA both match and exceed the antimicrobial functional capacity of bone marrow-derived PMNs. CD11b is an integrin on the surface of PMNs that mediates the transition from cell arrest to a migratory state capable of extravasation through inflamed endothelium[33,48,54]. A measure of PMN degranulation is the upregulation of CD11b *via* release from granule stores to the plasma membrane within minutes of chemotactic stimulation[48]. EGFP+CD11b+ GelMA PMNs were capable of > 50% upregulation in CD11b expression rapidly after PMA stimulation, whereas suspension cells only

registered a ~ 10% increase. These results suggest that PMNs expanded in cytokine-supplemented suspension cultures have delayed maturation and lack the signaling machinery necessary for chemotactic stimulation, lowering their capacity as function antimicrobial phagocytes.

Mature PMNs in the body generate nuclear extracellular traps (NETs) to ensnare bacteria in the wound environment. All cell cultures were able to generate NETs in response to *P. aeruginosa* stimulation; however, suspension-expanded PMNs demonstrated significantly less NETosis than bone-marrow isolated PMNs. These results further support the inferiority of suspension cultures to GelMA cultures in terms of antimicrobial capacity. Another important antimicrobial function of neutrophils is the ability to clear bacteria from an infected wound through phagocytosis. Here we note that EGFP+ cells phagocytosed fewer *S. aureus*-coated bioparticles than those expanded in suspension. However, both suspension and GelMA cultures on average phagocytosed a significantly greater number of bioparticles than bone marrow cells. This confirms that PMNs expanded in culture with growth factors, cytokines, and Flt3-ligand enriched media at baseline are more mature and capable of antibacterial functions.

Luciferase co-expressed with MRP8 as a mature neutrophil reported allowed us to assess growth dynamics employing IVIS spectral imaging in real-time without disturbing these culture systems. We expected to observe the radiance of these cultures increase with time in supplemented differentiation media. Unexpectedly, HSPCs in GelMA exhibited a strong FFLUC signal in the absence of differentiation factor supplementation, despite the absence of growth factors. This observation supports the hypothesis that GelMA constructs provide a more expansion-conducive 3D

microenvironment that increases the survival of HSPCs *via* paracrine activity. This effect is likely attributed to the optimal physical properties of GelMA that facilitate cell-matrix and homotypic adhesion and remodeling. Because this phenomenon was consistently observed in GelMA and not suspension cultures, we conclude that the 3D growth environment can be optimized to promote HSPC renewal and expansion, implying the importance of the mechanical properties of the matrix that promotes granulopoiesis[35].

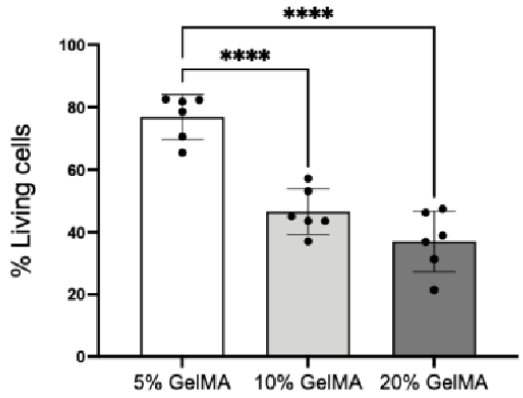
While suspension and GelMA cultures both exhibited comparable average radiance, the luminescence of GelMA cultures exhibited focal areas of PMN expansion, suggesting that granulopoiesis is promoted withing the 3D construct. The limited field of view of confocal imaging limited precise quantification of these areas of high cell density that support greater focal expansion of granulocytes. HSPC differentiation and expansion were confirmed by FACS analysis, revealing greater numbers of GMPs and PMNs produced in the GelMA matrix. The enhanced capacity of MRP8-FFLUC HSPCs to undergo granulopoiesis in GelMA was demonstrated by transplanting them into full-thickness skin wounds of C57BL/6J mice. Suspension cultures quickly dispersed in wounds after implantation whereas gels retained a strong focal bioluminescent signal after 5 days. Earlier we addressed how the expansion of HSPCs in GelMA may be limited in culture over time, unlike suspension cultures. However, for the use of adoptive transfer for local granulocyte expansion, encapsulating cells leads to more overall HSPCs in the wound environment. Previously, we have shown that early PMN expansion is critical for host survival against virulent *S. aureus*[22]. Further studies will focus on the delivery of HSPC-loaded GelMA gels directly to the site of a skin wound or infection in an immunodeficient model that requires PMN expansion for resolution[22].

Despite successes in optimizing PMN expansion withing HSPC GelMA discs demonstrated in this study, several limitations should be noted. The elevated expression of CD11b observed in both suspension and GelMA cultures compared to bone marrow suggests that the media cocktail containing IL-3 and IL-6 may prematurely activate PMNs[55,56]. This may lead to desensitization of PMNs due to premature activation when eventually applied therapeutically[57,58]. Many safety concerns must also be addressed before the implantation of GelMA constructs in the wounds of human patients. Difficulties surrounding successfully deploying this therapy include isolating a patient's own bone marrow cells, the time it takes to naturally degrade this gel *in vivo*, and the effects of delayed inflammation resolution[59–61]. A potential limitation of this system is that PMNs would need time to escape from their gel niche after maturation. However, PMNs are capable of migration in confined 3D spaces. Further, MMP14 expression was upregulated in cells encapsulated in GelMA compared to escaped cells, supporting our hypothesis that PMNs can degrade the gels and exit into the wound space. When we compare GelMA therapy to injecting suspended HSPCs directly into the wound site, cells rapidly diffuse out. Therefore, we believe encapsulation of HSPCs will still lead to more neutrophils effectively in the wound site despite the time needed to escape. PMNs also produce other factors that assist in immune defense, such as NETs, enzymes, and reactive oxygen species that would diffuse out of the gel space into the infection space.

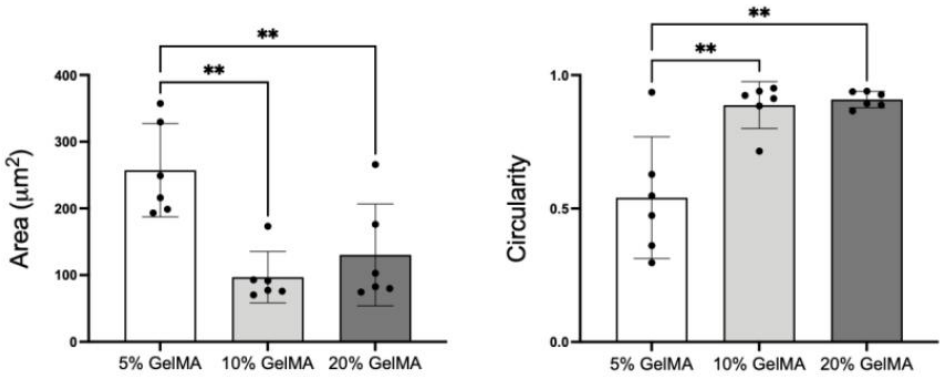
2.5 Conclusion

This study focused on the optimization of a 3D GelMA hydrogel to mimic the bone marrow niche for HSPC encapsulation and enhanced PMN expansion. There is a need to address the challenge of *ex vivo* PMN expansion as a viable means of providing functional PMNs for neutropenic patients who undergo chemotherapy or immunodeficient patients requiring acute innate immunotherapy. By establishing a biomimetic bone marrow environment for HSPCs, we demonstrated the importance of an appropriate 3D microenvironment to support HSPCs differentiation and PMN expansion while retaining phagocyte functionality. Furthermore, our findings elaborate on potential therapeutic applications, such as implanting encapsulated HSPCs at wound sites to boost innate immune function in acute infections in patients with neutropenia. Further work should concentrate on further optimization of the 3D substrate and evaluation of the full therapeutic potential of HSPC-seeded hydrogels in clinically relevant skin infection models such as antibiotic-resistant gram-negative and positive bacteria.

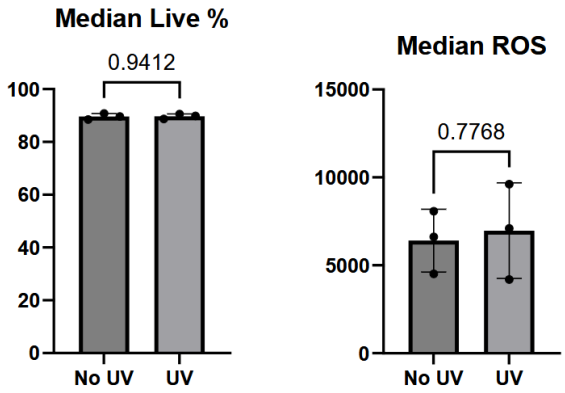
2.6 Supplemental Materials



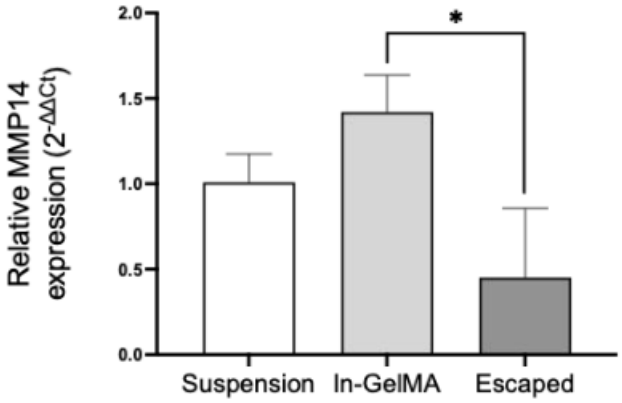
Supplementary Figure 2-1. Percentage of living cells in varying concentrations of GelMA hydrogels 24h after encapsulation



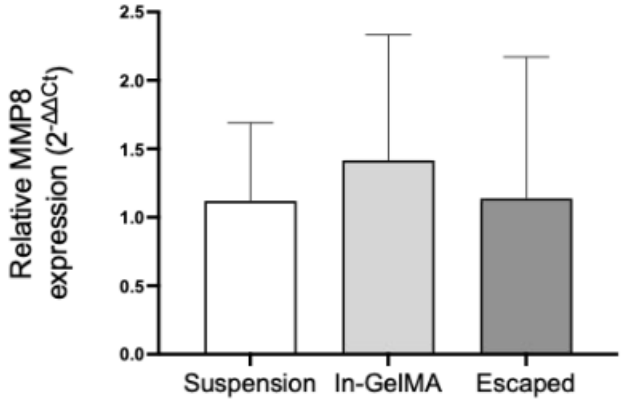
Supplementary Figure 2-2. Image quantification of cell area and circularity of cells in GelMA hydrogels



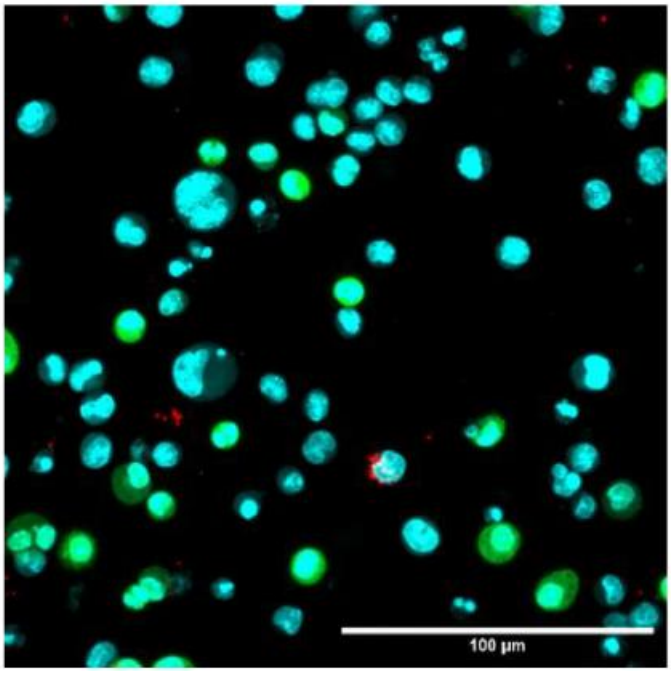
Supplementary Figure 2-3. HSPCs from C57BL/6J mice were isolated and seeded in supplemented media. One group of cells were then exposed to the same dose of UV light GelMA gels were exposed to during crosslinking. After 3 days in culture, the viability of cells was measured *via* flow cytometry using Zombie Yellow Fixable viability dye. Results show no difference in total cell viability between the two groups. After 3 days in culture, ROS was also measured in all live cells using CellROX deep red. Results show no significant difference in cellular oxidative stress. N = 3 for both experiments. P-values shown using student's unpaired t-test.



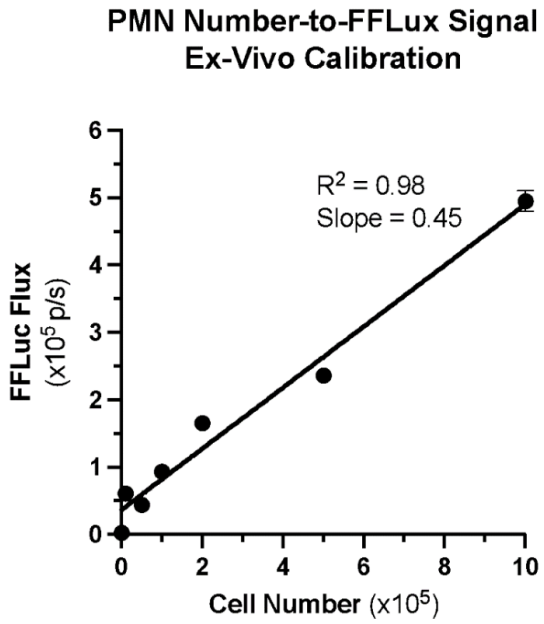
Supplementary Figure 2-4. Analysis of MMP expression and HSPC differentiation before gel escape. Relative gene expression of MMP14 in the HSPCs cultured in suspension, HSPCs in GelMA (in-GelMA0, and cells escaped from GelMA (escaped) following 7 days in culture. N = 3. * Denotes significance ($p < 0.05$).



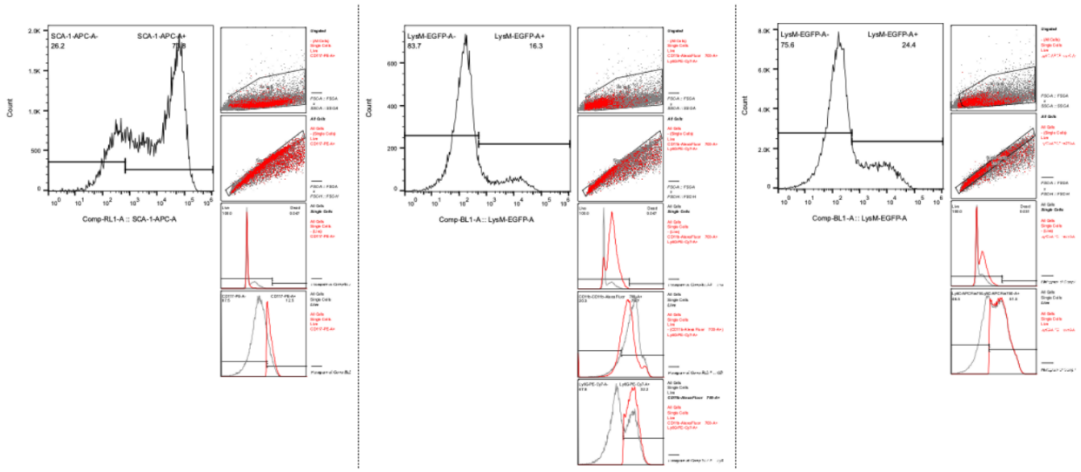
Supplementary Figure 2-5. Analysis of MMP expression and HSPC differentiation before gel escape. Relative gene expression of MMP8 in the HSPCs cultured in suspension, HSPCs in GelMA (in-GelMA0, and cells escaped from GelMA (escaped) following 7 days in culture. N = 3. * Denotes significance ($p < 0.05$).



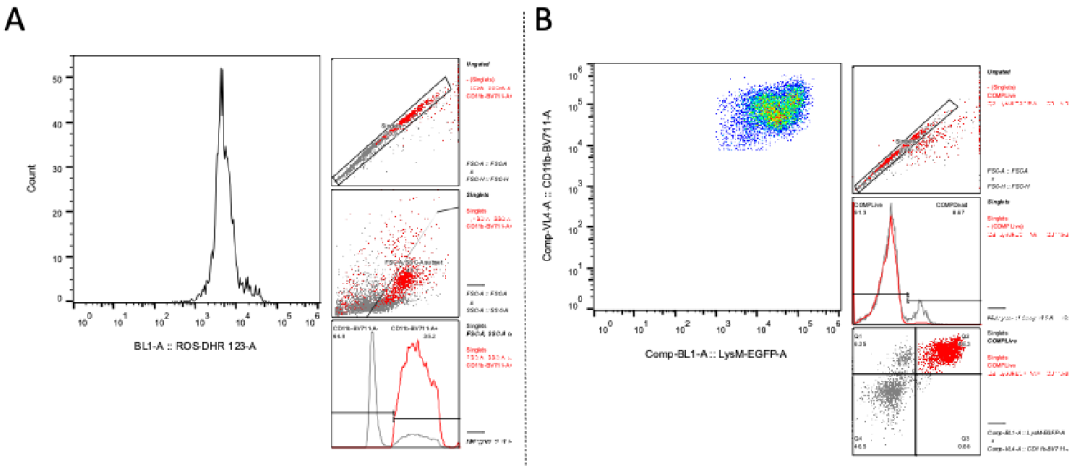
Supplementary Figure 2-6. 60x confocal image of HSPCs and differentiated cells encapsulated in GelMA after 7 days *in vitro*. DAPI (cyan), LysM (green), and CD117 (red).



Supplementary Figure 2-7. Mice expressing a Cre MRP8-EGFP promoter (Tg(S100A8-cre,-EGFP)1Ilw) were cross-bred with mice expressing a ffLuc-Lox reporter (Gt(ROSA)26Sortm1(Luc)Kael/J) to generate mice expressing Firefly luciferase (FFLuc) in granulocytes. Offspring received a subcutaneous dose of 5mg/mL of D-Luciferin and imaged in an IVIS Spectrum to identify mice expressing the FFLuc reporter (FFLuc+). Bone marrow neutrophils (CD11bhi Ly6Ghi confirmed by flow cytometry) were isolated from FFLuc+ mice and a known number of cells were placed in a 96-well plate containing 5mg/mL D-Luciferin. The plate was imaged in an IVIS Spectrum to correlate FFLuc total flux (p/s) with neutrophil number.



Supplementary Figure 2-8. Gating strategy for the phenotypic characterization of cell populations of HSPCs, PMNs, and GMPs. Compensation controls, unstained samples, and live/dead controls were used to gate cell populations.



Supplementary Figure 2-9. Gating strategy for the characterization of ROS activity and CD11b upregulation. Gating was informed from unstained controls or using unstained, Live/Dead, and compensation controls.

3 Chapter 3: An Integrated Microphysiological Model of Human Bone Marrow and Skin

Adapted from: "An Integrated Microphysiological Model of Human Bone Marrow and Skin" by Evan Cirves and Evelyn Zarate-Sanchez et al. submitted to Biofabrication. April 2026.

3.1 Introduction

Microphysiological systems (MPSs) are engineered platforms designed to recapitulate key structural, cellular, and functional features of human organ systems *in vitro*[62,63]. MPSs provide key advantages over traditional models—including both small animal and 2D *in vitro* cell cultures—by recapitulating 3D tissue architecture at high spatial and temporal resolution and thus facilitating real-time observation of cellular dynamics. The past decade of development has included the integration of multiple MPSs capable of mimicking in vivo interactions between organs (e.g., gut-liver[64,65], heart-liver-bone-skin[66], liver-heart[67]). While these multi-organ microphysiological systems (MOMPSs) provide the promise for enhanced understanding of inter-organ interactions, there remains important limitations. A critical challenge is maintaining appropriate relative scaling of organs and systemic circulation within the microfluidic environment. For example, an adult human has approximately 1.5 liters of bone marrow and 5 liters of blood in the systemic circulation. A typical microfluidic compartment housing bone marrow in an MPS is on the order of $1x10^8$ μm^3 [68]. To maintain the appropriate scaling of bone marrow to systemic circulation, this leaves a scant 8 mm of typical microfluidic channel (200 μm x 200 μm) for inter-organ connectivity and re-

circulation. Furthermore, MPSs generally comprise a specific microfluidic design for each organ. This feature adds significant complexity and logistical barriers (e.g., time, expertise) to the creation of MOMPSs which has slowed the adoption by the broader scientific field. Finally, MOMPSs are most easily employed when simulating interactions of two or more organ models via soluble mediators, and thus remain underutilized in immunology where complex, human-specific cellular trafficking is essential. For innate immunity this translates to the trafficking of neutrophils—or polymorphonuclear granulocytes (PMNs)—from the bone marrow to a peripheral site of injury or infection in the skin.

PMNs serve as the first line of innate immune defense against peripheral infections in the skin. These relatively short-lived cells are continuously replenished by differentiating hematopoietic stem and progenitor cells (HSPCs) in the bone marrow which produce on the order of 10^{11} neutrophils daily in healthy adults[7]. During acute or prolonged infection, the bone marrow undergoes an adaptive process—emergency granulopoiesis—which increases not only the number of mature neutrophils in circulation, but also immature neutrophils and CD34+ HSPCs[19].

Here we present a bone marrow microenvironment MPS (BMM-MPS) and a skin microenvironment MPS (SM-MPS) that are created using the same microfluidic device design to model these interactions between bone marrow and skin during infection. Both systems employ a simple, accessible three-chamber polydimethylsiloxane (PDMS) architecture that reduces fabrication and operational complications, and thus technical barriers to simulating multi-organ interactions. The BMM-MPS boasts a simple design that supports long-term granulopoiesis at rates similar to that present in vivo. The

design includes only three cell types in a vascularized niche: endothelial cells, bone marrow stromal cells, and HSPCs. Marrow-derived immune cells egress from the stromal niche into adjacent microfluidic channels to mimic entry into the peripheral circulation. The SM-MPS recreates a vascularized dermal niche using endothelial cells, dermal fibroblasts, and keratinocytes. Its design enables real-time visualization of neutrophil trafficking, retention, and inflammatory responses within the dermis.

To greatly simplify the integration of these MPSs, we collected cells egressing from the BMM-MPS and introduced them at physiological concentrations and fluid shear rate into an inflamed vascular channel of the SM-MPS. While the integration step involves manual transfer, it circumvents the difficult scaling requirements of skin, bone marrow, and the systemic circulation, while recapitulating inflammatory mobilization of marrow-derived cells and targeted homing to infected skin. Importantly, we observe endothelial attachment, diapedesis, phagocytosis, and early differentiation of hematopoietic progenitors within the dermal microenvironment. These findings support the feasibility of establishing an innate human immune response in vitro and a broadly accessible MOMPS framework for studying inter-organ immune cell crosstalk.

3.2 Materials & Methods

MPS device design and modeling: The microfluidic device used in both the BMM-MPS and SM-MPS consists of three parallel channels divided by 16 trapezoidal posts per side with 30 μm gaps between each post. This simulates the capillary burst valve and allows the loading of fibrin hydrogels without leaking into adjacent chambers[69]. The pores allow diffusion of signaling molecules and migration of cells between each chamber. Each chamber is approximately 4 mm long and 100 μm high in the z-direction. The central channel is 350 μm wide and the side channels are 250 μm wide. Different volumes of media were added to the inlet and outlet of a single channel to simulate convective flow across a single channel. Different volumes added to the top and bottom channels of the BMM-MPS created a hydrostatic pressure differential between the top and bottom channels driving interstitial flow.

MPS device preparation: A master mold of the device made of SU-8 on a silicon wafer was prepared using standard soft lithography methods[70]. A 100 μm layer of SU-8 3050 was spun onto a silicon wafer. Then the microfluidic design was patterned onto the wafer during a single mask lithography step. The mold was then silanized. Curing agent (Dow Corning, GMID# 02065622) was mixed with Polydimethylsiloxane (PDMS) in a 1:10 ratio, poured onto the mold, degassed, and allowed to bake overnight at 60°C. The cured PDMS was removed from the mold and had fluidic lines added by puncturing with either a 16- or 18-gauge syringe. The punctured devices were plasma bonded to either a glass coverslip (Thermo Fisher) or glass slide (Thermo Fisher). Devices were exposed to ultraviolet light for 30 minutes to ensure sterility before loading.

In vitro cell culture: Endothelial colony-forming endothelial cells (ECs) were isolated from cord blood as previously described by our group[70] and others[71]. All cord blood samples were collected in accordance with the University of California Institutional Review Board regulations. Briefly, all cells were cultured in tissue-treated culture flasks; ECs were specifically cultured on flasks additionally treated with 1% gelatin. All cells were cultured according to vendor protocols using appropriate culturing media at 37 °C and 5% CO_2. Other cells used were Bone Marrow Stromal Cells (BMSCs, Lonza, Cat# 2M-302), Normal Human Adult Epidermal Keratinocytes (NHEKs, Lonza, Cat# 00192627), and Normal Human Dermal Fibroblasts (NHDFs, Lonza, Cat# CC-2511). ECs were cultured in EGM-2 (Lonza, Cat# CC-3162). BMSCs were cultured in Mem α (Nucleosides, Cat# 12571063) with 10% heat-inactivated Fetal Bovine Serum (FBS, Gibco, Cat# 10082147) and Penicillin-Streptomycin (100 U/mL, Gibco, Cat# 15140122). NHEKs were cultured in KGM-Gold (Lonza, Cat# 00192060). NHDFs were cultured in FGM-2 (Lonza, Cat# CC-3132).

BMM-MPS Model: BMSCs and ECs were expanded to passages 3 and 5, respectively, before use. Cells were thawed and cultured for 10 days and 7 days, respectively, prior to loading into the BMM-MPS. CD34+ HSPCs were split into aliquots of $5x10^4$ cells/mL upon arrival to be thawed and used when other cells were lifted. BMSCs ($1x10^7$ cells/mL), ECs ($1x10^7$ cells/mL) and HSPCs ($1x10^6$ cells/mL) were mixed in a fibrin gel comprising 10 mg/mL fibrinogen from bovine plasma (Thermo Fisher, Cat# F8630-5G) and 5 U/mL thrombin (Sigma-Aldrich, Cat#9002-04-4) and injected into the central chamber of the device, and was allowed to gel for 10 minutes at 37 °C and 5% CO_2. The flanking channels were coated in 0.2% gelatin and perfused

with Granulopoietic Expansion Media (GEM). Devices were perfused with media as follows: 200 µL top inlet, 20 µL bottom inlet, and 0 µL outlets. Volumetric volumes were alternated daily for 7 days to create a vessel network. Afterwards, media was replenished every two days without alternating. Devices were incubated at 37°C, 5% CO_2 for 28 days.

The Granulopoietic Expansion Media (GEM) consists of a 1:1 ratio of EGM-2 and StemSpan™ SFEM II (STEMCELL, Cat# 09655) with the following added supplements: Interleukin 3 (IL-3, 10 ng/mL, Peprotech, Cat# 200-03-10UG), Interleukin 6 (IL-6, 10 ng/mL, Peprotech, Cat# 200-06-20UG), FMS-like tyrosine kinase 3 (Flt-3, 10 ng/mL, Peprotech, Cat# 300-19-10UG), and Stem Cell Factor (SCF, 100 ng/mL, Peprotech, Cat# 300-07-10UG).

SM-MPS Model: ECs, NHEKs, and NHDFs were expanded to passages 5, 4, and 6, respectively, before use. Cells were thawed and cultured for 5 days prior to lifting with Accutase™ and loading into the SM-MPS. NHDFs were resuspended at $1x10^7$ cells/mL before being loaded into the central channel comprising 10 mg/mL fibrinogen from bovine plasma (Thermo Fisher) and 5 U/mL thrombin. Devices were incubated for 30 minutes at 37°C, 5% CO_2 to allow the hydrogel to solidify. NHEKs and ECs were resuspended at approximately $1x10^7$ cells/mL before perfusing into opposite channels flanking the center channel and allowed to attach to the bottom of the device. After 2 hours, devices were perfused with DPBS to wash out any unbound cells. Media reservoirs were aspirated and device media was added as such: 150 µL and 100 µL of KGM-Gold were added to the epidermal channel inlets and outlets, respectively; 250 µL of EGM-2 was added to the inlet of the vascular channel. This allows convective flow

across the inside of both the epidermal and vascular channels, with higher wall shear-stress in the vascular channel. Because the total volume of both the epidermal and vascular channels is equivalent, there is no interstitial flow across the dermal compartment, and fluid exchange only occurs by diffusion.

BMM-MPS egress cell collection: Cells were harvested from the BMM-MPS by manual aspiration of the media from both the top and bottom outlets. For phagocytosis assays, neutrophils were isolated via negative selection using the EasySep™ Direct Human Neutrophil Isolation Kit (STEMCELL Technologies, Vancouver, BC, Canada; Cat #19666) according to the manufacturer's instructions.

Confocal imaging and immunohistochemistry assays: Devices were fixed in 4% paraformaldehyde (PFA, BOSTER, SKU# AR1068) for 2 hours and blocked overnight with 2% bovine serum albumin (BSA, Thermo Fisher) in DPBS. Antibodies in 0.1% BSA were delivered through the fluidic lines and devices were labeled overnight. Devices stained for Keratin 5 were permeabilized with Triton X-100. Nuclei were counterstained with DAPI at a final concentration of 5 μg/mL. Fluorescent and time-lapse images were acquired with a FV3000 Confocal microscope (Olympus). Multi-Area-Time-Lapse (MATL) acquisition was used so the entire length of the MPS could be imaged simultaneously. Image post-processing was done in Fiji/ImageJ. Image stitching was done in FV310.

For vessel network and endothelial junction labeling, devices were labeled with anti-CD31 APC antibody (1:100, Biolegend, Cat# 303116, Lot# B271124). Cells egressed from the BMM-MPS were images on coverslips using a 60x oil-immersion objective. For determining the distribution of ECs, NHDFs, and NHEKs in the SM-MPS,

ECs were labeled with CellTracker™ Green, NHDFs were labeled with CellTracker™ Orange, and NHEKs were labeled with CellTracker™ Far Red. For Keratin 5 labeling of the SM-MPS, devices were labeled with anti-cytokeratin 5 PE antibody (1:100, Abcam, Cat# ab224985, lot# GR3455185-1). For integrin labeling of the SM-MPS, devices were labeled either with anti-CD54 (ICAM-1) BD Horizon Brilliant™ Blue 515 antibody (1:100, Cat# 564685, Lot# 3130986) or anti-CD106 (VCAM-1) Alexa Fluor 594 antibody (1:100, Biolegend, Cat# 305812, Lot# B236197); quantification was performed using established methods[72]. For labeling differentiated immune cells in the SM-MPS, devices were labeled with anti-CD16 FITC antibody (1:100, Biolegend, Cat# 980112, Lot# B420425).

Permeability assays: Permeability of both models was performed using previously cited methods[68]. Briefly, for the BMM-MPS, 70 kDa FITC-dextran (5 μg/mL, Sigma-Aldrich, Cat# 53471-1G) was perfused into the top channel on day 7 post-device-seeding. Diffusion of dextran was recorded using Olympus FV3000 (5 min, 30FPS). Permeability (*P*) was quantified by defining a vessel Region of Interest (ROI) using the following relationship:

$$P = \left(\frac{dI_{sink}}{dt}\right) * \frac{1}{I_{max}} * \frac{A_{sink}}{2} * \frac{L}{SA} \quad (4)$$

where dI_{sink}/dt is the rate of change in background fluorescence intensity over time, I_{max} is the maximum mean intensity of the vessel, A_{sink} is the area of the background region, *L* is the vessel length, and *SA* is the vessel surface area. For non-uniform segments, *L* and vessel diameter were averaged from multiple linear measurements.

For the SM-MPS, permeability was measured across either the endothelial channel or keratinocyte channel using the same relationship and imaging settings

above for devices 3 days post-seeding. Four ROIs were chosen per device in Fiji/ImageJ by selecting a rectangle in the central channel directly inside where the outer channel and central channel come into contact between the PDMS device posts. For these internal ROIs the dI_{sink}/dt is the rate of change in measured fluorescence intensity over time, A_{sink} is the area of the ROI, L is the height of the MPS (100 μm), and SA is the contact surface area between the outer channel and the central channel (100 μm x 30 μm). I_{max} is the maximum mean intensity of FITC-Dextran in the outer channel.

Flow Cytometry: BMM-MPS egress cells (days 9-23) were collected every two days during that period by aspiration of the media from both the top and bottom outlet and fixed using 4% PFA and resuspended in cell staining buffer (Biolegend, Cat# 420201). Cells were stained for 1h with anti-CD38 PE antibody (1:1000, Biolegend, Cat# 303505), anti-CD34 BV421 (1:1000, Biolegend, Cat#343610), anti-CD16 PC7 (1:1000, Biolegend, Cat#360708), anti-CD45RA PerCP (1:1000, Biolegend, Cat#304155) and anti-CD66b AF700 (1:1000, Biolegend, Cat#305114). Cells were washed and analyzed using a Beckman Cytoflex 13-color detector flow cytometer (Beckman Coulter, Cat# B75408). Compensation controls, unstained samples, and fluorescence-minus-one controls were used to gate cell populations. OneComp eBeads™ Compensation Beads (ThermoFisher, Cat#01-1111-42) were used for compensation beads. Data analysis was performed using FlowJo software.

Phagocytosis Assay: Both blood-isolated PMNs and BMM-MPS egress cells were plated at matched densities in 96-well plates (N = 3). Samples were labeled with pHrodo™ Red Zymosan Bioparticles™ (Thermo Fisher, Cat# P35364). The assay was followed using manufacturer's instructions and imaged via confocal. Images were

analyzed in Fiji/ImageJ using automated segmentation workflows with fixed parameters across datasets to ensure reproducibility. Briefly, channels were separated to distinguish total cells from those containing zymosan, thresholded to remove background noise, and converted to binary masks. Total neutrophils were quantified using a lower particle size threshold (10 microns), whereas phagocytosis-positive cells were identified using a higher threshold (25 microns) to identify cells internalizing zymosan particles.

Artificial bacterial stimulation of the SM-MPS: To stimulate an artificial infection in the SM-MPS, a combination of factors was used to accomplish this: Pam_3CSK_4 (10 μg/mL), TNF-α (10 ng/mL), IL-1β (10 ng/mL), and IFN-γ (100 ng/mL). Pam_3CSK_4 (Invivogen, Cat# vac-pms) is a synthetic triacylated lipopeptide mimicking the lipopeptides of the bacterial wall by acting on TLR2 receptors[73]. In conjunction with IFN-γ (interferon gamma, Peprotech, Cat# 300-02-100UG), Pam_3CSK_4 acts to augment inflammatory responses from IFN-γ in endothelial cells[74]. Previous work also has been cited to show TNF-α (tumor necrosis factor alpha, Peprotech, Cat# 300-01A-50UG) and IL-1β (interleukin 1 beta, Peprotech, Cat# 200-01B-10UG) together are potent activators of endothelium[75]. EGM-2 was supplemented with these factors and added to SM-MPS devices 4 hours prior to measuring surface integrin expression or capture of immune cells. The combination is noted as Pγαβ for brevity.

RT-qPCR: ECs, NHDFs, and NHEKs were cultured in 96 well plates with appropriate culturing media—with or without supplemental inflammatory factors—and lifted after 24 hours. HSPCs were thawed from frozen and cultured in 48 well plates in granulopoietic expansion media for 24 hours before recovering. Cells were then processed using a Total RNA Purification Kit (STEMCELL Cat# 79004) using

manufacturer instructions. Purified mRNA was then reverse-transcribed with the High-Capacity cDNA Reverse Transcription Kit (Thermo Fisher, Cat# 4368814) and RiboLock RNase Inhibitor (Thermo Fisher, Cat# EO0381) in the SimpliAmp Thermal Cycler (Thermo Fisher) according to manufacturer instructions. RT-qPCR was performed on a QuantStudio 5 system (Applied Biosystems). Primers for ACTB (NM_001101), IL6 (NM_000600), IL8 (NM_000584), IL1B (NM_000576), and CEBPA (NM_004364) were purchased from IDT. Critical threshold values (C_t) were quantified for each gene. The ΔCt was quantified by subtracting the samples' C_t value of the housekeeping gene ACTB. The $\Delta\Delta C_t$ was quantified by subtracting the average ΔC_t of the control group. The relative expression values for each gene of interest are presented as $2^{-\Delta\Delta Ct}$.

Immune cell isolation and capture assay: Peripheral blood—from healthy, adult volunteers—was collected by venipuncture using sodium-heparin collection tubes (BD Vacutainer 10 ml, Cat# 367874) in agreement with an approved University of California, Davis Institutional Review Board protocol (#1541024-1). Neutrophils (and BMM-MPS egressed cells where applicable) were isolated using immunomagnetic separation via EasySep™ Direct Human Neutrophil Isolation Kit (STEMCELL, Cat # 19666) and resuspended in EGM-2.

2D and 3D Renderings: All 2D renderings were made in Biorender™. 3D renderings were made in Blender 5.0 and subsequently hand-processed in the Procreate app on an iPad Air (5th gen).

Statistical Analysis: Data are presented as means ± standard deviation. Statistical analysis was done using one-way ANOVA with post-hoc Tukey test, two-way ANOVA with Tukey's multiple comparisons test, or unpaired t-test when necessary. For data

following a non-normal distribution, Kruskal–Wallis test was used. $p < 0.05$ was considered significant. Statistical significance was indicated in each graph as $*p < 0.05$, $**p < 0.01$, $***p < 0.001$, and $****p < 0.0001$.

3.3 Results

3.3.1 Single Multi-Organ MPS Platform

PMNs are produced in the bone marrow and subsequently enter the systemic circulation to form a central part of the innate immune response (Figure 3-1).

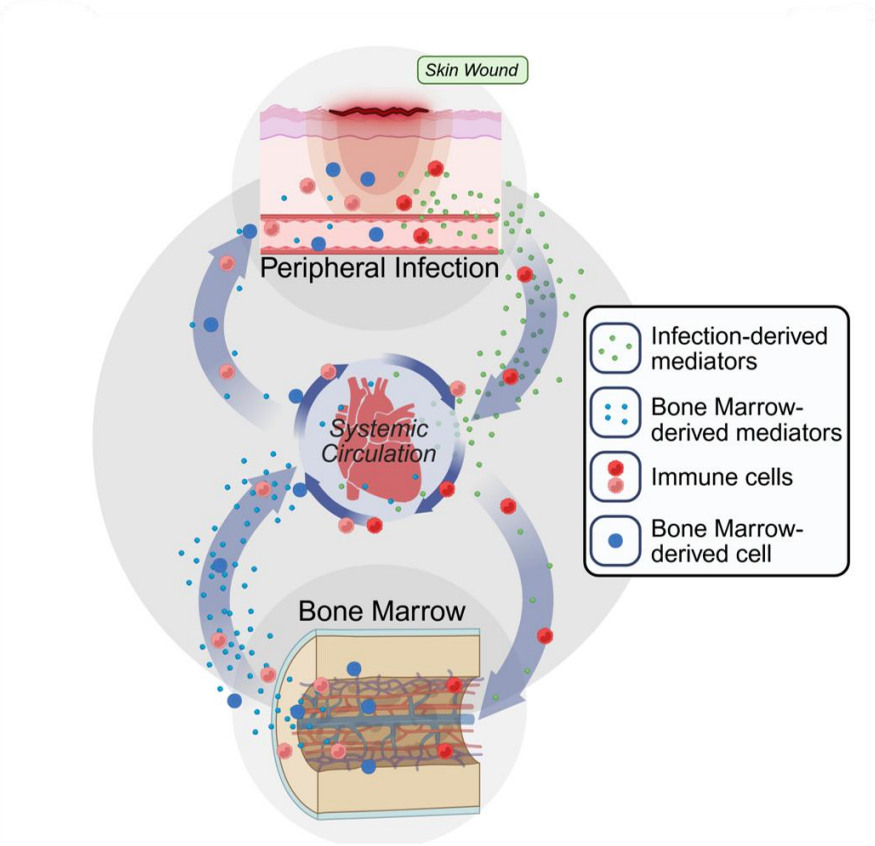


Figure 3-1. Immune cells produced in the bone marrow egress upon maturation into the systemic circulation. Sensing an inflamed skin environment, immune cells exit circulation toward infected tissue to combat the infection. Occasionally, immune cells traffic out of the skin and back to the bone marrow.

Inflammation caused by injury or infection alters the expression of adhesion molecules on the endothelium. The expression of adhesion molecules regulates PMN rolling, attachment, polarization, and extravasation from the circulation into the inflamed tissue. PMNs then attempt to resolve the infection by phagocytosing foreign particulate and generating local reactive oxygen species (ROS) among other antibacterial

functions[76]. In severe cases of peripheral infection or sepsis, a portion of PMNs can return to the bone marrow niche and stimulate emergency granulopoiesis, resulting in an increased quantity of bone marrow-derived cell production and egress[77].

We simulated this immune circuit by developing a simple model of both the bone marrow microenvironment (BMM-MPS) and the skin microenvironment (SM-MPS) using the same microfluidic device for both MPSs. This approach reduces both time and resources needed during the design and experimental phases of the project. The design of the single PDMS-based device includes three parallel microfluidic channels separated by (approximately 30 μm in width) pores that enable communication between the channels and therefore cells *via* diffusion and convection of soluble mediators. The device is created using standard soft lithography (Figure 3-2).

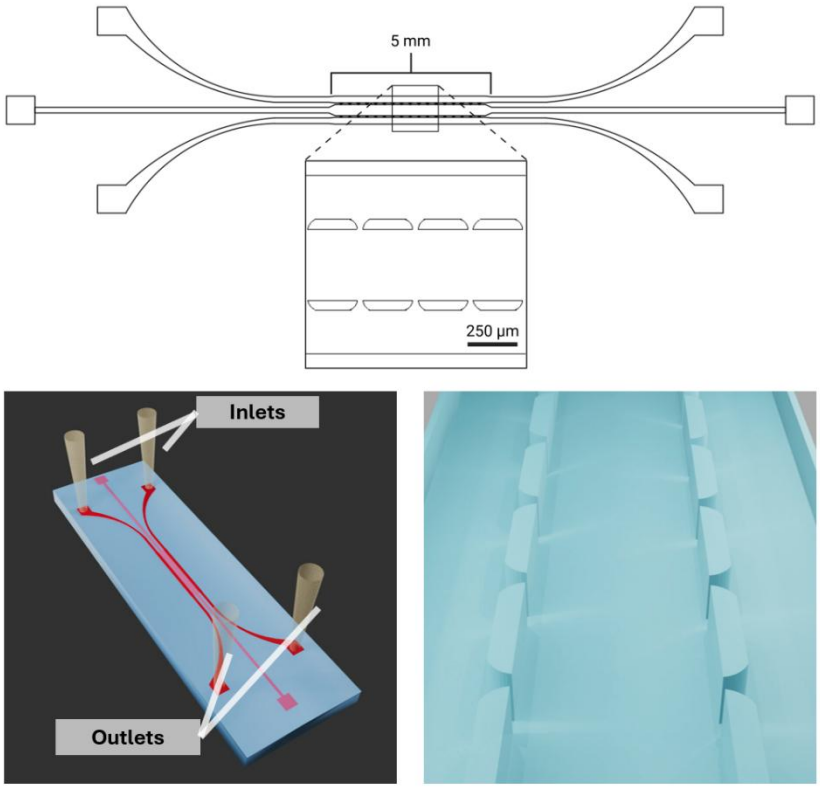


Figure 3-2. (top) 2D CAD design of the multi-organ microfluidic device. Higher magnification sub-image shows 30 μm pores between posts, allowing diffusion of dissolved factors between parallel channels.

(Bottom Left) 3D-rendered external view of device. Cells within a hydrogel are loaded into the central channel (pink), and media is perfused through the outer microfluidic lines (red) using hydrostatic pressure. (Bottom Right) An internal 3D-rendered view of the device.

Media reservoirs made by standard pipette tips allow soluble mediators and/or cells to be delivered to the outer channels. A hydrostatic pressure difference between the outer lines generates interstitial flow through the pores and across the central channel (see Methods).

3.3.2 Bone Marrow Microenvironment MPS

The BMM-MPS features a single niche consistent with models of the perivascular niche[68]. The central chamber in the BMM-MPS is seeded with cord blood-derived endothelial cells (ECs,1×10^7 cells/mL)[78], bone marrow stromal cells (BMSCs, 1×10^7 cells/mL), and CD34+ hematopoietic stem/progenitor cells (HSPCs, 1×10^6 cells/mL) encapsulated in fibrin (10 mg/mL). This approach is similar to the perivascular niche in our previous report[68]. The tissue microenvironment is fed with granulopoietic expansion media (see methods) in the outer channel under a hydrostatic pressure that creates physiological interstitial flow (~1 μm/s) through the central chamber (Figure 3-3).

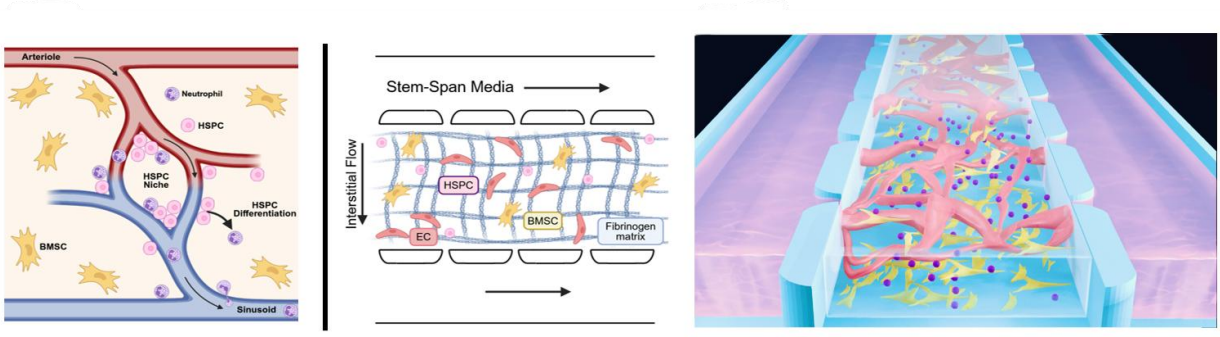


Figure 3-3. (left) A schematic of the bone marrow microenvironment in which hematopoietic stem and progenitor cells (HSPCs), supported by BMSCs and endothelial cells, produce neutrophils that egress from the bone marrow niche and enter the adjacent microfluidic line simulating the systemic circulation. (middle) The bone marrow microenvironment-MPS (BMM-MPS). (right) 3D-render of BMM-MPS with a complete, perfusable microcapillary network, bone marrow stomal cells (yellow), and HSPCs (purple) approximately five days after loading.

The cells self-assemble to create a perfusable vascular network within the first seven days (Figure 3-4).

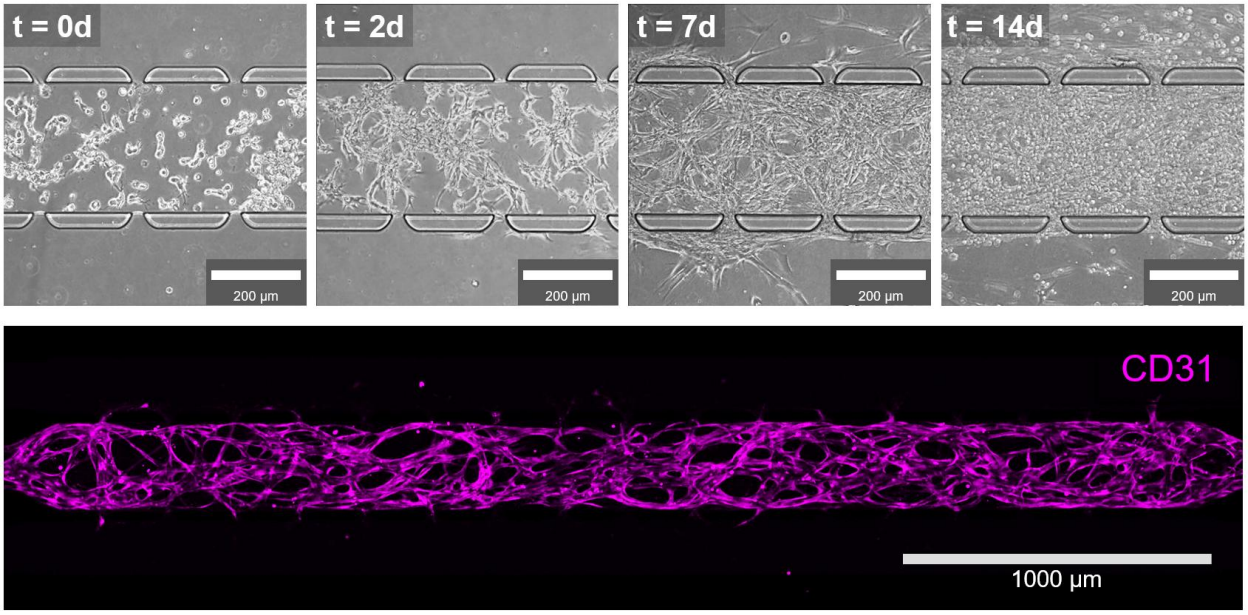


Figure 3-4. (top) Central chamber of the MPS is seeded with ECs, BMSCs and CD34+ HSPCs. Cells self-assemble to create a vascular network. (bottom) Image of endothelial cell network, labeled with anti-CD31 (magenta), in BMM-MPS 7 days post-loading of devices.

Beginning approximately 9 days post-loading, cells begin to emerge (egress) from the central niche and enter the adjacent microfluidic lines. These cells are collected between 15-23 days post-loading for further analysis. The egressed cells comprise PMNs at different stages of maturation: myelocyte, metamyelocytes, banded and mature PMNs as evidenced by nuclear DAPI staining (Figure 3-5 & **Error! Reference source not found.**).

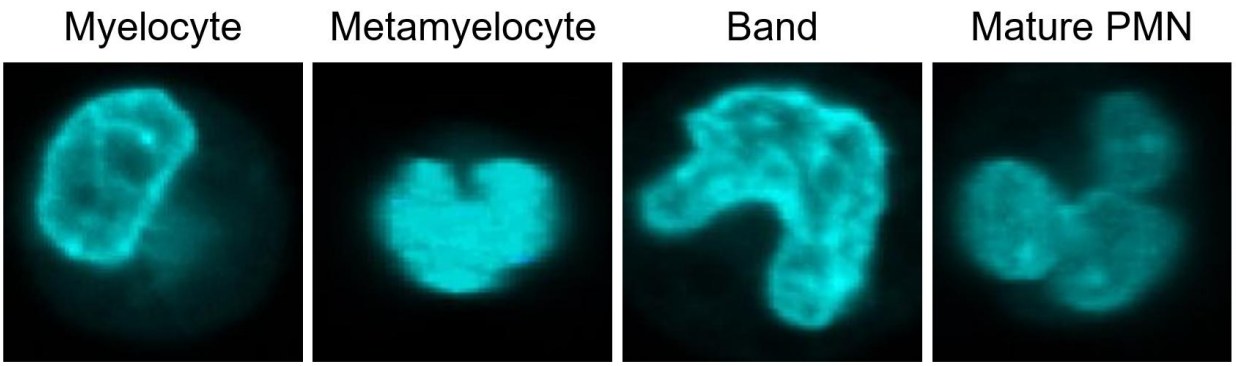


Figure 3-5. Nuclear staining of egressed cells using DAPI (cyan).

Permeability of the vessel network to 70 kDa FITC-Dextran was 8.7 ± 3.3 x 10^{-6} cm/s with no difference between consecutive devices (Figure 3-6)[79,80].

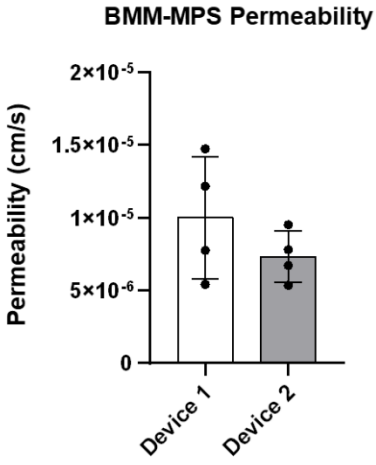


Figure 3-6. Permeability of 70 kDa FITC-Dextran through vasculature within the BMM-MPS. “ns” denotes a p-value of > 0.05.

Flow cytometry analysis of pooled egressed cells (N = 9 devices) demonstrates that approximately 9-16% of cells are HSPC-like (CD34+CD45RA-), 4-5% of cells are GMP-like (CD34+CD38-CD45RA+), and 8-27% of cells are consistent with mature PMNs (CD34-CD66b+) (Figure 3-7).

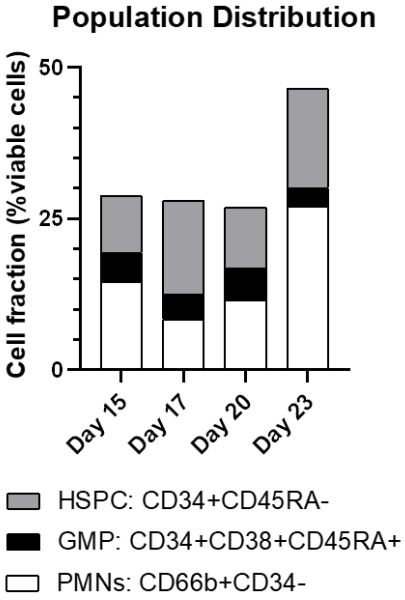


Figure 3-7. Flow cytometry analysis of the population distribution of Hematopoietic Stem and Progenitor Cells (HSPCs), Granulocyte-Monocyte Progenitors (GMPs), and PMNs of cells egressing from a pool of 9 BMM-MPS chips collected every 2-3 days.

Further quantification of cell egress demonstrated that approximately 3.0 cells were generated per HSPC per day (or 1 x 10^9 cells per liter per day) (Fig. 2F).

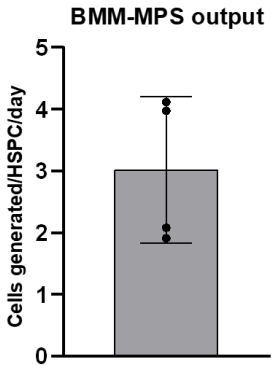


Figure 3-8. The average total number of cells exiting the BMM-MPS every day over 11 days.

Cells produced by the BMM-MPS were assessed for their ability to undergo phagocytosis. Cells were pooled from BMM-MPS devices over a 3-day period for 9 devices. These cells were then negatively selected for mature neutrophils using the EasySep™ Direct Human Neutrophil Isolation Kit (STEMCELL). Cells from the BMM-

MPS phagocytosed pHrodo™ Red Zymosan Bioparticles™ (ThermoFisher) as effectively as whole blood neutrophil controls (Figure 3-9 & Supplementary Figure 3-2).

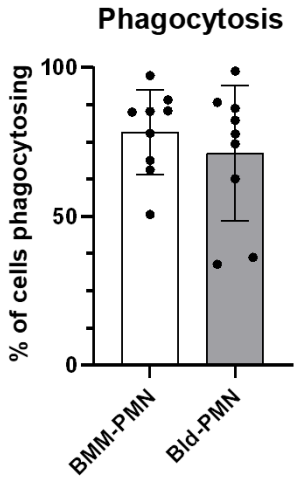


Figure 3-9. Percentage of cells undergoing phagocytosis of Zymosan Bioparticles™ (ThermoFisher) from neutrophils negatively selected from either the BMM-MPS egressing cells (BMM-PMN) or from adult whole blood (Bld-PMN). A total of 9 observations were collected (N = 3 well-plates × 3 ROIs per plate).

3.3.3 Skin Microenvironment MPS

The SM-MPS uses the same microfluidic device design as the BMM-MPS. The SM-MPS incorporates primary adult dermal fibroblasts (1 x 10^7 cells/mL) in a 10 mg/ml fibrin matrix in the central chamber. To simulate the vascular compartment, cord blood-derived ECs are seeded to form a confluent monolayer. This model simplifies the visualization and quantification of cell attachment and extravasation. To model the epidermis, the top chamber is seeded with a monolayer of normal human epidermal keratinocytes (Figure 3-10).

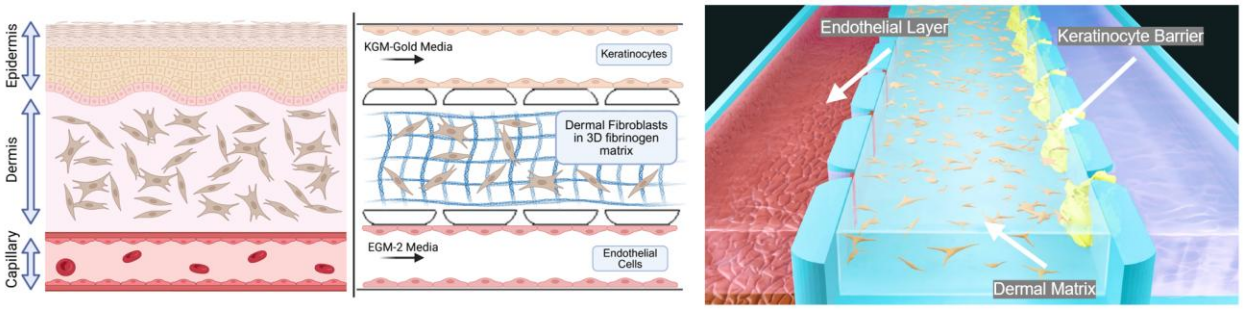


Figure 3-10. (left) A schematic of the skin microenvironment-MPS (SM-MPS) including keratinocytes, dermal fibroblasts, and supporting microcirculation. (middle) The skin microenvironment-MPS (SM-MPS). (right) 3D-render of SM-MPS with a complete, perfusable endothelial vessel (left), dermal fibroblasts in fibrin, and keratinocytes (yellow) forming a barrier between the middle and right channel.

Though initially seeded evenly throughout the top channel, the keratinocytes—over 72 hours—migrate slowly and penetrate through the microfluidic pores into the dermal compartment, providing a tight barrier that isolates the dermal compartment from the outer microfluidic line (Figure 3-11).

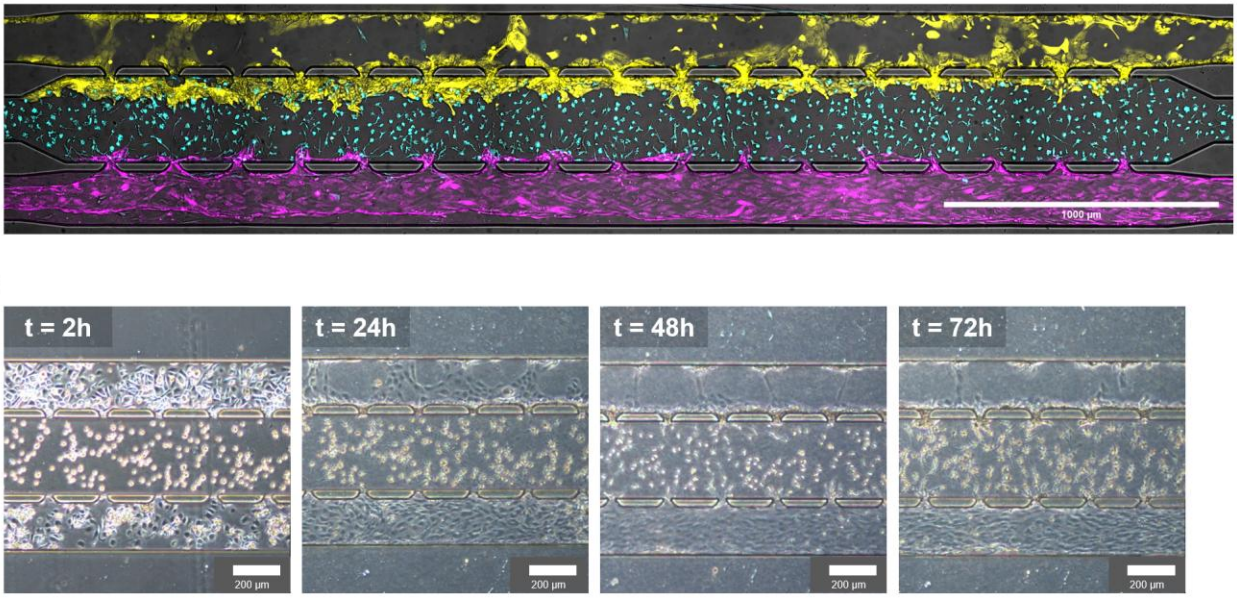


Figure 3-11. (top) The full-length of the SM-MPS three days post-loading showing keratinocytes (yellow), dermal fibroblasts (cyan), and ECs (magenta), all labeled with separate CellTracker™ dyes. (bottom) SM cells are loaded into the MPS and cultured over 72 hours before used.

Immunohistochemical labeling shows all keratinocytes are Keratin 5 positive, consistent with the basal layer of epidermis (Figure 3-12). An air-liquid interface is not

employed for this model as our interest focuses on the immune contributions from the basal keratinocytes adjacent to the dermis.

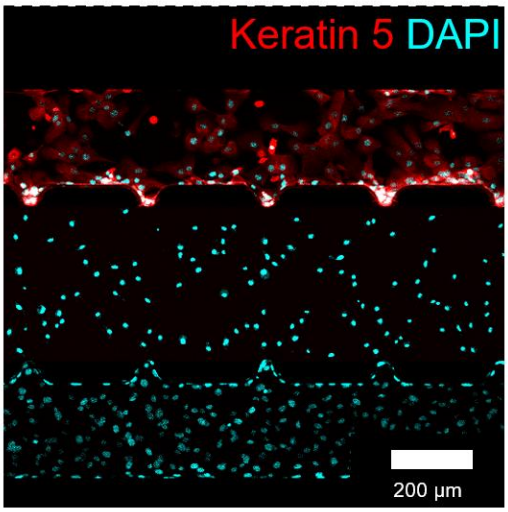


Figure 3-12. SM-MPS labeled with anti-Keratin 5 (red) and DAPI nuclear stain (cyan).

Additionally, the dermal fibroblasts remain well-confined to the dermal compartment, showing podia protrusions and matrix reorganization, but little to no migration or cell proliferation outside the fibrin matrix. ECs form a confluent monolayer throughout the vascular channel as evidenced by anti-CD31 labeling of tight junctions (Fig. 3D), and z-stack confocal imaging 3 days post-seeding showing ECs along the sides, top, and bottom of the vascular compartment.

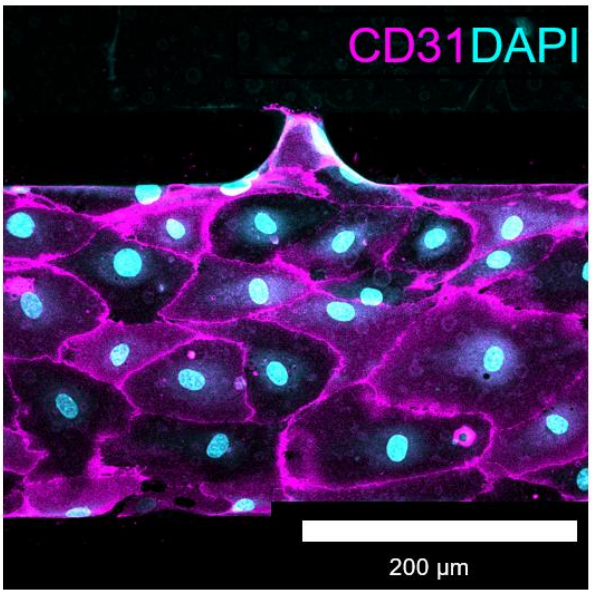


Figure 3-13. High resolution image of the EC channel labeled with anti-CD31 (magenta) and DAPI nuclear stain (cyan).

Both the endothelial and keratinocyte channels were perfused with 70kDa FITC-Dextran to analyze barrier permeability. The keratinocyte layer was nearly impermeable ($10 \pm 5.3 \times 10^{-8}$ cm/s) whereas the permeability of the EC layer was approximately an order of magnitude higher ($2.3 \pm 1.1 \times 10^{-6}$ cm/s), consistent with previously reported values for in vitro endothelial permeability (Figure 3-14)[68,75,81].

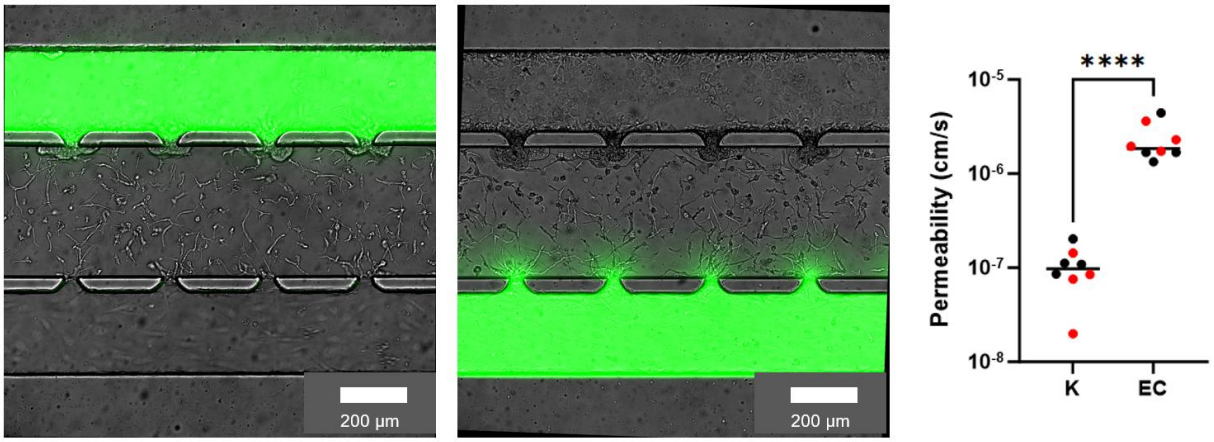


Figure 3-14. (left) 5 minutes post-perfusion of 70kDa FITC-Dextran in the top epidermal channel, and (middle) 5 minutes post-perfusion of 70kDa FITC-Dextran in the bottom EC channel. (right) Quantification of permeability of 70kDa FITC-Dextran across either the EC or keratinocyte barrier. Red and black data points represent measurements of multiple pores from different devices, respectively. **** $p < 0.0001$.

3.3.4 SM-MPS Response to Inflammation

To simulate bacterial inflammation, the SM-MPS was exposed to artificial Toll-like receptor 2 (TLR2) agonist Pam_3CSK_4 and a mixture of three inflammatory cytokines (IFN-γ, TNF-α, and IL-1β). This combination replicates septic conditions inside the SM and together are referred to as Pγαβ for brevity (see Methods). The expression of vascular endothelial adhesion molecules ICAM-1 and VCAM-1 is increased 3- to 4-fold after 4 hours of Pγαβ exposure (Figure 3-15).

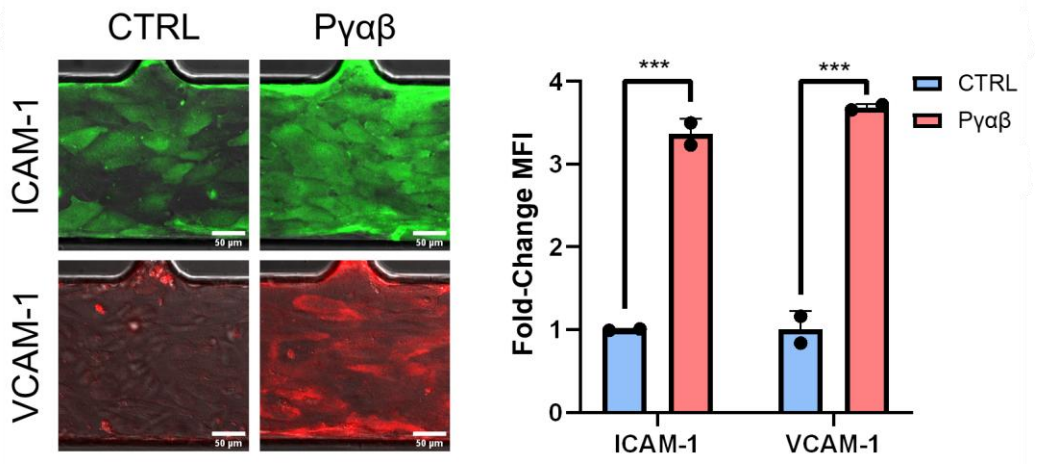


Figure 3-15. ICAM-1 (green) and VCAM-1 (red) expression in the endothelial cells of the SM-MPS after 4 hours of stimulation with Pam_3CSK_4, IFN-γ, TNF-α, & IL-1β (Pγαβ). * $p < 0.05$; ** $p < 0.01$; *** $p < 0.001$; **** $p < 0.0001$.

Monocultures of SM cells were also evaluated for gene expression of pro-inflammatory cytokines and granulopoietic factors. The presence of Pam_3CSK_4 increases the expression of IL-6, IL-8, and IL-1β in endothelial cells and fibroblasts, but only IL-8 significantly in keratinocytes. The expression of these molecules is significantly further increased in the presence of Pγαβ which simulates a more robust inflammatory response in the absence of resident immune tissue cells (Figure 3-16).

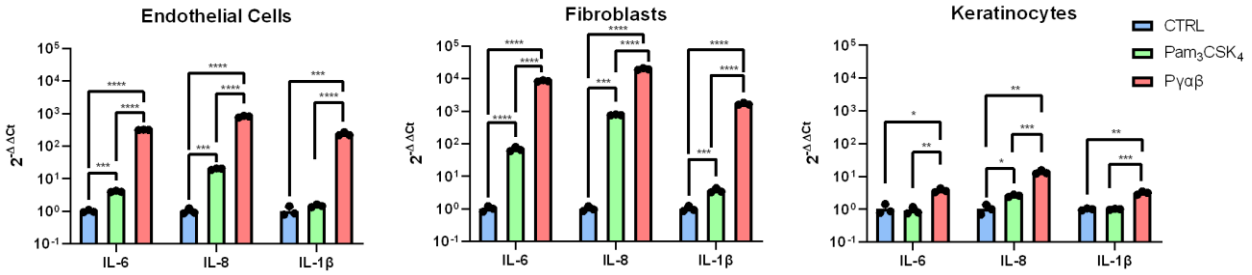


Figure 3-16. Gene expression of IL-6, IL-8, and IL-1β in SM cells stimulated for 24 hours with Pam_3CSK_4 or Pγαβ separately in well plates. * $p < 0.05$; ** $p < 0.01$; *** $p < 0.001$; **** $p < 0.0001$.

We next introduced adult, human, blood-isolated PMNs (Bld-PMN) into the SM-MPS model of inflammation. The SM-MPS was stimulated for 4 hours with Pγαβ and then Bld-PMNs were perfused through the vascular compartment over 20 minutes (Figure 3-17).

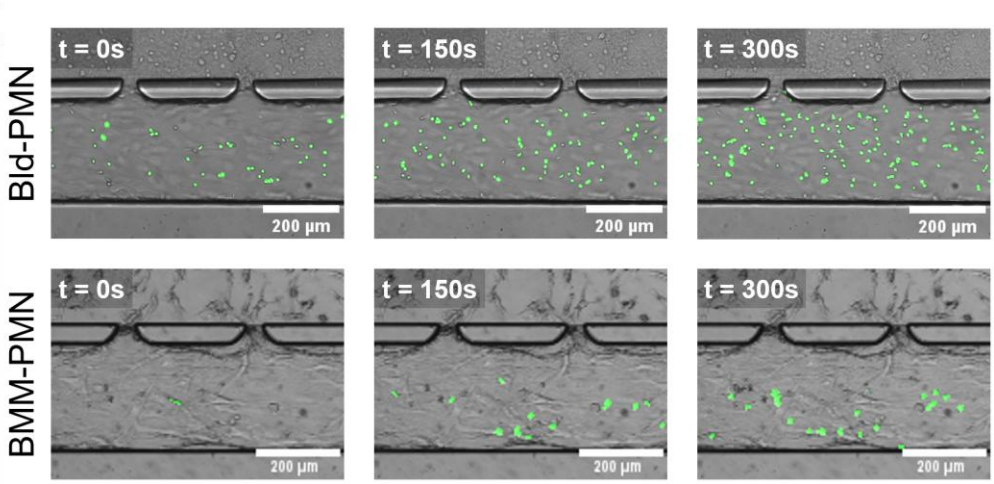


Figure 3-17. Static high-resolution image of Bld-PMNs and BMM-PMNs attaching to the vasculature of inflamed SM-MPS.

Bld-PMNs adhere to the endothelial layer, with a progressive accumulation over 5 minutes leading to an ~ 8-fold increase compared to control. After 20 minutes, devices were flushed to remove any unbound cells, showing that PMNs adhered robustly to the inflamed SM-MPS (Figure 3-18).

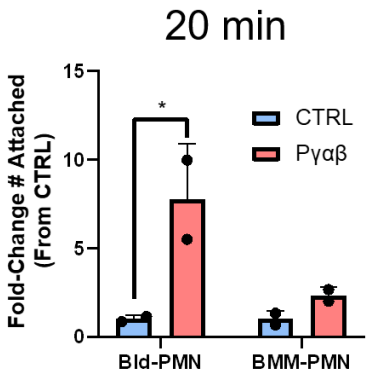


Figure 3-18. Quantification of cells attached to either an unstimulated or Pγαβ stimulated SM-MPS. * $p < 0.05$.

This process was then repeated with egressed cells from the BMM-MPS, denoted BMM-PMN (Figure 3-17). BMM-PMN also bind to the endothelium following Pγαβ, but to a lesser degree—a 2-fold increase compared to control (Figure 3-18). We next introduced pHrodo™ Zymosan Bioparticles™ in the SM-MPS, stimulated with Pγαβ, and then introduced either Bld-PMN or BMM-PMN. Both Bld-PMN and BMM-PMN demonstrated robust phagocytosis of the particles (Fig. 4E).

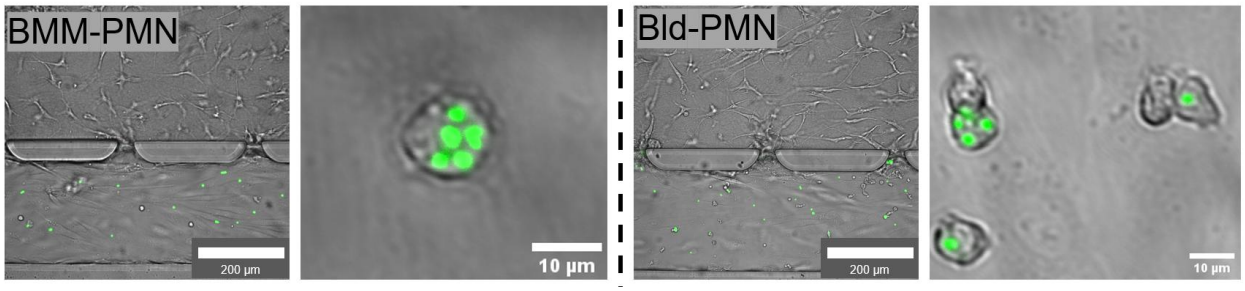


Figure 3-19. Static high-resolution image (wide angle and close-up of single cell) of BMM-MPS egressed cells (left) and Bld-PMNs (rights) adhered to a Pγαβ-stimulated SM-MPS and subsequently perfused with pHrodo™ Zymosan Bioparticles™ revealing phagosomes (green).

3.3.5 Progenitor Response in the SM-MPS

The presence of progenitor cells (CD34+) in the BMM-PMN population (Figure 3-7) is consistent with bone marrow production and release but also highlights a difference between this cell population and Bld-PMNs. This difference may account for

differences in cell attachment (Figure 3-18). As such, we assessed the ability of CD34+ HSPCs to bind to and potentially differentiate within the SM-MPS. Primary cord-blood HSPCs were thawed, labeled with CellTracker™, and immediately perfused into an inflamed (Pγαβ) SM-MPS over 20 minutes and compared to Bld-PMNs. HSPCs bound to the endothelium (Figure 3-20).

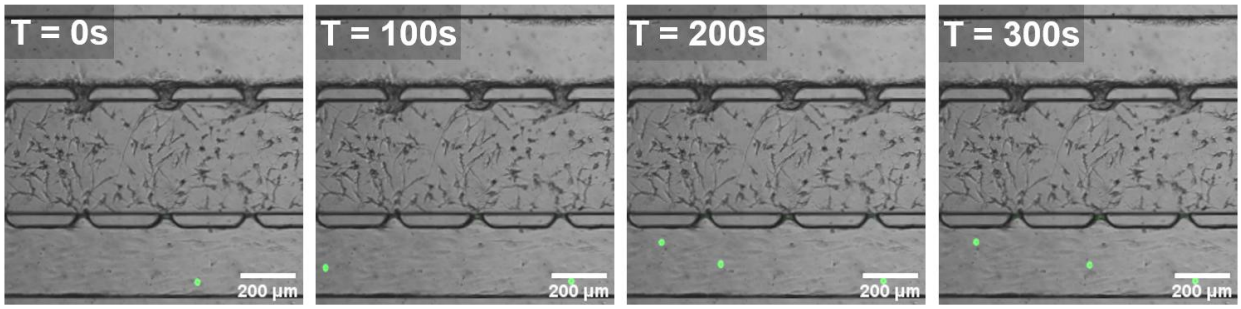


Figure 3-20. Primary HSPC donor cells are perfused along inflamed SM-MPS endothelium.

Control peripheral blood PMNs binding to the Pγαβ-stimulated SM-MPS vasculature was, again, 8-fold greater compared to unstimulated SM-MPS (Figure 3-21); in contrast, binding of the HSPCs showed a positive trend consistent with observations (Figure 3-20) but was not statistically significant (Figure 3-21).

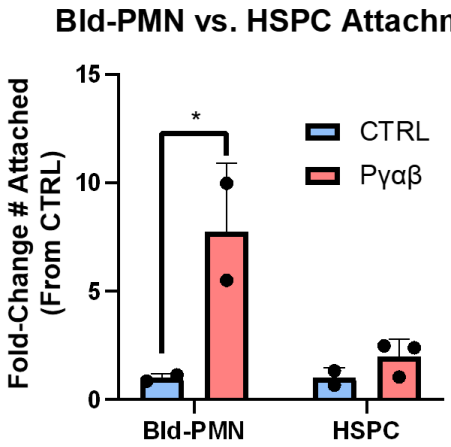


Figure 3-21. Fold-change in number of blood-isolated PMNs or primary HSPCs attached to the EC layer after 20 minutes of perfusion and subsequent flushing of unbound cells. SM-MPS was either unstimulated or inflamed with Pγαβ.

24 hours following endothelial attachment in the SM-MPS, approximately 50% and 20% of the initially (first 20 minutes) attached Bld-PMNs and HSPCs, respectively, remained firmly bound (Figure 3-22).

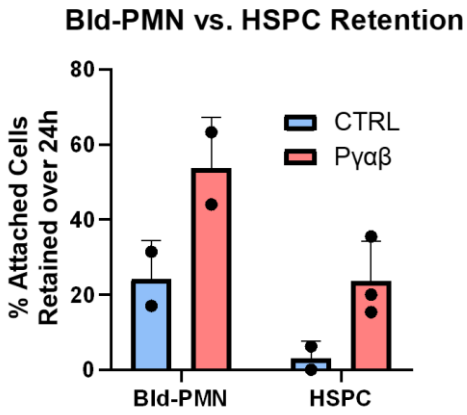


Figure 3-22. Percentage of blood-isolated PMNs or HSPCs retained in the SM-MPS 24 hours after initial perfusion. * $p < 0.05$.

To test whether local granulopoiesis could occur, we next introduced granulopoietic expansion media for six days in the vascular channel. On day 7, abundant small round cells were observed and remain attached to the endothelium, and immunohistochemical staining revealed a subpopulation of CD16+ cells consistent with granulopoiesis (Fig. 5D).

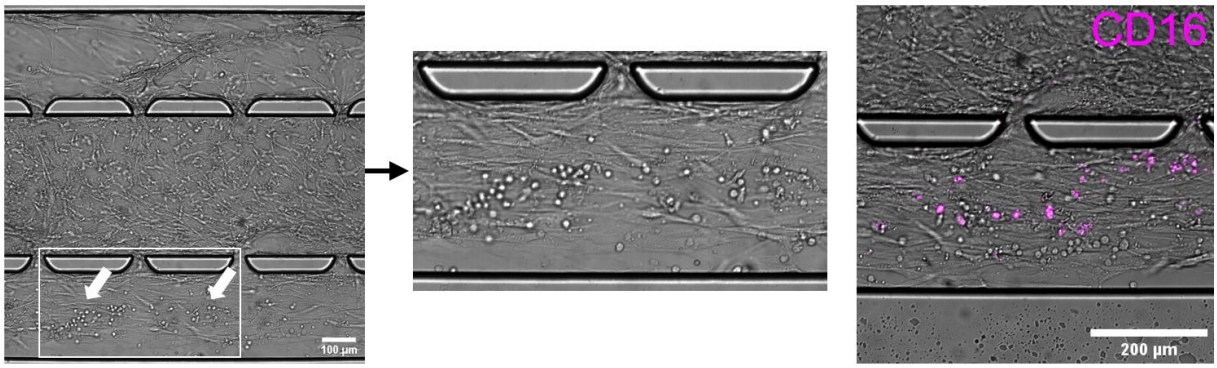


Figure 3-23. SM-MPS, 20 min post-perfusion, is flushed and supplemented with granulopoietic expansion media for 7 days. Greater numbers of granule-like immune cells are then seen in the SM-MPS (middle panel is higher magnification view of region surrounded by white box in right panel). SM-MPS fixed and labeled with anti-CD16 (magenta).

Discussion

Integrating MOMPSs is inherently challenging as each micro-organ system requires specialized media, organ-specific endothelium, precise scaling, and potentially unique microfluidic devices. Our primary goal was to model bone marrow and skin organ systems, separately at first, using the same microfluidic device design; then, manually integrate the organ systems at physiological scale and function. This strategy greatly simplifies the design requirements and reduces the logistical barriers of coordinating disparate platforms. We used this approach to simulate bacterial inflammation in the skin and the subsequent recruitment and trafficking of neutrophils from the bone marrow to eliminate the infection. Our simple model of human bone marrow releases a diverse population of cells that includes hematopoietic stem/progenitor cells, myeloid progenitor cells, and mature neutrophils capable of phagocytosis. When introduced into the model of bacterial inflammation and infection in the skin, these cells adhere to the endothelium, migrate into the dermis, and demonstrate active phagocytosis of pathogenic material. Finally, we demonstrate that HSPCs adhere to inflamed endothelium in the skin microenvironment and can undergo local granulopoiesis in the vascular compartment. Our results demonstrate that a simplified approach (single microfluidic design, manual transfer of cells at scale) can lower the barrier to simulate complex biological events in multi-organ physiology.

Bone marrow microenvironment. We created a remarkably simple model of human bone marrow by including only three cell populations (HSPCs, ECs, and BMSCs) in a fibrin matrix. This strategy is consistent with the perivascular niche of human bone marrow

and leverages our previous report[68] which created both the perivascular niche and the endosteal niche in a single MPS. This single niche recapitulates several basic features of human bone marrow including granulopoiesis, egress of cells from the marrow compartment, and maintenance of a population of HSPCs for up to 25 days. The population of cells that egress from the marrow is diverse and includes not only mature neutrophils (CD66b+/CD34-), but also more immature progenitors including HSPCs themselves (CD34+/CD45RA-). While it is difficult to compare directly with cells that egress from adult human bone marrow, this diverse population is consistent with cells present in the systemic circulation, particularly when considering the variable lifespan of PMNs, and the ability of progenitors to mature after leaving the bone marrow. The total production of cells from the BMM-MPS (3 x 10^9 cells per liter per day or 3.0 cells per HSPC per day) is lower than that produced by adult human bone marrow (nominally ~ 1 x 10^{11} cells per liter per day)[7]. The lower production could be due to a myriad of differences including, but not limited to, a lower number of HSPCs, altered microenvironment stimuli including soluble mediators, and the lack of osteoblasts and/or mineralized bone. Previously reported 3D *in vitro* models of human bone marrow have included additional features such as osteoblasts and mineralized bone[68,82–84]. The presence of these features likely influences the maturation of progenitors and response to exogenous stimuli but also increase complexity and cost. As such, depending on the goals or purpose of the model, our simple approach provides a low-cost option that captures important fundamental features of adult human bone marrow.

Skin microenvironment. Our approach to creating a skin microenvironment was similar to that of the bone marrow. We sought a simple model capable of recreating features relevant to our goals of mimicking neutrophil attachment to the vascular endothelium, trafficking within an inflamed microenvironment, and phagocytosis. We chose to layer a microfluidic channel with endothelial cells to maximize visualization of neutrophil attachment. *In vivo*, endothelial cells (~ 5-15%) and fibroblasts (~ 50-70%) comprise the two most common cell types, though the dermis contains additional cell types including pericytes (~ 2-8%), macrophages (~ 5-10%), dendritic cells (~ 2-5%), mast cells (~ 1-5%), and lymphocytes (~ 1-3%)[85–87].These additional cells types provide many different functions in the skin, and can also produce soluble mediators integral to the inflammatory response. For simplicity, we chose to simulate features of the inflammatory response (i.e., ICAM-1 and VCAM-1 endothelial expression) by providing a cocktail of common inflammatory mediators—INF-γ, IL-1β and TNF-α. We acknowledge that additional soluble mediators from in vivo resident immune cells could amplify the released damage-associated molecular patterns (DAMPs) that resulted in immune cell recruitment and the responses we observed. We also utilized the synthetic TLR2 agonist Pam_3CSK_4 to simulate bacterial infection without needing to integrate bacterial cultures into this system. TLR2 stimulation of dermal fibroblasts increases expression of additional inflammatory mediators such as IL-6 that will contribute the inflammatory milieu of the skin microenvironment[88,89]. For the epidermis, we chose to include keratinocytes with a liquid interface, which is technically simpler than an air-liquid interface, but maintains the phenotype of the basal cells (Keratin 5+, Figure 3-12). The basal cells are the most important epidermal cells to impact the immune

microenvironment[90]. Interestingly, even in the absence of the superficial layer of keratinocytes, the permeability of the basal layer was especially low, consistent with the barrier function of the epidermis.

Integration of multiple organs. Integration of multiple organ systems in a single MPS can be cumbersome and involve significant time, expense, and technical expertise. In addition, it is difficult to replicate cell trafficking behavior across *in vivo* biological barriers, and to scale volumes of the micro-organs and integrated plumbing to reflect in vivo conditions. We sought to investigate the interaction between bone marrow-derived cells and bacterial-infected skin. To simplify this process, we created separate MPS systems for bone marrow and skin using the same microfluidic design. Then, collected the cells that egress from the BMM-MPS, and introduced them into the inflamed/infected SM-MPS. This approach has the obvious advantage that it eliminates the need for complex plumbing to integrate the two MPSs, and thus allows simple observations of how bone marrow-derived cells interact with an inflamed/infected skin microenvironment. We were able to replicate fundamental features of this interaction including endothelial attachment of the bone marrow-derived cells and phagocytosis of simulated bacterial particles. Bld-PMNs adhered to the EC surface ~ 8 times greater when the SM-MPS was treated with Pγαβ which was ~ 4-fold larger than the BMM-PMNs. The reduced binding from the BMM-PMNs is likely due to the greater heterogeneity of this cell population including the larger presence of progenitor cells (e.g., CD34+) which we demonstrated had lower binding rates. The lower rate of binding

for the progenitor cells is consistent with lower expression of LFA-1 and VLA-4[91], the binding partners of ICAM-1 and VCAM-1, respectively.

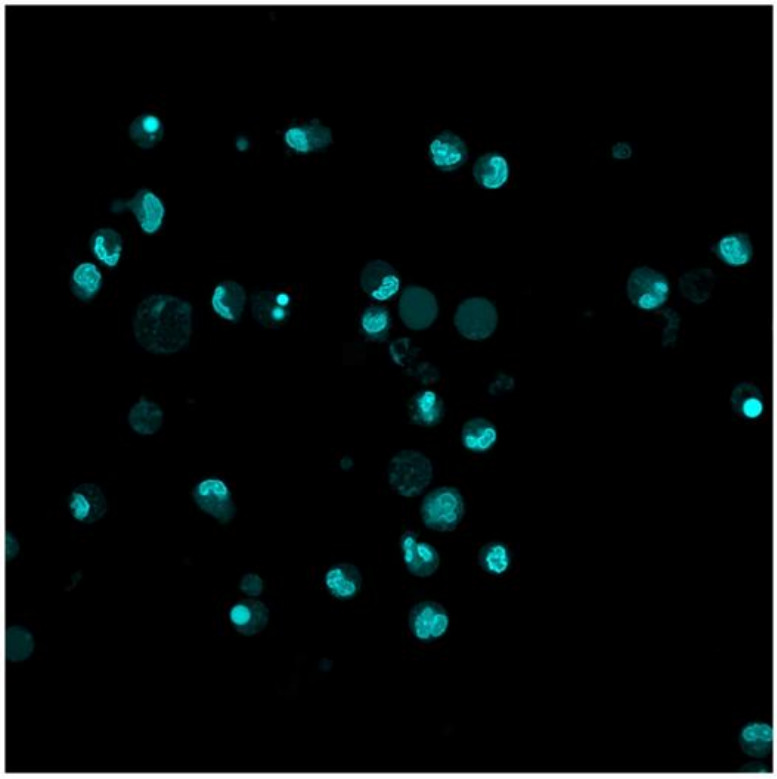
While our current study did not provide new molecular-level mechanistic insight, it revealed that HSPCs themselves can attach to the endothelium and undergo local granulopoiesis (CD16+) within the vascular compartment, providing a possible mechanism to combat bacterial skin infections. The theory of extramedullary granulopoiesis in skin to combat infection was first discovered in murine models, and now for the first time is being directly tested in integrated human microphysiological models[21]. It is also easy to imagine studying the interaction of bone marrow and skin in the opposite direction using the two MPSs; that is, examining the impact of skin-derived soluble mediators on the behavior of the bone marrow. Although not technically difficult, care must be taken to appropriately simulate the dilution of soluble mediators in the systemic circulation. The obvious disadvantage of our approach to integrate the bone marrow and skin is the absence of the systemic circulation which not only provides dilution for cells and soluble mediators, but also opportunities for both cells and mediators to interact (and be consumed) by other organ systems.

3.4 Conclusion

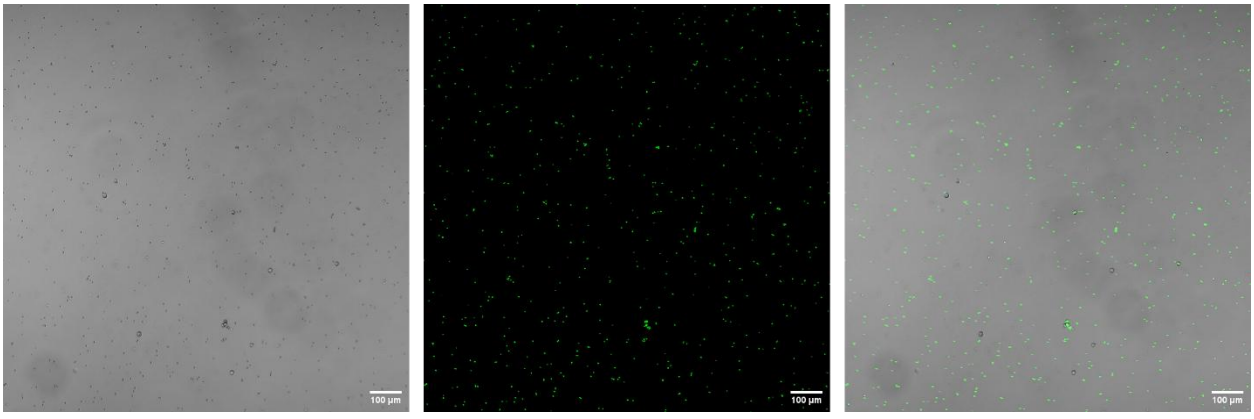
The dual-MPS framework presented here successfully recapitulates the critical human immune circuit between the bone marrow and the skin using a single, simple microfluidic platform. By utilizing the same polydimethylsiloxane (PDMS) architecture for both microenvironments, we significantly reduced the fabrication complexity and technical barriers often associated with integrated multi-organ systems. The bone marrow microenvironment model (BMM-MPS) sustained long-term hematopoiesis and granulopoiesis for over 23 days. This system achieved a production rate of approximately 3.0 cells generated per HSPC per day, with a subpopulation consistent with mature PMNs that have the capacity for phagocytosis. The skin microenvironment model (SM-MPS) effectively recreated a vascularized dermis protected by a keratinocyte barrier. The endothelium demonstrated an appropriate inflammatory response, and by manually transferring cells from the marrow to an inflamed skin environment, we provided a scalable solution to the scaling and metabolic challenges of multi-organ integration. This method avoided the use of cumbersome external pumps, challenging scaling requirements, and divergent media requirements that might otherwise compromise organ-specific phenotypes. A key finding of this study is the successful recruitment and local differentiation of CD34+ HSPCs within the dermal vascular compartment. The observation of marrow-derived cells undergoing local granulopoiesis (indicated by CD16+ sub-populations) highlights a potential physiological mechanism for combating peripheral bacterial infections. Ultimately, this dual-MPS approach demonstrates that the integration of complex organ models is feasible and

accessible, offering a robust platform for studying human-specific immune crosstalk and systemic inflammatory responses *in vitro*.

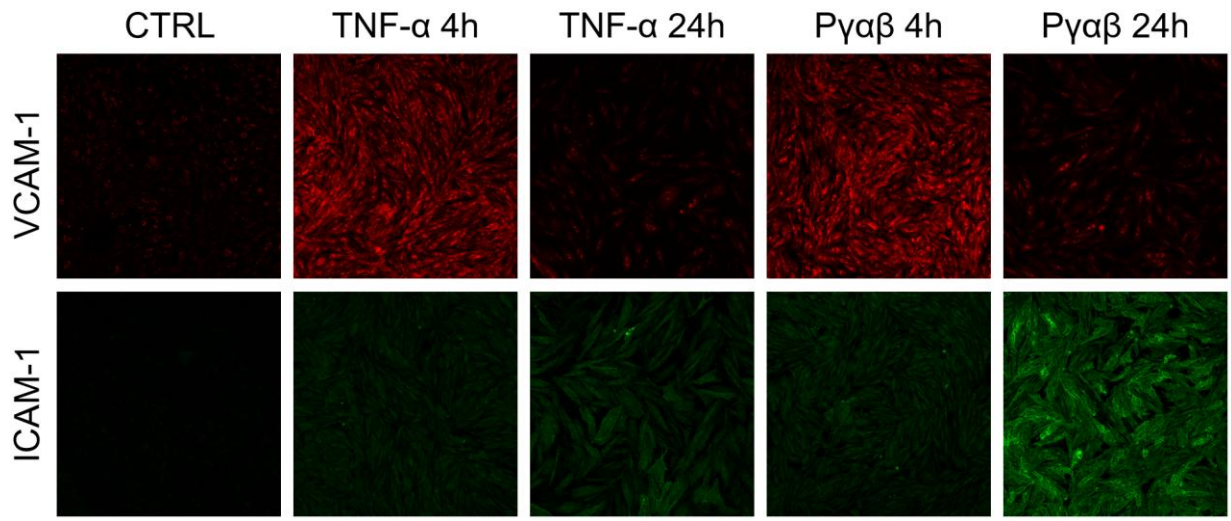
3.5 Supplemental Materials



Supplementary Figure 3-1. 60x magnification of egressed cells collected from the BMM-MPS and stained with DAPI nuclear stain (cyan).



Supplementary Figure 3-2. 10x magnification of neutrophil-isolated egressed cells collected from the BMM-MPS phagocytosing pHrodo™ Red Zymosan Bioparticles™ (ThermoFisher) in a 96-well plate. (left) brightfield; (middle) Zymosan phagosomes (green); (right) converged image



Supplementary Figure 3-3. ECs were seeded in well plates, fed with EGM-2, and allowed to grow to confluency for 3 days. ECs where then stimulated with either TNF-α (10ng/mL) or Pγαβ (see methods) for 4 or 24 hours in EGM-2. After the selected time, cells were fixed and labeled with either anti-VCAM-1 (red) or anti-ICAM-1 (green) antibody. Results align with findings that VCAM-1 expression peaks at t = 4 hours post-stimulation whereas ICAM-1 expression continues to climb for 24 hours post-stimulation. Pγαβ triggers greater ICAM-1 expression compared to solely TNF-α at 24 hours.

4 Chapter 4: Recruitment and Local Granulopoiesis of HSPCs in a 3D Skin Model

Adapted from "Recruitment and local granulopoiesis of human hematopoietic stem/progenitor cells in a skin-on-a-chip" By Evan Cirves et al. submitted to Lab-on-a-Chip. May 2026.

4.1 Introduction

Global healthcare is grappling with a resurgence of antibiotic-resistant bacterial pathogens that challenge the efficacy of modern drugs, resulting in over 1 million direct deaths every year[1]. For example, methicillin-resistant *Staphylococcus aureus* (MRSA) represents a single pathogen responsible for over, on average, 125,000 hospitalizations in the U.S. annually[2]. As antibiotic resistance continues to rise, the clinical reality necessitates a more granular understanding of the host-pathogen interface where the innate immune system attempts to clear these resistant pathogens. The primary line of defense against these invaders is the polymorphonuclear granulocyte (PMN)—or neutrophil. These cells are viewed as short-lived effector cells with a half-life that is normally less than 24 hours[92]. PMNs are the daughter cells of hematopoietic stem and progenitor cells (HSPCs) that reside in the bone marrow to produce, on average, over 10^{11} PMNs per day[7]. The traditional paradigm of combating infection has been PMNs produced by HSPCs in the bone marrow subsequently travel through the systemic circulation to the site of infection to clear the bacteria. However, previous murine models have challenged this traditional view by claiming that HSPCs also travel *via* the systemic circulation to the site of dermal wounds to locally produce neutrophils to

combat infection[20–22]. Our previous work includes a proof-of-concept clinical application of combining HSPCs with a hydrogel scaffold implanted in a murine dermal wound to assist in wound-healing and antibacterial activity[93]. However, substantial immunological and biological differences between animal and human systems underscores importance of testing this concept in human-relevant experimental platforms and derive therapeutic applications.

The pathogen-infected tissues present many of the essential components required for HSPC migration and granulopoiesis. PMN attachment (expressing high levels of LFA-1[94,95] and low levels of VLA-4) to the endothelium is primarily regulated through ICAM-1 interactions, whereas HSPC attachment (high in VLA-4[96], low in LFA-1) is regulated through VCAM-1[97]. Although both adhesion molecules are expressed by inflamed endothelium, their expression peaks at distinct stages of infection, thereby enabling the inflamed endothelium to recruit and adhere circulating HSPCs. Moreover, HSPCs express CXCR4 which binds SDF-1 to mediate tethering to bone marrow niches during homeostasis and to endothelium during inflammation[98]. Most studies expound on this, though few studies elaborate that excessively high SDF-1 concentrations drives active movement of leukocytes away from its source[99,100]. Importantly, HSPCs can undergo emergency granulopoiesis in response to pathogen-associated factors (i.e., LPS, TLR2 agonists) that are commonly present during severe infection[15–18]. As such, HSPCs, which exist in the systemic circulation in low numbers[19], could potentially traffic to the site of an infection, and undergo local granulopoiesis in the presence of TLR2 agonists.

Organ-on-a-chip systems have emerged as promising *in vitro* alternatives capable of recreating key aspects of the multicellular architecture of human tissues. Several vascularized microfluidic models, including previously developed bone marrow, tumor, and cardiac systems, have demonstrated utility for studying drug responses and immune cell trafficking[68,75,81]. However, while prior studies have modeled immune migration of neutrophils and T cells, local HSPC granulopoiesis withing the tissue microenvironment remains unexplored. Recapitulating this process requires careful control over fluid flows, morphogen gradients, and tissue cellular compositions to create biologically faithful microenvironments that captures HSPC transport, differentiation, and local granulopoiesis.

Here we present a human Skin-on-a-chip microphysiological system to model the interactions of HSPCs and PMNs with the skin microenvironment mimicking a bacterial infection. The three-chamber polydimethylsiloxane (PDMS) device recreates a vascular layer (comprising endothelial cells), a dermal layer (comprising dermal fibroblasts in a fibrin gel), and an epidermal layer (comprising adult keratinocytes). HSPCs and PMNs can be introduced into the vascular layer at physiological shear. The design allows for real-time visualization of HSPC and PMN attachment and retention in the device. HSPCs robustly attach to the vascular layer, but do not undergo transendothelial migration like PMNs. Despite this, we observe that HSPCs undergo early differentiation in the dermal vascular niche to create PMN-like cells capable of phagocytosis. These findings suggest that human HSPCs can contribute to clearing bacterial infection through a mechanism of local granulopoiesis within the vascular compartment of the

skin and demonstrate the potential to create HSPC-based therapies for antibiotic-resistant infections.

4.2 Materials & Methods

Microfluidic device design and modeling: The microfluidic device used consists of three parallel channels divided by 16 trapezoidal posts per side with 30 μm gaps between each post. This simulates the capillary burst valve and allows the loading of fibrin hydrogels without leaking into adjacent chambers[69]. The pores allow diffusion of signaling molecules and migration of cells between each chamber. Each chamber is approximately 4 mm long and 100 μm high in the z-direction. The central channel is 350 μm wide and the side channels are 250 μm wide. Different volumes of media were added to the inlet and outlet of a single channel to simulate convective flow across a single channel.

MPS device preparation: A master mold of the device made of SU-8 on a silicon wafer was prepared using standard soft lithography methods[70]. A 100 μm layer of SU-8 3050 was spun onto a silicon wafer. Then the microfluidic design was patterned onto the wafer during a single mask lithography step. The mold was then silanized. Curing agent (Dow Corning, GMID# 02065622) was mixed with Polydimethylsiloxane (PDMS) in a 1:10 ratio, poured onto the mold, degassed, and allowed to bake overnight at 60°C. The cured PDMS was removed from the mold and had fluidic lines added by puncturing with either a 16- or 18-gauge syringe. The punctured devices were plasma bonded to either a glass coverslip (Thermo Fisher) or glass slide (Thermo Fisher). Devices were exposed to ultraviolet light for 30 minutes to ensure sterility before loading.

In vitro cell culture: Endothelial colony-forming endothelial cells (ECFC-ECs) were isolated from cord blood as previously described by our group[70] and others[71]. All cord blood samples were collected in accordance with the University of California Institutional

Review Board regulations. Briefly, all cells were cultured in tissue-treated culture flasks; ECs were specifically cultured on flasks additionally treated with 1% gelatin. All cells were cultured according to vendor protocols using appropriate culturing media at 37 °C and 5% CO_2. Other cells used were Normal Human Adult Epidermal Keratinocytes (Ks, Lonza, Cat#00192627), and Normal Human Dermal Fibroblasts (DFs, Lonza, Cat# CC-2511). Endothelial cells were cultured in EGM-2 (Lonza, Cat# CC-3162). Keratinocytes were cultured in KGM-Gold (Lonza, Cat# 00192060). Dermal Fibroblasts were cultured in FGM-2 (Lonza, Cat# CC-3132).

The Granulopoietic Expansion Media consists of a 1:1 ratio of EGM-2 and StemSpan™ SFEM II (STEMCELL, Cat# 09655) with the following added supplements: Interleukin 3 (IL-3, 10 ng/mL, Peprotech, Cat# 200-03-10UG), Interleukin 6 (IL-6, 10 ng/mL, Peprotech, Cat# 200-06-20UG), FMS-like tyrosine kinase 3 (Flt-3, 10 ng/mL, Peprotech, Cat# 300-19-10UG), and Stem Cell Factor (SCF, 100 ng/mL, Peprotech, Cat# 300-07-10UG).

Skin-on-a-chip model: ECs, Ks, and DFs were expanded to passages 5, 4, and 6, respectively, before use. Cells were thawed and cultured for 5 days prior to lifting with Accutase™ and loading into the SC. DFs were resuspended at $1x10^7$ cells/mL before being loaded into the central channel comprising 10 mg/mL fibrinogen from bovine plasma (Thermo Fisher) and 5 U/mL thrombin. Devices were incubated for 30 minutes at 37°C, 5% CO_2 to allow the hydrogel to solidify. Ks and ECFC-ECs were resuspended at approximately $1x10^7$ cells/mL before perfusing into opposite channels flanking the center channel and allowed to attach to the bottom of the device. After 2 hours, devices were perfused with DPBS to wash out any unbound cells. Media reservoirs were

aspirated and device media was added as such: 150 µL and 100 µL of KGM-Gold were added to the epidermal channel inlets and outlets, respectively; 250 µL of EGM-2 was added to the inlet of the vascular channel. This allows convective flow across the inside of both the epidermal and vascular channels, with higher wall shear-stress in the vascular channel. Because the total volume of both the epidermal and vascular channels is equivalent, there is no interstitial flow across the dermal compartment, and fluid exchange only occurs by diffusion.

Confocal imaging and immunohistochemistry assays: Devices were fixed in 4% paraformaldehyde (PFA, BOSTER, SKU# AR1068) for 2 hours and blocked overnight with 2% bovine serum albumin (BSA, Thermo Fisher) in DPBS. Antibodies in 0.1% BSA were delivered through the fluidic lines and devices were labeled overnight. Nuclei were counterstained with DAPI at a final concentration of 5 µg/mL. Fluorescent and time-lapse images were acquired with a FV3000 Confocal microscope (Olympus). Multi-Area-Time-Lapse (MATL) acquisition was used so the entire length of the MPS could be imaged simultaneously. Image post-processing was done in Fiji/ImageJ. Image stitching was done in FV310. For determining the distribution of ECs, DFs, and Ks in the SM-MPS, ECs were labeled with CellTracker™ Green, NHDFs were labeled with CellTracker™ Orange, and NHEKs were labeled with CellTracker™ Far Red. For integrin-pair labeling of the SC, devices were labeled either with anti-CD54 (ICAM-1) BD Horizon BrilliantTM Blue 515 antibody (1:100, Cat# 564685, Lot# 3130986), anti-CD106 (VCAM-1) Alexa Fluor 594 antibody (1:100, Biolegend, Cat# 305812, Lot# B236197), or anti-CXCL12 (SDF-1) (1:100, Peprotech, Cat# 500-P87A-100UG, Lot# 0219M092RB)

with secondary antibody donkey anti-rabbit AF647 (1:1000, Invitrogen, Cat# A31573, Lot# 2359136); quantification was performed using established methods[72].

AMD3100 blocking assay: PMNs were collected from blood and HSPCs were thawed from aliquots and allowed to incubate for 30 minutes in CellTracker™ Green in EGM-2 for 30 minutes (37 °C, 5% CO2). After spinning down and resuspension, cells were then incubated for 2 hours in EGM-2 supplemented with or without (AMD3100, 1μM, Selleck Chemicals Cat# S3013). After blocking, cells were perfused into SCs. Cells were counted at the end of 30 minutes and 24 hours.

Flow Cytometry: HSPCs were differentiated in well plates for 7 or 14 days in granulopoietic expansion media changed every 2 days. Cells were fixed in 4% PFA and resuspended in cell staining buffer (Biolegend, Cat# 420201). Cells were stained for 1h with anti-CD34 BV421 (1:1000, Biolegend, Cat#343610) and anti-CD66b AF700 (1:1000, Biolegend, Cat#305114). Cells were washed and analyzed using a Beckman Cytoflex 13-color detector flow cytometer (Beckman Coulter, Cat# B75408). Compensation controls, unstained samples, and fluorescence-minus-one controls were used to gate cell populations. OneComp eBeads™ Compensation Beads (ThermoFisher, Cat#01-1111-42) were used for compensation beads. Data analysis was performed using FlowJo software.

Phagocytosis Assay: SCs were perfused with pHrodo™ Red Zymosan Bioparticles™ (Thermo Fisher, Cat# P35364). The assay was followed using manufacturer's instructions and imaged via confocal. Images were analyzed in Fiji/ImageJ.

Artificial bacterial stimulation of the SM-MPS: To stimulate an artificial infection in the SC, a combination of factors was used to accomplish this: Pam_3CSK_4 (10 µg/mL), TNF-α (10 ng/mL), and IL-1β (10 ng/mL). Pam_3CSK_4 (Invivogen, Cat# vac-pms) is a synthetic triacylated lipopeptide mimicking the lipopeptides of the bacterial wall by acting on TLR2 receptors[101]. Previous work also has been cited to show TNF-α (tumor necrosis factor alpha, Peprotech, Cat# 300-01A-50UG) and IL-1β (interleukin 1 beta, Peprotech, Cat# 200-01B-10UG) together are potent activators of endothelium[102]. EGM-2 was supplemented with these factors and added to SC devices 4 hours prior to measuring surface integrin expression or capture of immune cells.

RT-qPCR: ECs, DFs, and Ks were cultured in 96 well plates with appropriate culturing media—with or without supplemental inflammatory factors—and lifted after 24 hours. Cells were then processed using a Total RNA Purification Kit (STEMCELL Cat# 79004) using manufacturer instructions. Purified mRNA was then reverse-transcribed with the High-Capacity cDNA Reverse Transcription Kit (Thermo Fisher, Cat# 4368814) and RiboLock RNase Inhibitor (Thermo Fisher, Cat# EO0381) in the SimpliAmp Thermal Cycler (Thermo Fisher) according to manufacturer instructions. RT-qPCR was performed on a QuantStudio 5 system (Applied Biosystems). Primers for ACTB (NM_001101), IL6 (NM_000600), IL8 (NM_000584), IL1B (NM_000576), SCF (NM_003994) and SDF-1 (NM_000609) were purchased from IDT. Critical threshold values (C_t) were quantified for each gene. The ΔC_t was quantified by subtracting the samples' C_t value of the housekeeping gene ACTB. The $\Delta\Delta C_t$ was quantified by subtracting the average ΔC_t of the control group. The relative expression values for each gene of interest are presented as $2^{-\Delta\Delta Ct}$.

Immune cell isolation and capture assay: Peripheral blood—from healthy, adult volunteers—was collected by venipuncture using sodium-heparin collection tubes (BD Vacutainer 10 ml, Cat# 367874) in agreement with an approved University of California, Davis Institutional Review Board protocol (#1541024-1). Neutrophils were isolated using immunomagnetic separation via EasySep™ Direct Human Neutrophil Isolation Kit (STEMCELL, Cat # 19666) and resuspended in EGM-2.

2D and 3D Renderings: All 2D renderings were made in Biorender™. 3D renderings were made in Blender 5.0 and subsequently hand-processed in the Procreate app on an iPad Air (5th gen).

Statistical Analysis: Data are presented as means ± standard deviation. Statistical analysis was done using one-way ANOVA with post-hoc Tukey test, two-way ANOVA with Tukey's multiple comparisons test, or unpaired t-test when necessary. For data following a non-normal distribution, Kruskal–Wallis test was used. $p < 0.05$ was considered significant. Statistical significance was indicated in each graph as $*p < 0.05$, $**p < 0.01$, $***p < 0.001$, and $****p < 0.0001$.

4.3 Results

4.3.1 Skin-on-a-Chip (SC) Platform

We sought to create a robust and reproducible microfluidic model of the skin that included the vascular system (capillary), the dermis, and the epidermis such that we could simulate the most fundamental features of immune cell trafficking in response to a bacterial infection. The Skin-on-a-Chip (SC) platform comprises 3 separate parallel microfluidic channels separated by sixteen 30 μm pores, allowing for cell-cell trafficking and communication *via* soluble factors between channels (Figure 4-1, Supplementary Figure 4-1).

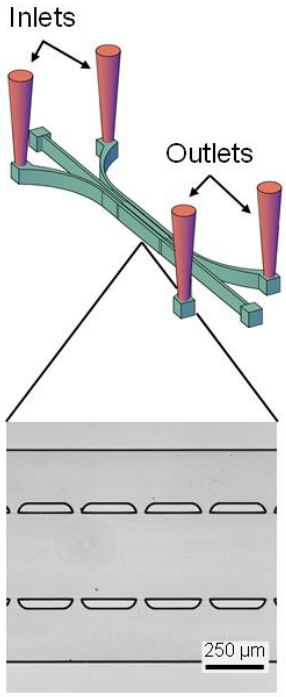


Figure 4-1. (Top) 3D rendering of channels within microfluidic device (green) and pipette tip inlets and outlets (red) for creating vascular flow in one outer channel, and the keratinocyte layer in the opposite outer channel. (Bottom) brightfield image of an empty microfluidic device showing three chambers separated by 250 μm trapezoidal posts with 30 μm pores between.

The device itself is made from polydimethylsiloxane (PDMS) bound to a glass slide using standard soft-lithography techniques[68,75]. Pipette tips are used to create a

pressure gradient along the channels that drive physiological shear flow of culture media with or without immune cells. SCs are created by first seeding primary adult dermal fibroblasts (DFs) in the central/dermal channel in a 10 mg/mL fibrin matrix (see methods) (Figure 4-2).

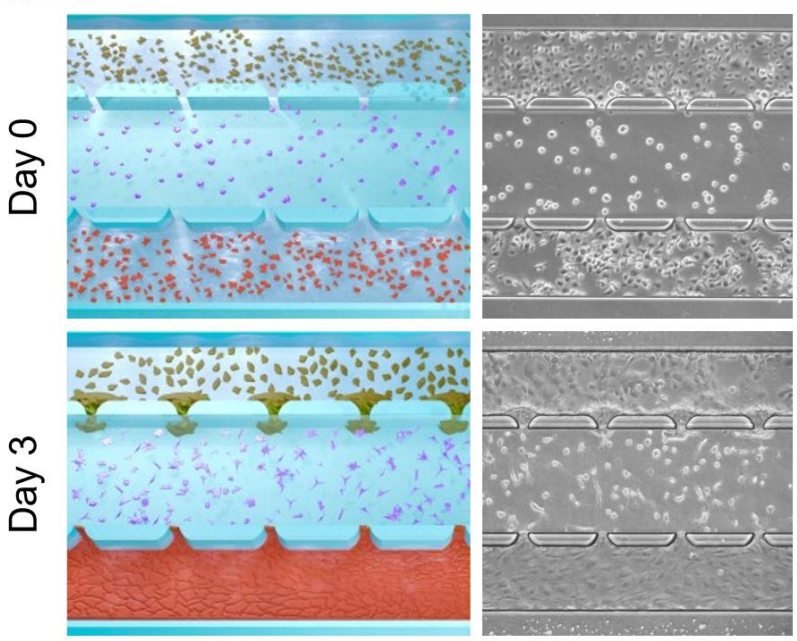


Figure 4-2. (Left) 3D representation of cells seeded in the microfluidic device to create the skin-on-a-chip at days 0 and 3 and (right) brightfield images.

The dermal channel is flanked on both sides with monolayers of either primary adult keratinocytes (Ks) creating the epidermal channel, or cord blood-derived endothelial colony forming cell endothelial cells (ECFC-ECs or just ECs) creating the vascular channel (Figure 4-2, Figure 4-3).

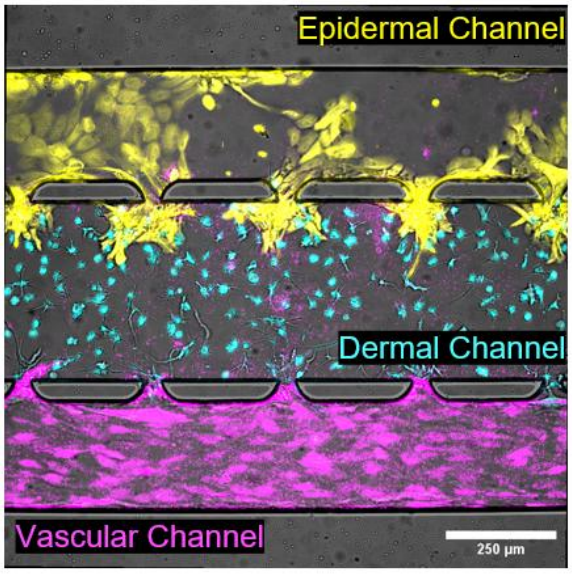


Figure 4-3. Cells in the skin-on-a-chip labelled with CellTrackerTM showing endothelialized channel representing the vascular conduit (magenta), dermal fibroblasts (cyan) in fibrin representing the dermis, and keratinocyte layer representing the epidermis (yellow).

Daily, devices are supplemented with both EGM-2 media and KGM-Gold for 3 days to create a confluent EC layer mimicking the microcirculation, and a K layer occupying the epidermal channel. The Ks in the epidermal channel over 3 days of culturing grow and occlude the pores leading to the dermal channel, thus creating a tight barrier similar to the epidermis *in vivo*.

Our SC mimics key physiological features of normal skin: 1) a tight epidermal layer; 2) an extracellular matrix (ECM) with dermal fibroblasts; and 3) a perfusable vasculature. This model can be used to observe traditionally well-known features of PMN-based responses in the skin microenvironment, where PMNs can attach to the endothelium, and undergo transendothelial migration across the EC layer toward a skin infection to clear pathogenic matter (). Herein, we utilize the SC to model the response of HSPCs in the circulation to a bacterial infection in the skin.

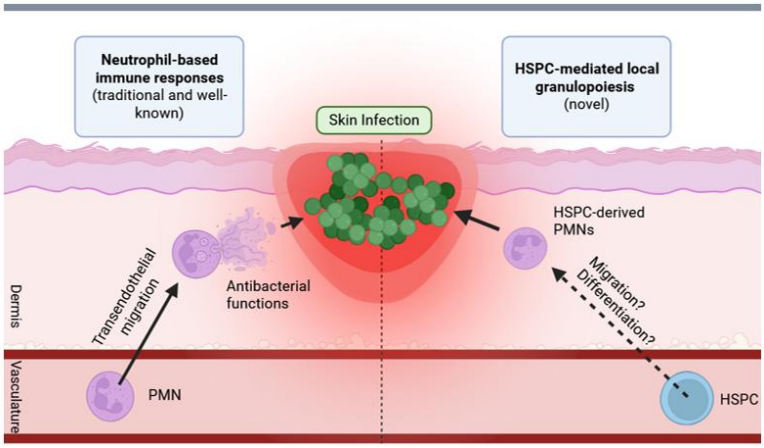


Figure 4-4. Graphical rendering of the theory of local granulopoiesis. Mechanisms of PMN transendothelial migration and antibacterial function are well-understood, but how HSPCs contribute (dashed line) to clearing infection is unknown.

4.3.2 Skin-on-a-Chip response to simulated inflammation

To model the inflammatory responses related to bacterial inflammation, soluble inflammatory mediators were delivered *via* the vascular channel to simulate the inflammatory milieu of a bacterial infection. SCs were stimulated with a combination of 10 ng/mL TNF-α and 10 ng/mL IL-1β (combination denoted as αβ) since they are known as potent inflammatory activators of ECs[75], or 1 μg/mL Pam_3CSK_4 (denoted P) which is a synthetic Toll-like receptor 2 (TLR2) agonist responsible for priming cells for an anti-bacterial inflammatory response. Also used was a combination of these two in a 1/100th (1:100 P+αβ) concentration. ICAM-1 and VCAM-1 expression on the surface of the SC endothelium after 24 hours and 4 hours of exposure, respectively, was quantified (Figure 4-5).

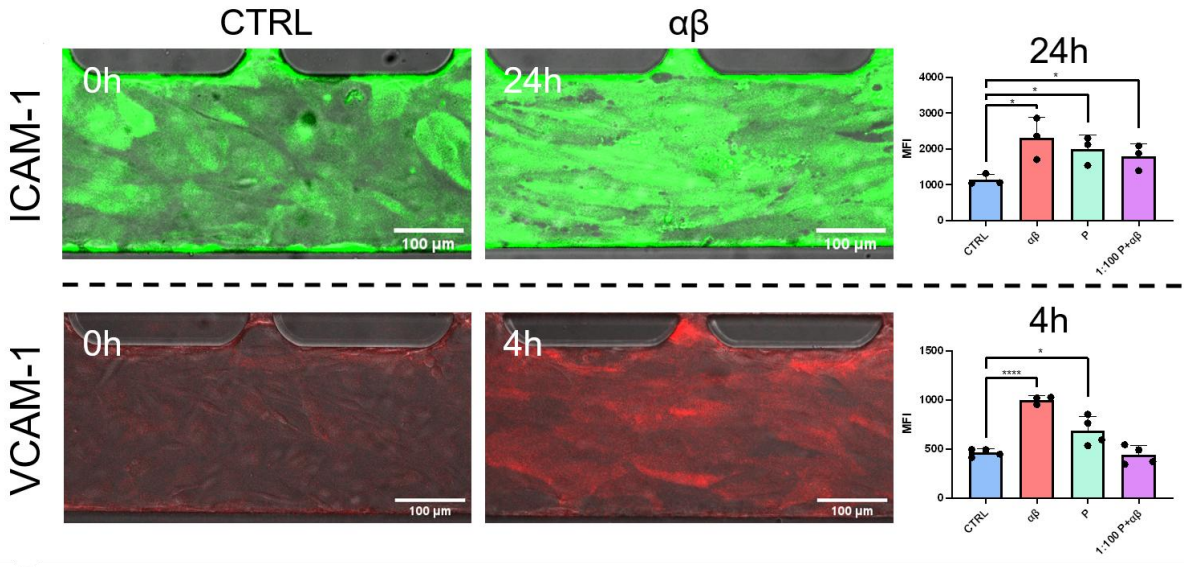


Figure 4-5. Immunohistochemical confocal images of ICAM-1 and VCAM-1 expression on the surface of ECs in the SC. SCs were imaged at t = 0h initially and t = 24h or t = 4h for maximal ICAM-1 and VCAM-1 expression, respectively. Quantitative analysis of Mean Fluorescence Intensity (MFI) of markers on EC surface is also shown under different stimuli conditions (N = 3-4 for MFI analysis; αβ – TNF-α and IL-1β; P – Pam_3CSK_4).

The time points were chosen since VCAM-1 has been shown to have maximal expression at 4 hours post-inoculation, whereas ICAM-1 rises at 4 hours, but continues to rise over 24 hours[97]. Image quantification shows over a doubling of MFI of ICAM-1 and VCAM-1 expression when stimulated with αβ. This upregulation was also observed with SCs stimulated with P and 1:100 P+αβ, though these effects were less pronounced than αβ. Previous studies have demonstrated that sustained exposure to TNF-α over twelve hours can be cytotoxic to cells[103,104]. HSPCs cultured in well plates validates this assumption (Supplementary Figure 4-2). As such, the αβ condition was only used for stimulating the SC within a 4-hour window; longer-term studies did not include an αβ condition.

We next examined the individual contributions of skin cells to the initial inflammatory response. The three cell types in the SC (ECs, DFs, and Ks) were cultured in well plates as monolayers separately for 2 days. mRNA expression of IL-6, GCSF,

SCF, and SDF-1 did not change in stimulated Ks, with the notable exception that P elicited a 4-fold increase in IL-8 (Figure 4-6).

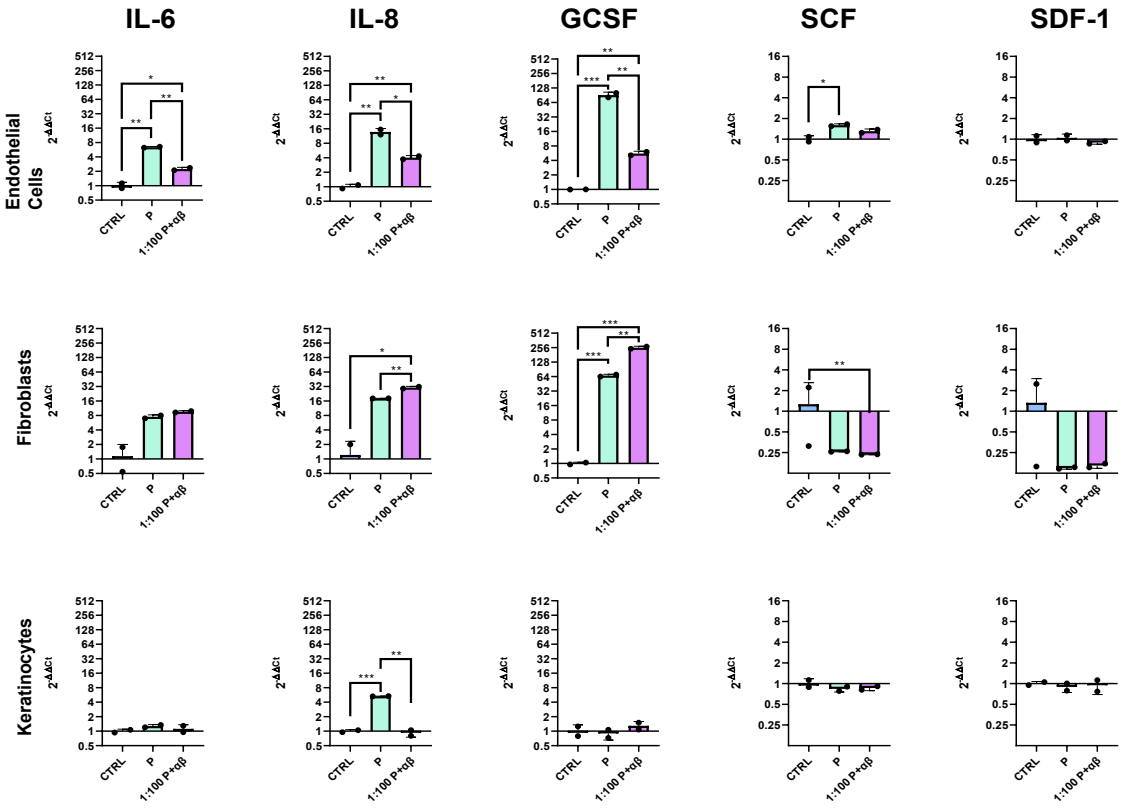


Figure 4-6. RT-qPCR mRNA expression analysis of IL-6, IL-8, GCSF, SCF, and SDF-1 in ECs, DFs, and Ks, separately cultured as monolayers (N = 2). For RT-qPCR analysis, statistics were compared using $\Delta\Delta C_t$ values. *p < 0.05; **p < 0.01; ***p < 0.001;

IL-6 upregulation, associated generally with a pro-inflammatory profile, was most pronounced in ECs and DFs[105]. IL-8 and GCSF, pro-inflammatory cytokines also typically associated with the terminal differentiation of HSPCs into PMNs, was elevated in ECs and DFs[106,107]. Notably, P stimulation caused the highest mRNA upregulation in ECs, whereas 1:100 P+αβ caused the highest upregulation in DFs. SCF and SDF-1 are associated with HSPC self-renewal and homing[98,108]. P stimulation of ECs produced a ~ 60% increase in mRNA expression of SCF, and DFs showed ~ 50% decrease in expression. SDF-1 expression was unchanged in ECs, DFs, and Ks. These results

suggest that ECs and DFs could support the differentiation of HSPCs into PMNs in an inflammatory milieu, though not long-term.

4.3.3 PMN and HSPC attachment and migration dynamics

To examine whether HSPCs might differentiate into PMNs, we next perfused both HSPCs and PMNs into the SC to evaluate differences in binding to an inflamed endothelium. PMNs were isolated from adult whole blood following an IRB approved protocol at the University of California, Davis, while HSPCs (Lonza) were thawed from cryopreserved aliquots. Both cell types were labeled with CellTracker™ to facilitate visualization and quantification, and resuspended in EGM-2 to a working concentration between 1 x 10^5 to 1 x 10^6 cells/mL. 20 µL of labeled cells were perfused into the vascular channel over 30 minutes (Figure 4-7).

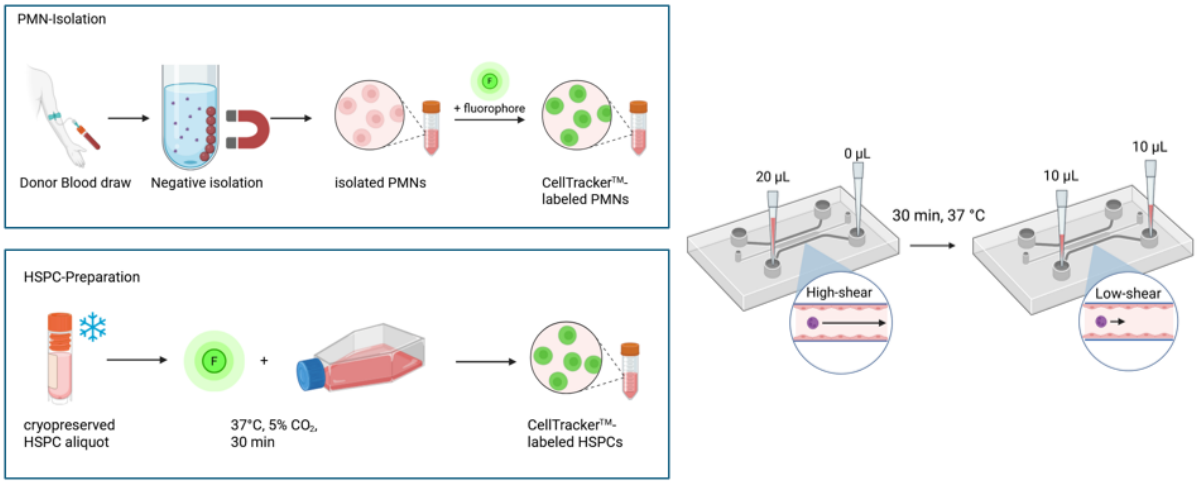


Figure 4-7. (Left) Graphical representation of PMN and HSPC isolation and labeling. (Right) Graphical representation of immune cell perfusion into the SC *via* a gravity-driven pressure differential between inlet and outlet tips. SCs are exposed to inflammatory stimuli to mimic bacterial infection for 4 hours prior to perfusion of immune cells.

After 30 minutes, 200 µL of EGM-2 was added to the inlet to wash out any unbound cells. Both HSPCs and PMNs robustly attach to the endothelium (Figure 4-8). αβ-stimulated endothelium in the SC captured approximately 7 and 5 times more

HSPCs and PMNs compared to unstimulated control, respectively (Figure 4-8). P and 1:100 P+αβ stimulated SCs captured HSPCs and PMNs in greater quantities than controls, though not to the same degree as αβ stimulation.

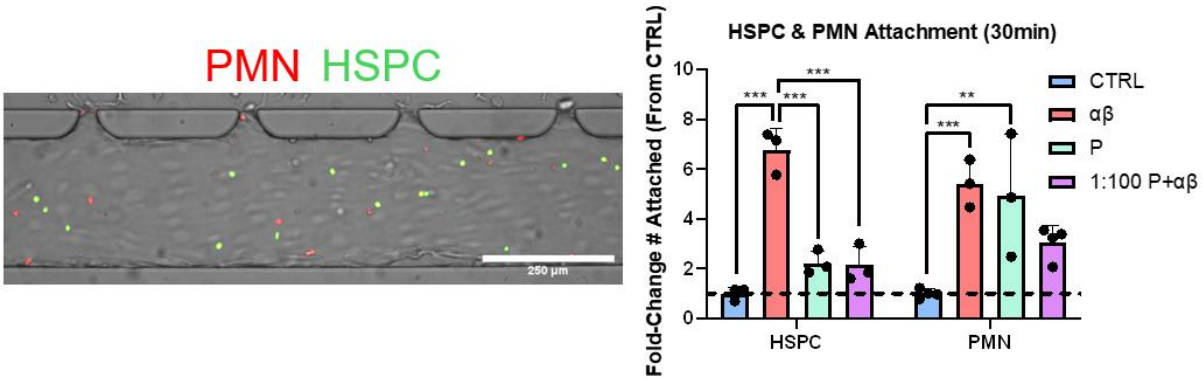


Figure 4-8. (Left) Confocal images 30 minutes post-perfusion showing PMNs (red) and HSPCs (green) bound to the endothelium of the vascular conduit of the SC following stimulation with TNF-α & IL-1β. (Right) Quantification of bound cells to ECs 30 minutes post-perfusion under different inflammatory stimuli of the SC normalized to control (CTRL).

Perfusing HSPCs and PMNs alone or simultaneously (total cell count constant) did not impact EC attachment (Figure 4-9).

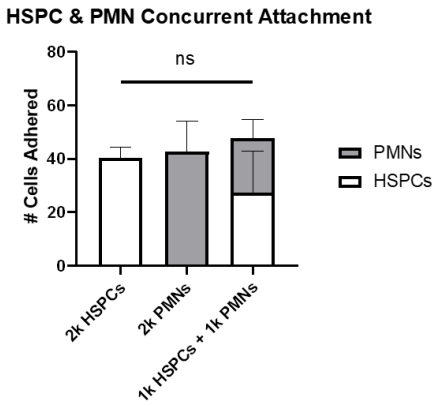


Figure 4-9. Either 2,000 HSPCs, 2,000 PMNs, or 1,000 HSPCs and 1,000 PMNs were perfused into the SC, and cell attachment quantified 30 minutes later (N = 3-5).

After flushing the SCs of unbound cells, around 50% of both HSPCs and PMNs that were initially bound to the αβ-stimulated EC after 30 minutes post-perfusion were

still found either on the EC surface or migrated into the dermal compartment 24 hours later (Figure 4-10).

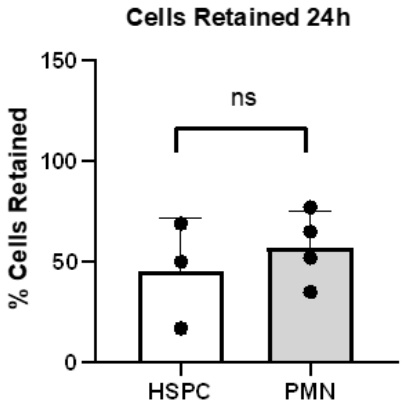


Figure 4-10. Percentage of attached cells at 30 minutes that remained bound to the EC or migrated into the central compartment of the SC 24-hours post-perfusion (N = 3-4).

However, over half of the PMNs found in the SC at 24 hours had migrated into the dermal compartment, whereas all the HSPCs remained attached to the endothelium (Figure 4-11). This remarkable difference between HSPCs and PMNs suggests a different mechanism by which each cell type might contribute to anti-bacterial function.

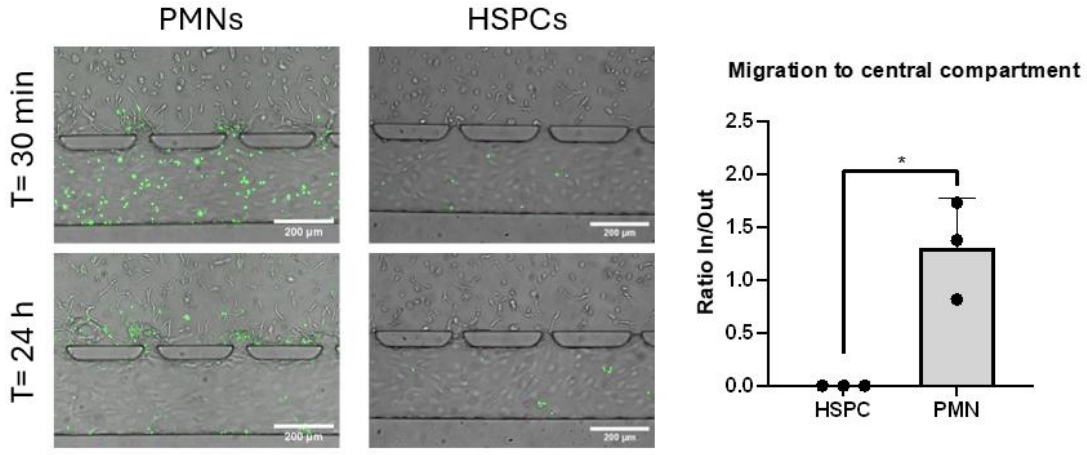


Figure 4-11.(Left) Static confocal images of HSPCs or PMNs (green) migrating into the central compartment over 24 hours and (Right) quantification of the ratio of the number of cells (HSPCs or PMNs) that migrated into the central compartment divided by the number that remained bound to the endothelium after 24 hours. *p < 0.05; **p < 0.01; ***p < 0.001; ****p < 0.0001.

4.3.4 The SDF-1/CXCR4 axis in cell binding and retention

SDF-1 is a chemokine that plays a key role in the homing and retention of HSPCs in their native bone marrow niche[109]. While the endothelial expression of SDF-1 was not impacted by inflammatory stimulation (Figure 4-6), we next examined whether the simple presence of SDF-1 on the endothelium and its binding axis with CXCR4 would potentially explain the tight binding of the HSPCs to the endothelium (Figure 4-11). The EC monolayer was stimulated with αβ for 4 hours before fixing and labeling with anti-SDF-1 antibody (Figure 4-12). Unlike ICAM-1 and VCAM-1, which significantly upregulate on the surface of ECs in the presence of pro-inflammatory factors, SDF-1 expression on the surface of ECs does not change with exogenous stimuli (Figure 4-12), consistent with the mRNA expression shown earlier.

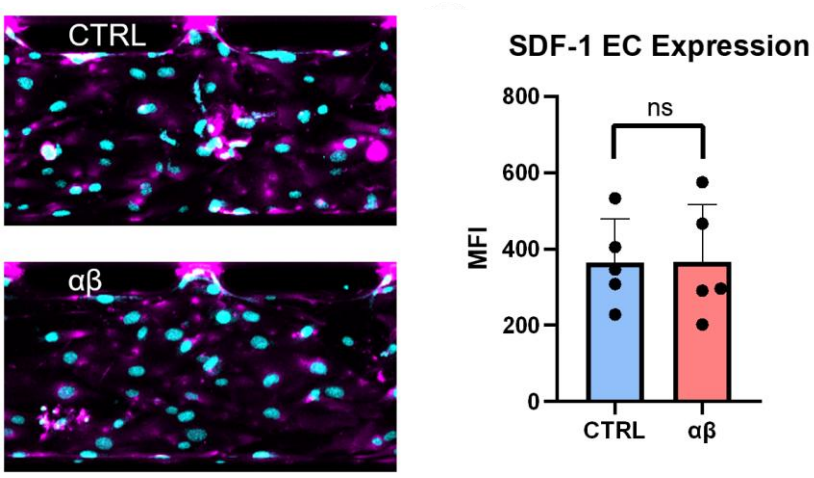


Figure 4-12. (Left) SDF-1 (magenta) expression and DAPI (cyan) in the EC layer in the SC stimulated with TNF-α & IL-1β (αβ) or CTRL for 4 hours. (Right) Quantification of ROIs (N = 5) from 2 SCs measuring the Mean Fluorescence Intensity (MFI) of surface SDF-1 expression of ECs.

We next tested whether an exogenous SDF-1 gradient known to drive migration of HSPCs could stimulate the transendothelial migration of attached HSPCs. 100 μg/mL of recombinant SDF-1 was added to the epidermal channel of a SC while maintaining a zero concentration in the vascular channel for 4 hours. In this experiment, the SC was

created in the absence of Ks to allow for robust diffusion and the subsequent concentration gradient of SDF-1 in the dermal compartment as we have shown earlier in a similar system[101]. HSPCs again attached to the inflamed endothelium 30 minutes post-perfusion but, again, were unable to migrate into the dermal compartment (Supplementary Figure 4-3).

Though SDF-1 supplementation did not impact HSPC retention, we probed whether disruption of binding to CXCR4 impaired the ability of HSPCs to bind to and be retained within the SC. Pre-incubation of the HSPCs or PMNs in AMD3100 (1 μM), a small molecule competitive inhibitor of CXCR4, before introducing into the SC did not impact initial binding (30 minutes) to the inflamed endothelium as expected (Figure 4-13).

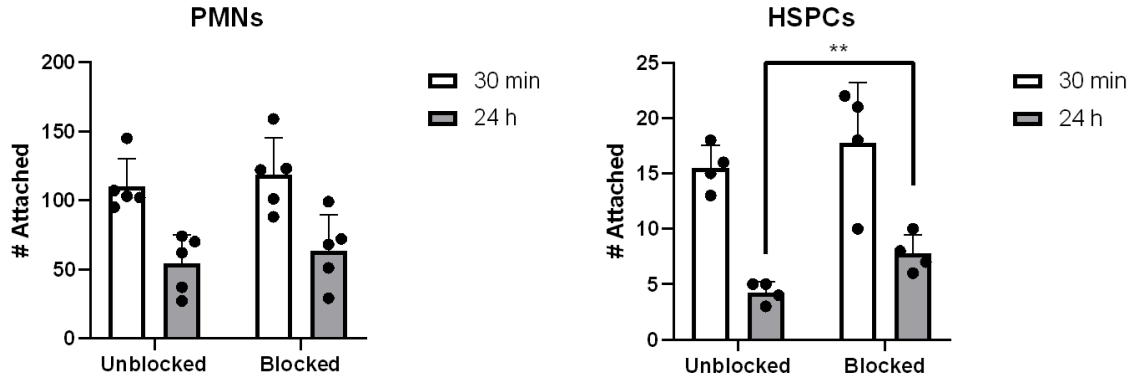


Figure 4-13. Attachment of PMNs and HSPCs to the inflamed (αβ) endothelium in the SC following blocking with 1 μM AMD3100 for 2 hours prior to perfusing into SC. *$p < 0.05$; **$p < 0.01$.

After 24 hours in the SC while continually exposing the cells to AMD3100, retained PMNs were lower as previously observed (Figure 4-10), but were not impacted by AMD3100. In contrast, HSPCs retained on the vascular endothelium were increased in the presence of AMD3100, though only slightly (Figure 4-13). Supplementation of SDF-1, or disruption of CXCR4 signaling did not lead to HSPC migration into the dermal

compartment. In fact, CXCR4 blocking improved HSPC retention on the endothelium. This effect was small but does suggest that disrupting the CXCR4 axis does not reduce HSPCs retention in the SC, contrasting observations in the bone marrow.

4.3.5 Anti-bacterial response of HSPC-derived granulocytes in SC

Since HSPCs were not observed to migrate into the dermis and undergo granulopoiesis, we next tested whether the HSPCs that could attach to the endothelium could undergo granulopoiesis in the vascular compartment. HSPCs were perfused into the inflamed (TNF-α and IL-1β) SC and any unbound cells after 30 minutes were flushed out. No evidence of HSPC differentiation was observed over the ensuing 14 days. In a follow-up experiment, we repeated the delivery of HSPCs into the inflamed SC, removed unbound cells after 30 minutes, except now supplemented the SC with granulopoietic expansion media (see methods) and incubated for two weeks. This condition resulted in the significant expansion of cells within the vascular compartment that phenotypically resembled PMNs (Figure 4-14).

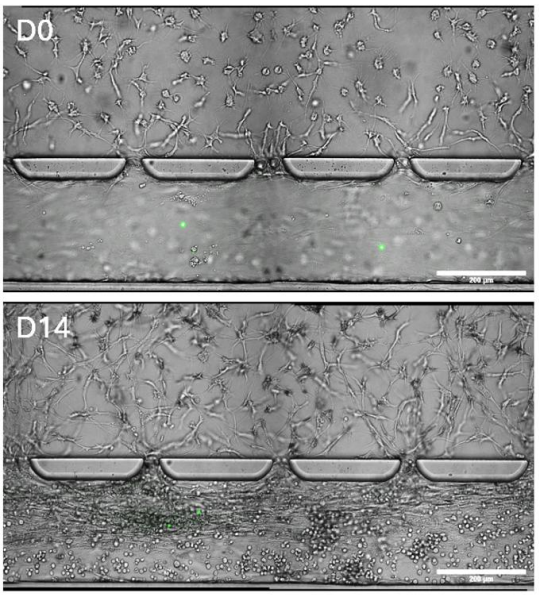


Figure 4-14. Confocal image of HSPCs (green) being perfused into the SC at day 0 (30 min post-perfusion). SCs were fed with granulopoietic expansion media on day 0 and allowed to incubate for 14 days with no shear. Confocal image of HSPCs expanded in SC after 14 days is shown.

To demonstrate that the expanded cells are functional, SCs were then perfused with pHrodo™ Zymosan Bioparticles™ at day 14 which confirmed that the cells in the vascular compartment were PMN-like and able to phagocytose bacterial material (Figure 4-15).

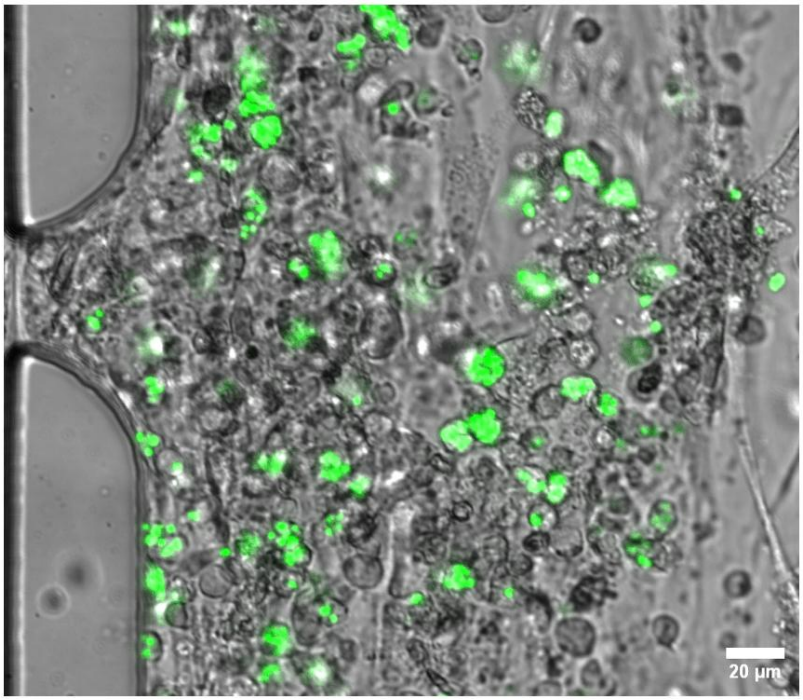


Figure 4-15. Close-up image of phagocytosis assay. At day 14, the SC was perfused with pHrodo™ Zymosan BioparticlesTM assay lysate, and HSPC-differentiated granulocytes are seen consuming zymosan particulate (green).

The expanded cells in the vascular compartment were also mobile but did not migrate into the dermis. HSPCs were also expanded in well plates outside the SC, and flow cytometry revealed a large portion, approximately 35%, are mature PMN-like granulocytes at day 14 of expansion (Supplementary Figure 4-4). Finally, to examine whether the HSPCs could differentiate in a pathogenic-specific manner that wound transcriptionally shift the phenotype of PMNs, HSPCs were perfused into SCs and differentiated for 14 days with granulopoietic expansion media either with or without supplemental Pam_3CSK_4 to simulate a bacterial infection. The PMN-like cells were then flushed out and processed for mRNA expression (Figure 4-16). LCN2 expression increased about 3-fold in cells treated with Pam3CSK4, whereas CAMP, CLEC7A, and MX1 all reduced their mRNA expression by around 50%, consistent with an anti-bacterial-specific response.

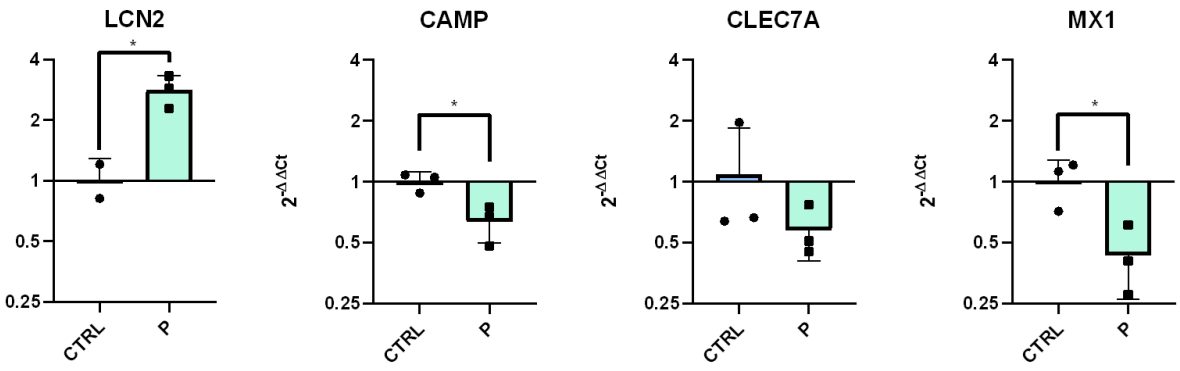


Figure 4-16. Immune cells in (Figure 4-15) were perfused out of the SC and collected. Subsequent RT-qPCR mRNA expression analysis of LCN2, CAMP, CLEC7A, and MX1 on those cells was performed. (N = 2-3). For RT-qPCR analysis, statistics were compared using $\Delta\Delta C_t$ values. *$p < 0.05$.

4.4 Discussion

We created a robust microfluidic human skin-on-a-chip model to gain insight into the mechanism(s) by which circulating HSPCs may contribute to anti-bacterial function. The SC model was comprised of a vascular compartment (endothelialized microfluidic channel), a dermal compartment (dermal fibroblasts in a fibrin gel), and an epidermal compartment (confluent layer of keratinocytes). HSPCs introduced into the vascular compartment at physiological shear robustly adhered to the inflamed endothelium. The HSPCs—unlike PMNs which could undergo transendothelial migration—remain localized in the vascular compartment. Over the course of two weeks, the SC supported the differentiation of PMN-like cells from the attached HSPCs. In addition, the differentiated cells demonstrated anti-bacterial functionality such as phagocytosis, and a phenotype consistent with a PMN targeting bacteria. These results suggest that HSPCs can contribute anti-bacterial function by undergoing local granulopoiesis within the vascular lumen and demonstrate the potential for HSPC-based therapy to combat resistant bacterial skin infections in humans.

Treating our SC with classic mediators of acute inflammation (TNF-α and IL-1β) produced a robust and appropriate upregulation of endothelial VCAM-1 and ICAM-1[97]. Both PMNs from adult peripheral blood and HSPCs showed enhanced attachment to the inflamed endothelium at a similar pattern and frequency at physiological shear. However, once attached, the two cell types showed markedly different behavior. More than 50% of the attached PMNs migrated across the endothelium and into the dermal compartment within 24 hours, whereas none of the HSPCs demonstrated this migration. PMNs engage three key mechanisms during transendothelial migration. First, high

surface expression of LFA-1 on PMNs[95] binds and activates ICAM-1 on the EC leading to cytoskeletal EC actin contraction and exploitable inter-endothelial cell gaps[110]. Second, PMNs have a small and malleable nucleus allowing the PMN to squeeze or fit through the larger gaps between the EC[102]. Third, the PMN secretes a host of proteolytic enzymes (MMP-8, MMP-9, neutrophil elastase, cathepsin G) to remodel the ECM of the basement membrane and interstitial tissue to facilitate migration[111]. In contrast, HSPCs have lower expression of LFA-1[91], have a more rigid nucleus[102,112], and secrete less proteolytic enzymes[113,114]. All these factors could contribute to our observation that HSPCs were unable to cross the endothelium and enter into the dermal channel.

The SDF-1/CXCR4 axis plays a critical role in the bone marrow microenvironment[98]. SDF-1 (CXCL12) is produced within the bone marrow by stromal and endothelial cells, and has been shown to be a key regulator and homing signal for CXCR4 expressing cells. HSPCs express CXCR4 which contributes to retention, survival, and quiescence[115,116]. As such, we investigated the possibility that SDF-1 expression within the vascular and dermal niches of the skin might play a similar role. ECFC-ECs cultured as monolayers do not create a detectable difference in SDF-1 mRNA expression when stimulated (Figure 4-6). Baseline SDF-1 expression is detectable on endothelial cells in the SC, though also no change in expression is detected when stimulated (Figure 4-12). This observation may be consistent with low levels of EC expression and the soluble nature of SDF-1 which can bind to ECM proteins. An imposed exogenous SDF-1 gradient did not stimulate HSPC transendothelial migration as seen in PMNs. We next observed that blocking CXCR4 on HSPCs led to a small but significant increase in

retention of the HSPCs 24 hours following initial attachment. Some reports state that moderate doses of SDF-1 act on CXCR4 during attachment and rolling by transiently increasing VLA-4 expression on cells and thus binding affinity to VCAM-1, which would increase retention of HSPCs in the vascular niche[117]. However, further studies note that excessively high ECM SDF-1 concentration may induce chemorepulsion. If the endothelium in our model expresses excessive SDF-1, this may explain HSPC retention[99,118]. Regardless, our results are not definitive in claiming CXCR4 blocking improves HSPC retention *via* this mechanism, but evidently disrupting the SDF-1/CXCR4 axis has no negative impact on retention of HSPCs in our model.

Our results are consistent with prior studies and confirm that transendothelial migration of HSPCs is a rare event[119]. Nonetheless, we considered the possibility that HSPCs could contribute anti-microbial activity in the skin by undergoing local granulopoiesis within the vascular compartment. This was based on our observation that HSPCs could, indeed, attach and remain attached to an inflamed endothelium, but also the observations by others that the microcirculation in a wound environment can collapse leading to a low-shear regime[120]. In this environment, PMNs from the systemic circulation have difficulty reaching the infection site in adequate numbers to replace expiring PMNs[121]. While HSPCs must overcome the same limitations within the circulation, far fewer of them need to arrive at the wound site, and they show extended longevity with the potential to undergo local granulopoiesis and self-renewal. Similar observations of granulopoiesis in low-shear vascular regimes of the liver has been reported[120,122]. Our observations support these findings, and challenge prior murine

studies about HSPC recruitment and local granulopoiesis that did not interrogate closely the exact location of HSPCs within a wound niche[20–22].

We observed local granulopoiesis of HSPCs in the SC, following the addition of an exogenous granulopoietic expansion media. This result would suggest that the skin microenvironment may not be able to support granulopoiesis *in vivo*. However, our SC model has only three cell types for simplicity, and the presence of other cells types *in vivo*—such as resident dermal macrophages, dendritic cells, and mast cells—may augment the environment for granulopoiesis through production of pro-granulopoietic chemokines naturally found in the bone marrow. Instigating granulopoiesis in vitro, has been reported by us[68] and others[123] using bone marrow specific stromal cells, but, as is the case in our current study, granulopoietic expansion media was necessary—highlighting the difficulty to recreate an appropriate in vitro environment for HSPC differentiation and expansion using only support cells. Importantly, our results show that ECs and dermal fibroblasts produce IL-6, IL-8, and GCSF which all contribute to terminal differentiation of HSPCs into PMNs in the skin niche[105–107]. Interestingly, we also observed that Pam_3CSK_4-inflamed ECs express higher SCF mRNA whereas DFs produce less. This is consistent with long-term replication of HSPCs without exhaustion during differentiation within the vascular niche.

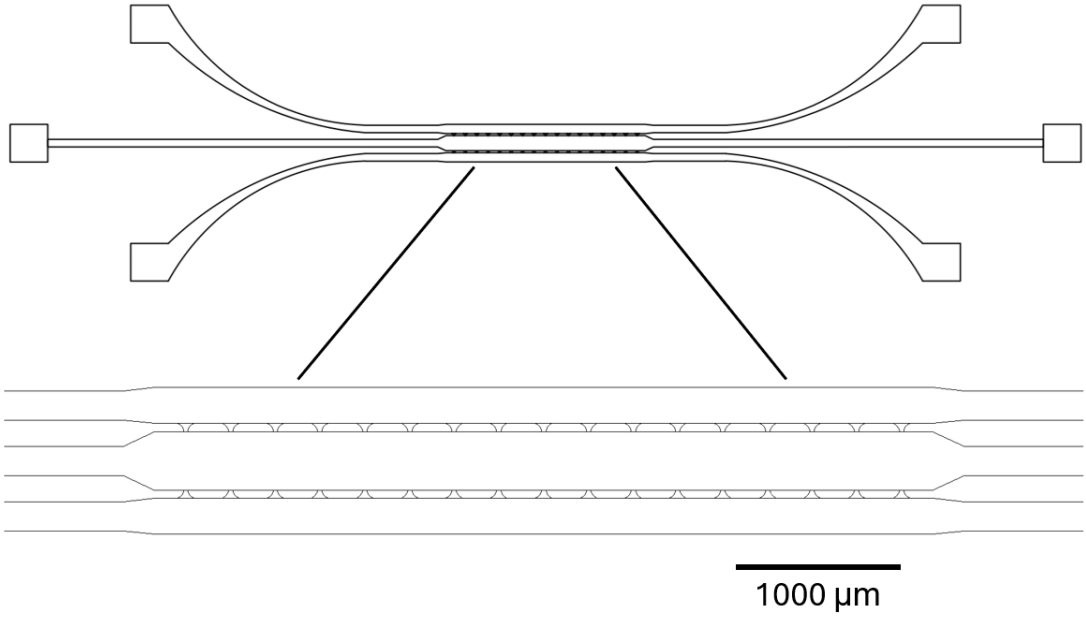
The PMN-like cells produced in the SC can phagocytose Zymosan particulate, consistent with anti-bacterial function. Previous studies using PMNs derived from mouse HSPCs (in encapsulated hydrogels cultured with similar granulopoietic expansion media for the delivery into skin wounds) also show phagocytic action of HSPC-derived PMNs, along with other immune-active properties such as CD11b

upregulation, reactive oxygen species (ROS) production and NETosis[93]. Our results also show that these derived PMNs, in the presence of Pam_3CSK_4, express more LCN2 (Lipocalin-2). LCN2 is an anti-bacterial protein responsible for depleting bacteria of iron needed for replication[124]. In contrast, expression of CLEC7A (antifungal[125]) and MX1 (antiviral[126]) was downregulated in the presence of Pam_3CSK_4. This gene expression pattern suggests that HSPCs can differentiate within the vascular niche in a manner specific to counteract the stimulus. Of note is our observation that CAMP (Cathelicidin, responsible for direct bacterial cell wall lysis[127]) was decreased in response to Pam_3CSK_4. A possible explanation of this finding is that CAMP is stored in PMN secondary granules of mature PMNs, and the PMN-like cells in the in the vascular niche in our model are relatively immature[16].

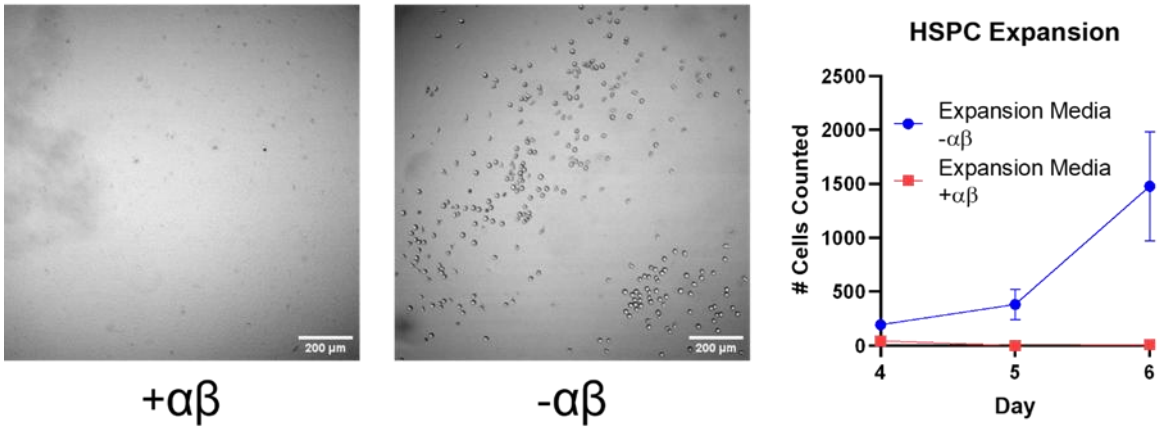
4.5 Conclusion

The SC platform presented here successfully recapitulates crucial features of inflammation in a model of human skin to examine interactions between HSPCs and PMNs with the skin microenvironment. The skin model was capable of responding to exogenous pro-inflammatory (e.g., TNF-α, IL-1β, Pam_3CSK_4) stimuli typically observed during infection by upregulating integrin pair markers ICAM-1 and VCAM-1, and increasing expression of pro-granulopoietic factors (e.g., IL-6, IL-8, GCSF, SCF). HSPCs and PMNs were thus able to robustly adhere to inflamed SCs, though PMNs were able to undergo transendothelial migration deeper into the SC dermis whereas HSPCs remained located in the vascular niche. A key finding of this study is the dissimilar migration capacities repeatedly observed between HSPCs and PMNs. An exogenous SDF-1 gradient was unsuccessful at triggering HSPC migration into the SC dermis. AMD3100 blocking of CXCR4 did not impair HSPC recruitment to the vascular channel. HSPCs that were expanded on the vasculature in the SC were capable of phagocytosis, a hallmark antibacterial function. Differentiated cells exposed to TLR2 agonist Pam_3CSK_4 expressed increased LCN2 and diminished CLEC7A and MX1 mRNA expression—indicative that PMN-like cells expanded in the presence of a particular stimulus adapt to counteract the source of the specific stimuli. Ultimately, this study offers novel insights into how HSPCs may undergo targeted, local granulopoiesis in the skin vasculature in a manner adaptive to the pathogen(s) present at the site of infection.

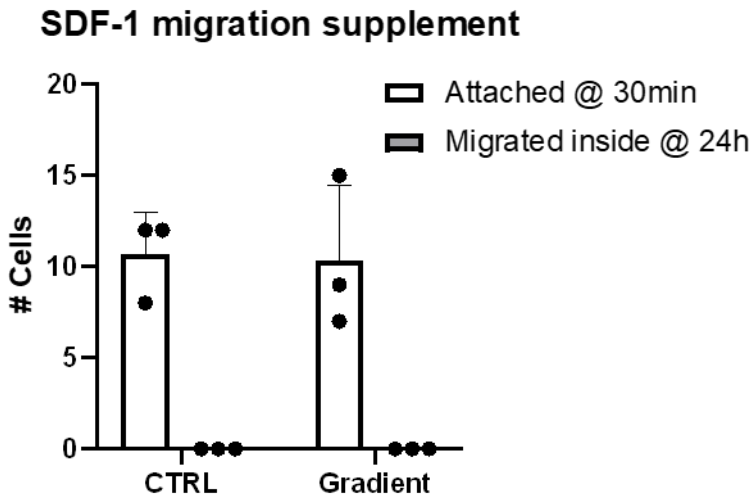
4.6 Supplemental Materials



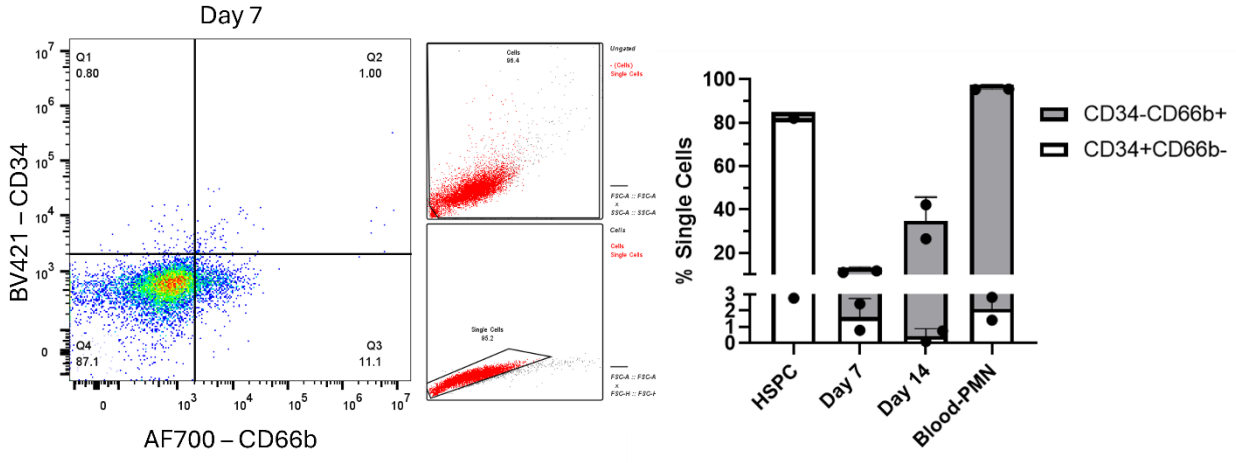
Supplementary Figure 4-1. (Top) CAD silhouette of the inside of the microfluidic device with (bottom) zoom in of internal channels.



Supplementary Figure 4-2. Brightfield images showing the expansion of HSPCs in well plates supplemented with granulopoietic expansion media either in the presence of αβ (left) or without (middle). (right) quantification of the expansion of HSPCs in well plates during the exponential growth phase. N = 4 from 4 different wells.



Supplementary Figure 4-3. The K channel of the SC was fed with EGM-2 with 100 ng/mL SDF-1 (Peprotech) and the bottom EC channel fed with solely EGM-2 for 4 hours before being perfused with HSPCs. CTRL consisted of no SDF-1 added. HSPCs bound in both the CTRL and gradient case in 30 minutes, though no HSPCs migrated into the central compartment in either after 24 hours.



Supplementary Figure 4-4. (Left) Flow cytometry graphs of the population distribution of HSPCs and PMNs of cells cultured for 7 days in a well plate in granulopoietic expansion media. (Right) Analysis of HSPC cultures expanded for 7 or 14 days (N = 2) compared to HSPC aliquots and blood-isolated PMNs. N = 1 for one aliquot of vendor-acquired HSPCs.

5 Chapter 5: Future Directions

These studies have culminated in creating a biological equivalent of skin that has been used to investigate the role of dermal granulopoiesis in humans. While the skin-on-a-chip model successfully identified a distinct divergence in mechanism between PMNs and HSPCs, it remains a simplified model. Translating these baseline microphysiological human findings into actionable clinical immunotherapies requires systematically increasing the biological, molecular, and pathogenic complexity of the microenvironment. Thus, we propose three specific investigative prongs that will guide the next studies in dermal granulopoiesis.

The first prong is increasing the biological sophistication of the SC model. The goal here is to try to move away from exogenous cytokine cocktails to support granulopoiesis and leverage endogenous cellular signaling. The resident skin cells already employed—endothelial cells, dermal fibroblasts, and keratinocytes—cannot sufficiently produce enough cytokines to drive granulopoiesis on their own. Therefore, the SC needs added resident immune cells to drive this response. The first cell type that should be investigated are dermal macrophages. Protocols exist that turn easily-cultured immortalized THP-1 monocytes into M2-like macrophages typically found in the dermis. Dermal macrophages are a primary source of G-CSF and IL-8 that would aid in vascular granulopoiesis without the aid of exogenous supplementation. These cells can easily be cultured in the lead-up time to culturing all the other cell types before perfusing them into the SC. Other cells that warrant individual investigation are dendritic cells—who promote wound healing and react to stress and inflammation—and mast cells—which quickly drive allergic responses and inflammation. A final option is to use a skin model

that incorporates skin tissue biopsies to provide the greatest biological similarity, but would result in large donor-to-donor differences.

Other studies should involve co-trafficking of PMNs with HSPCs. In a “pave the way” fashion, PMNs definitely undergo transendothelial migration in the SC model into deeper and more inflamed layers of the skin. This begs the question whether PMN diapedesis results in more permeable EC junctions and a reorganized ECM in the dermis that allows HSPCs to follow after. These studies can also be performed with monocytes and macrophages as above, but the ultimate goal is to repeat HSPC attachment and trafficking in the skin microenvironment with other blood-originated immune cells to observe differences in migration.

The second prong concerns further analysis of CXCR4/VLA-4/LFA-1 signaling on HSPCs and PMNs to alter attachment profiles that would highlight which mechanisms are most responsible for attachment and migration in the skin niche. It is crucial to move from broad chemical inhibition (AMD3100) to more precise genetic knockdowns to achieve more definitive and diverse results. Simple siRNA transfection of HSPCs and PMNs (whether primary-isolated or immortalized HL-60 cultures) would suffice to silence CXCR4, VLA-4, and LFA-1 receptors in these cells. Based on these studies, silencing of VLA-4 on HSPCs should significantly compromise their ability to bind to the SC. PMNs have very little VLA-4 and large quantities of LFA-1, so silencing LFA-1 should achieve the same effect. But importantly, silencing of CXCR4 on HSPCs will definitively answer our observation that CXCR4 signaling is not required for attachment and retention of HSPCs to the inflamed skin niche. Validating this result would be a significant discovery since it counters prior assumptions that the CXCR4/SDF-1

signaling axis is critical for HSPC retention—or, at least, it remains important in retention in the bone marrow, but not in extramedullary sites.

The final prong concerns incorporating pathogen-specific co-cultures into a skin model. This skin model can be the SC we already completed these studies with, or a new model described in this section. While our model incorporates Pam_3CSK_4, a synthetic peptide that robustly targets the TLR2 receptor that partially simulates bacterial infections, actual bacterial cultures would more completely recreate the antibacterial response in skin—for instance, targeting other antibacterial-sensors like Toll-like-receptor 4. This would include culturing and heat-inactivating *S. aureus* (Gram-positive) and *P. aeruginosa* (Gram-negative) and directly perfusing into the epidermal compartment to naturally allow factors to diffuse naturally down through the keratinocyte layer. However, our model of the skin creates such a tight barrier between the epidermal and dermal compartments, an “injured” model would need trialed, such as adding bacteria to both the epidermal and vascular compartments. This will help verify whether local human HSPCs differentiate into functionally distinct neutrophil subsets that selectively upregulate genes like LCN2 and downregulate others like MX1 based on the subset of bacterial strain species present. Perhaps the difference in bacterial strain (Gram positive versus negative) will elicit different responses in genetic adaptation as well.

In the future, we hope to take this skin model and adapt it to begin investigating macro-level clinical therapies in humans. By completing these prongs, the SC platform will develop into a highly predictive immunotherapy-screening tool. Deeper molecular understanding of human vascular granulopoiesis will ultimately unlock targeted cellular

therapies and advanced biomaterial-based interventions to safely treat intractable, chronic, or antibiotic-resistant infections in vulnerable, neutropenic patient populations.

6 Appendix

6.1 Glossary

AML	Acute myeloid leukemia
BMM-MPS	Bone marrow microenvironment MPS
BMSC	Bone marrow stromal cell
DAMP	Damage-associated molecular pattern
EC	Endothelial cell
ECM	Extracellular Matrix
EGFP-LysM	Enhanced green fluorescent protein-lysozyme M
FACS	Fluorescence-Activated Cell Sorting
FFLUC	Firefly luciferase
Flt3	FMS-like tyrosine kinase 3
G-CSF	Granulocyte-colony stimulating factor
GelMA	Gelatin Methacrylate
GEM	Granulopoietic Expansion Media
HSPC	Hematopoietic stem and progenitor cell
ICAM-1	Intracellular Adhesion Molecule 1
IL-3	Interleukin-3
IL-6	Interleukin-6
IVIS	In Vivo Imaging System
LFA-1	Lymphocyte Function-Associate Antigen 1
MMP	Matrix metalloprotease
MOMPS	Multi-organ microphysiological system
MPS	Microphysiological System
MRP8	Myeloid-related protein 8
MRSA	Methicillin-resistant Staphylococcus aureus
MSC	Mesenchymal stem cell
NET	Neutrophil Extracellular Trap
NHDF	Normal human dermal fibroblast
NHEK	Normal human epidermal keratinocyte
PDMS	Polydimethylsiloxane
PFA	Paraformaldehyde
PMA	Phorbol 12-myristate 13-acetate (PMA)
PMN	Polymorphonuclear leukocyte
Pγαβ	Pam3CSK4, IFN-γ, TNF-α, IL-1β (combined)
ROI	Region of interest
ROS	Reactive Oxygen Species
SCF	Stem cell factor
SDF-1/CXCL12	Stromal-Cell-Derived Factor 1
SM-MPS	Skin microenvironment MPS
TLR2	Toll-like receptor 2

VCAM-1	Vascular Cell Adhesion Molecule 1
VLA-4	Very Late Antigen 4

6.2 References Cited

1. Naghavi, M. *et al.* Global burden of bacterial antimicrobial resistance 1990–2021: a systematic analysis with forecasts to 2050. *The Lancet* **404**, 1199–1226 (2024).
2. Kuehnert, M. J. *et al.* Methicillin-resistant–Staphylococcus aureus Hospitalizations, United States. *Emerg. Infect. Dis.* **11**, 868–872 (2005).
3. Mölne, L., Verdrengh, M. & Tarkowski, A. Role of Neutrophil Leukocytes in Cutaneous Infection Caused by Staphylococcus aureus. *Infect. Immun.* **68**, 6162–6167 (2000).
4. Verdrengh, M. & Tarkowski, A. Role of neutrophils in experimental septicemia and septic arthritis induced by Staphylococcus aureus. *Infect. Immun.* **65**, 2517–2521 (1997).
5. Basu, S., Hodgson, G., Katz, M. & Dunn, A. R. Evaluation of role of G-CSF in the production, survival, and release of neutrophils from bone marrow into circulation. *Blood* **100**, 854–861 (2002).
6. Cheretakis, C., Leung, R., Sun, C. X., Dror, Y. & Glogauer, M. Timing of neutrophil tissue repopulation predicts restoration of innate immune protection in a murine bone marrow transplantation model. *Blood* **108**, 2821–2826 (2006).
7. Furze, R. C. & Rankin, S. M. Neutrophil mobilization and clearance in the bone marrow. *Immunology* **125**, 281–288 (2008).
8. Young, R. L. *et al.* Neutrophil extracellular trap (NET)-mediated killing of Pseudomonas aeruginosa: evidence of acquired resistance within the CF airway, independent of CFTR. *PloS One* **6**, e23637 (2011).
9. Brinkmann, V. *et al.* Neutrophil extracellular traps kill bacteria. *Science* **303**, 1532–1535 (2004).
10. Winterbourn, C. C., Kettle, A. J. & Hampton, M. B. Reactive Oxygen Species and Neutrophil Function. *Annu. Rev. Biochem.* **85**, 765–792 (2016).
11. Lee, W. L., Harrison, R. E. & Grinstein, S. Phagocytosis by neutrophils. *Microbes Infect.* **5**, 1299–1306 (2003).
12. Hämäläinen, S. *et al.* Neutropenic fever and severe sepsis in adult acute myeloid leukemia (AML) patients receiving intensive chemotherapy: Causes and consequences. *Leuk. Lymphoma* **49**, 495–501 (2008).
13. Sung, L. *et al.* Effectiveness of supportive care measures to reduce infections in pediatric AML: a report from the Children's Oncology Group. *Blood* **121**, 3573–3577 (2013).
14. Valle, A. *et al.* Reduction of Circulating Neutrophils Precedes and Accompanies Type 1 Diabetes. *Diabetes* **62**, 2072–2077 (2013).
15. Urao, N., Liu, J., Takahashi, K. & Ganesh, G. Hematopoietic Stem Cells in Wound Healing Response. *Adv. Wound Care* **11**, 598–621 (2022).
16. Malengier-Devlies, B., Metzemaekers, M., Wouters, C., Proost, P. & Matthys, P. Neutrophil Homeostasis and Emergency Granulopoiesis: The Example of Systemic Juvenile Idiopathic Arthritis. *Front. Immunol.* **12**, 766620 (2021).
17. Kim, C. H. Homeostatic and pathogenic extramedullary hematopoiesis. *J. Blood Med.* **1**, 13–19 (2010).
18. Yáñez, A. *et al.* Detection of a TLR2 agonist by hematopoietic stem and progenitor cells (HSPCs) impacts the function of the macrophages they produce. *Eur. J. Immunol.* **43**, 2114–2125 (2013).

19. Paudel, S., Ghimire, L., Jin, L., Jeansonne, D. & Jeyaseelan, S. Regulation of emergency granulopoiesis during infection. *Front. Immunol.* **13**, (2022).
20. Kim, M.-H. *et al.* Neutrophil survival and c-kit+-progenitor proliferation in Staphylococcus aureus–infected skin wounds promote resolution. *Blood* **117**, 3343–3352 (2011).
21. Granick, J. L. *et al.* Staphylococcus aureus recognition by hematopoietic stem and progenitor cells via TLR2/MyD88/PGE2 stimulates granulopoiesis in wounds. *Blood* **122**, 1770–1778 (2013).
22. Falahee, P. C. *et al.* α-Toxin Regulates Local Granulocyte Expansion from Hematopoietic Stem and Progenitor Cells in *Staphylococcus aureus*– Infected Wounds. *J. Immunol.* **199**, 1772–1782 (2017).
23. Yamada, M. *et al.* Bone marrow-derived progenitor cells are important for lung repair after lipopolysaccharide-induced lung injury. *J. Immunol.* **172**, 1266–1272 (2004).
24. Si, Y., Tsou, C.-L., Croft, K. & Charo, I. F. CCR2 mediates hematopoietic stem and progenitor cell trafficking to sites of inflammation in mice. *J. Clin. Invest.* **120**, 1192–1203 (2010).
25. Hirai, H. *et al.* C/EBPβ is required for 'emergency' granulopoiesis. *Nat. Immunol.* **7**, 732–739 (2006).
26. Nauseef, W. M. & Borregaard, N. Neutrophils at work. *Nat. Immunol.* **15**, 602–611 (2014).
27. Marfin, A. A. & Price, T. H. Granulocyte Transfusion Therapy. *J. Intensive Care Med.* **30**, 79–88 (2015).
28. Torres-Acosta, M. A., Harrison, R. P., Csaszar, E., Rito-Palomares, M. & Brunck, M. E. G. Ex vivo Manufactured Neutrophils for Treatment of Neutropenia—A Process Economic Evaluation. *Front. Med.* **6**, (2019).
29. Silva, E. A., Kim, E.-S., Kong, H. J. & Mooney, D. J. Material-based deployment enhances efficacy of endothelial progenitor cells. *Proc. Natl. Acad. Sci.* **105**, 14347–14352 (2008).
30. Sleep, E. *et al.* Injectable biomimetic liquid crystalline scaffolds enhance muscle stem cell transplantation. *Proc. Natl. Acad. Sci.* **114**, E7919–E7928 (2017).
31. Rustad, K. C. *et al.* Enhancement of mesenchymal stem cell angiogenic capacity and stemness by a biomimetic hydrogel scaffold. *Biomaterials* **33**, 80–90 (2012).
32. Gonzalez-Fernandez, T., Sikorski, P. & Leach, J. K. Bio-instructive materials for musculoskeletal regeneration. *Acta Biomater.* **96**, 20–34 (2019).
33. Kolaczkowska, E. & Kubes, P. Neutrophil recruitment and function in health and inflammation. *Nat. Rev. Immunol.* **13**, 159–175 (2013).
34. Mahadik, B. P., Bharadwaj, N. A. K., Ewoldt, R. H. & Harley, B. A. C. Regulating dynamic signaling between hematopoietic stem cells and niche cells via a hydrogel matrix. *Biomaterials* **125**, 54–64 (2017).
35. Gilchrist, A. E., Lee, S., Hu, Y. & Harley, B. A. C. Soluble Signals and Remodeling in a Synthetic Gelatin-Based Hematopoietic Stem Cell Niche. *Adv. Healthc. Mater.* **8**, 1900751 (2019).
36. Faust, N., Varas, F., Kelly, L. M., Heck, S. & Graf, T. Insertion of enhanced green fluorescent protein into the lysozyme gene creates mice with green fluorescent granulocytes and macrophages. *Blood* **96**, 719–726 (2000).

37. Kim, M.-H. *et al.* Dynamics of Neutrophil Infiltration during Cutaneous Wound Healing and Infection Using Fluorescence Imaging. *J. Invest. Dermatol.* **128**, 1812–20 (2008).
38. Safran, M. *et al.* Mouse Reporter Strain for Noninvasive Bioluminescent Imaging of Cells that have Undergone Cre-Mediated Recombination. *Mol. Imaging* **2**, 15353500200303154 (2003).
39. Wang, G. *et al.* Identification of the Transgene Integration Site and Host Genome Changes in MRP8-Cre/ires-EGFP Transgenic Mice by Targeted Locus Amplification. *Front. Immunol.* **13**, (2022).
40. Gresham, R. C. H., Kumar, D., Copp, J., Lee, M. A. & Leach, J. K. Characterization of Induction and Targeting of Senescent Mesenchymal Stromal Cells. *Tissue Eng. Part C Methods* **28**, 239–249 (2022).
41. Gonzalez-Fernandez, T., Tenorio, A. J., Campbell, K. T., Silva, E. A. & Leach, J. K. Alginate-Based Bioinks for 3D Bioprinting and Fabrication of Anatomically Accurate Bone Grafts. *Tissue Eng. Part A* **27**, 1168–1181 (2021).
42. Campbell, K. T., Stilhano, R. S. & Silva, E. A. Enzymatically degradable alginate hydrogel systems to deliver endothelial progenitor cells for potential revasculature applications. *Biomaterials* **179**, 109–121 (2018).
43. Vigata, M. *et al.* Gelatin Methacryloyl Hydrogels for the Localized Delivery of Cefazolin. *Polymers* **13**, 3960 (2021).
44. Jansen, L. E., Birch, N. P., Schiffman, J. D., Crosby, A. J. & Peyton, S. R. Mechanics of intact bone marrow. *J. Mech. Behav. Biomed. Mater.* **50**, 299–307 (2015).
45. Anderson, L. S., Reynolds, M. B., Rivara, K. R., Miller, L. S. & Simon, S. I. A Mouse Model to Assess Innate Immune Response to Staphylococcus aureus Infection. *J. Vis. Exp. JoVE* 10.3791/59015 (2019) doi:10.3791/59015.
46. Parks, W. C., Wilson, C. L. & López-Boado, Y. S. Matrix metalloproteinases as modulators of inflammation and innate immunity. *Nat. Rev. Immunol.* **4**, 617–629 (2004).
47. Wysoczynski, M. *et al.* Defective engraftment of C3aR−/− hematopoietic stem progenitor cells shows a novel role of the C3a–C3aR axis in bone marrow homing. *Leukemia* **23**, 1455–1461 (2009).
48. Dixit, N. & Simon, S. I. Chemokines, selectins and intracellular calcium flux: temporal and spatial cues for leukocyte arrest. *Front. Immunol.* **3**, (2012).
49. Timmins, N. E. *et al.* Clinical scale ex vivo manufacture of neutrophils from hematopoietic progenitor cells. *Biotechnol. Bioeng.* **104**, 832–840 (2009).
50. Pluen, A., Netti, P. A., Jain, R. K. & Berk, D. A. Diffusion of Macromolecules in Agarose Gels: Comparison of Linear and Globular Configurations. *Biophys. J.* **77**, 542–552 (1999).
51. van Donkelaar, C. C., Chao, G., Bader, D. L. & Oomens, C. W. J. A reaction–diffusion model to predict the influence of neo-matrix on the subsequent development of tissue-engineered cartilage. *Comput. Methods Biomech. Biomed. Engin.* **14**, 425–432 (2011).
52. Hasty, K. A., Hibbs, M. S., Kang, A. H. & Mainardi, C. L. Secreted forms of human neutrophil collagenase. *J. Biol. Chem.* **261**, 5645–5650 (1986).

53. Markart, P., Korfhagen, T. R., Weaver, T. E. & Akinbi, H. T. Mouse Lysozyme M Is Important in Pulmonary Host Defense against Klebsiella pneumoniae Infection. *Am. J. Respir. Crit. Care Med.* **169**, 454–458 (2004).
54. Cappenberg, A., Kardell, M. & Zarbock, A. Selectin-Mediated Signaling-Shedding Light on the Regulation of Integrin Activity in Neutrophils. *Cells* **11**, 1310 (2022).
55. Weber, G. F. *et al.* Interleukin-3 amplifies acute inflammation and is a potential therapeutic target in sepsis. *Science* **347**, 1260–1265 (2015).
56. Borish, L., Rosenbaum, R., Albury, L. & Clark, S. Activation of neutrophils by recombinant interleukin 6. *Cell. Immunol.* **121**, 280–289 (1989).
57. Kienle, K. *et al.* Neutrophils self-limit swarming to contain bacterial growth in vivo. *Science* **372**, eabe7729 (2021).
58. Ali, H., Richardson, R. M., Haribabu, B. & Snyderman, R. Chemoattractant Receptor Cross-desensitization*. *J. Biol. Chem.* **274**, 6027–6030 (1999).
59. Pineault, N. & Abu-Khader, A. Advances in umbilical cord blood stem cell expansion and clinical translation. *Exp. Hematol.* **43**, 498–513 (2015).
60. Heltmann-Meyer, S. *et al.* Gelatin methacryloyl is a slow degrading material allowing vascularization and long-term use in vivo. *Biomed. Mater.* **16**, 065004 (2021).
61. Sansbury, B. E. & Spite, M. Resolution of Acute Inflammation and the Role of Resolvins in Immunity, Thrombosis, and Vascular Biology. *Circ. Res.* **119**, 113–130 (2016).
62. Low, L. A., Mummery, C., Berridge, B. R., Austin, C. P. & Tagle, D. A. Organs-on-chips: into the next decade. *Nat. Rev. Drug Discov.* **20**, 345–361 (2021).
63. Ingber, D. E. Human organs-on-chips for disease modelling, drug development and personalized medicine. *Nat. Rev. Genet.* **23**, 467–491 (2022).
64. Yang, J. *et al.* Integrated-gut-liver-on-a-chip platform as an in vitro human model of non-alcoholic fatty liver disease. *Commun. Biol.* **6**, 310 (2023).
65. Choe, A., Ha, S. K., Choi, I., Choi, N. & Sung, J. H. Microfluidic Gut-liver chip for reproducing the first pass metabolism. *Biomed. Microdevices* **19**, 4 (2017).
66. Ronaldson-Bouchard, K. *et al.* A multi-organ chip with matured tissue niches linked by vascular flow. *Nat. Biomed. Eng.* **6**, 351–371 (2022).
67. Zhang, Y. S. *et al.* Multisensor-integrated organs-on-chips platform for automated and continual in situ monitoring of organoid behaviors. *Proc. Natl. Acad. Sci. U. S. A.* **114**, E2293–E2302 (2017).
68. Glaser, D. E. *et al.* Organ-on-a-chip model of vascularized human bone marrow niches. *Biomaterials* **280**, 121245 (2022).
69. Cho, H., Kim, H.-Y., Kang, J. Y. & Kim, T. S. How the capillary burst microvalve works. *J. Colloid Interface Sci.* **306**, 379–385 (2007).
70. Moya, M. L., Hsu, Y.-H., Lee, A. P., Hughes, C. C. W. & George, S. C. In Vitro Perfused Human Capillary Networks. *Tissue Eng. Part C Methods* **19**, 730–737 (2013).
71. Ingram, D. A. *et al.* Identification of a novel hierarchy of endothelial progenitor cells using human peripheral and umbilical cord blood. *Blood* **104**, 2752–2760 (2004).
72. Shihan, M. H., Novo, S. G., Le Marchand, S. J., Wang, Y. & Duncan, M. K. A simple method for quantitating confocal fluorescent images. *Biochem. Biophys. Rep.* **25**, 100916 (2021).

73. Funderburg, N. T. *et al.* The Toll-like receptor 1/2 agonists Pam3CSK4 and human β-defensin-3 differentially induce interleukin-10 and nuclear factor-κB signalling patterns in human monocytes. *Immunology* **134**, 151–160 (2011).
74. Tsolmongyn, B. *et al.* A Toll-like receptor 2 ligand, Pam3CSK4, augments interferon-γ-induced nitric oxide production via a physical association between MyD88 and interferon-γ receptor in vascular endothelial cells. *Immunology* **140**, 352–361 (2013).
75. Shirure, V. S. *et al.* Mitigating neutrophil trafficking and cardiotoxicity with DS-IkL in a microphysiological system of a cytokine storm. *Lab. Chip* **23**, 3050–3061 (2023).
76. Döhrmann, S., Cole, J. N. & Nizet, V. Conquering Neutrophils. *PLOS Pathog.* **12**, e1005682 (2016).
77. Rhythmic Modulation of the Hematopoietic Niche through Neutrophil Clearance: Cell. https://www.cell.com/fulltext/S0092-8674(13)00516-3.
78. Chen, X. *et al.* Rapid anastomosis of endothelial progenitor cell-derived vessels with host vasculature is promoted by a high density of cotransplanted fibroblasts. *Tissue Eng. Part A* **16**, 585–594 (2010).
79. Shirure, V. S. *et al.* Tumor-on-a-chip platform to investigate progression and drug sensitivity in cell lines and patient-derived organoids. *Lab. Chip* **18**, 3687–3702 (2018).
80. Shirure, V. S., Lezia, A., Tao, A., Alonzo, L. F. & George, S. C. Low levels of physiological interstitial flow eliminate morphogen gradients and guide angiogenesis. *Angiogenesis* **20**, 493–504 (2017).
81. Shirure, V. S., Lezia, A., Tao, A., Alonzo, L. F. & George, S. C. Low levels of physiological interstitial flow eliminate morphogen gradients and guide angiogenesis. *Angiogenesis* **20**, 493–504 (2017).
82. Koenig, L. *et al.* A microfluidic bone marrow chip for the safety profiling of biologics in pre-clinical drug development. *Commun. Biol.* **8**, 754 (2025).
83. Chou, D. B. *et al.* On-chip recapitulation of clinical bone marrow toxicities and patient-specific pathophysiology. *Nat. Biomed. Eng.* **4**, 394–406 (2020).
84. Marturano-Kruik, A. *et al.* Human bone perivascular niche-on-a-chip for studying metastatic colonization. *Proc. Natl. Acad. Sci.* **115**, 1256–1261 (2018).
85. Rognoni, E. & Watt, F. M. Skin Cell Heterogeneity in Development, Wound Healing, and Cancer. *Trends Cell Biol.* **28**, 709–722 (2018).
86. Steele, L. *et al.* A single-cell and spatial genomics atlas of human skin fibroblasts reveals shared disease-related fibroblast subtypes across tissues. https://doi.org/10.1038/s41590-025-02267-8 (2025) doi:10.1038/s41590-025-02267-8.
87. Wang, L., Wang, B., Kou, E., Du, L. & Zhu, Y. New insight into the role of fibroblasts in the epithelial immune microenvironment in the single-cell era. *Front. Immunol.* **14**, (2023).
88. Yao, C. *et al.* Toll-like receptor family members in skin fibroblasts are functional and have a higher expression compared to skin keratinocytes. *Int. J. Mol. Med.* **35**, 1443–1450 (2015).
89. Zheng, X.-Q. *et al.* Treponema pallidum recombinant protein Tp47 enhanced interleukin-6 secretion in human dermal fibroblasts through the toll-like receptor 2 via

the p38, PI3K/Akt, and NF-κB signalling pathways. *Biochim. Biophys. Acta Mol. Cell Res.* **1870**, 119540 (2023).
90. Jiang, Y. *et al.* Cytokinocytes: the diverse contribution of keratinocytes to immune responses in skin. *JCI Insight* **5**, e142067.
91. Pruijt, J. F. M., van Kooyk, Y., Figdor, C. G., Willemze, R. & Fibbe, W. E. Murine Hematopoietic Progenitor Cells With Colony-Forming or Radioprotective Capacity Lack Expression of the β2-Integrin LFA-1. *Blood* **93**, 107–112 (1999).
92. Bonilla, M. C. *et al.* How Long Does a Neutrophil Live?—The Effect of 24 h Whole Blood Storage on Neutrophil Functions in Pigs. *Biomedicines* **8**, 278 (2020).
93. Cirves, E. *et al.* Neutrophil Granulopoiesis Optimized Through Ex Vivo Expansion of Hematopoietic Progenitors in Engineered 3D Gelatin Methacrylate Hydrogels. *Adv. Healthc. Mater.* **n/a**, 2301966.
94. Fekadu, J., Modlich, U., Bader, P. & Bakhtiar, S. Understanding the Role of LFA-1 in Leukocyte Adhesion Deficiency Type I (LAD I): Moving towards Inflammation? *Int. J. Mol. Sci.* **23**, 3578 (2022).
95. Lefort, C. T. & Ley, K. Neutrophil arrest by LFA-1 activation. *Front. Immunol.* **3**, 157 (2012).
96. Ruminski, P. G., Rettig, M. P. & DiPersio, J. F. Development of VLA4 and CXCR4 Antagonists for the Mobilization of Hematopoietic Stem and Progenitor Cells. *Biomolecules* **14**, 1003 (2024).
97. Spoelstra, F. M., Postma, D. S., Hovenga, H., Noordhoek, J. A. & Kauffman, H. F. Interferon-gamma and interleukin-4 differentially regulate ICAM-1 and VCAM-1 expression on human lung fibroblasts. *Eur. Respir. J.* **14**, 759–766 (1999).
98. Vagima, Y. *et al.* Pathways implicated in stem cell migration: the SDF-1/CXCR4 axis. *Methods Mol. Biol. Clifton NJ* **750**, 277–289 (2011).
99. Vianello, F. *et al.* Murine B16 Melanomas Expressing High Levels of the Chemokine Stromal-Derived Factor-1/CXCL12 Induce Tumor-Specific T Cell Chemorepulsion and Escape from Immune Control1. *J. Immunol.* **176**, 2902–2914 (2006).
100. Vianello, F., Olszak, I. T. & Poznansky, M. C. Fugetaxis: active movement of leukocytes away from a chemokinetic agent. *J. Mol. Med.* **83**, 752–763 (2005).
101. Hwang, P. Y., Brenot, A., King, A. C., Longmore, G. D. & George, S. C. Randomly Distributed K14+ Breast Tumor Cells Polarize to the Leading Edge and Guide Collective Migration in Response to Chemical and Mechanical Environmental Cues. *Cancer Res.* **79**, 1899–1912 (2019).
102. Manley, H. R., Keightley, M. C. & Lieschke, G. J. The Neutrophil Nucleus: An Important Influence on Neutrophil Migration and Function. *Front. Immunol.* **9**, 2867 (2018).
103. Chun, N. *et al.* T cell–derived tumor necrosis factor induces cytotoxicity by activating RIPK1-dependent target cell death. *JCI Insight* **6**, (2021).
104. Chan, F. K.-M. *et al.* A Role for Tumor Necrosis Factor Receptor-2 and Receptor-interacting Protein in Programmed Necrosis and Antiviral Responses *. *J. Biol. Chem.* **278**, 51613–51621 (2003).
105. Tanaka, T., Narazaki, M. & Kishimoto, T. IL-6 in Inflammation, Immunity, and Disease. *Cold Spring Harb. Perspect. Biol.* **6**, a016295 (2014).

106. Hageb, A., Farjia, M., Osei-Sarpong, C. & Silvestre-Roig, C. Ontogenetic drivers of neutrophil heterogeneity. *Exp. Hematol.* **151**, 104863 (2025).
107. Laterveer, L., Lindley, I. J. D., Hamilton, M. S., Willemze, R. & Fibbe, W. E. Interleukin-8 Induces Rapid Mobilization of Hematopoietic Stem Cells With Radioprotective Capacity and Long-Term Myelolymphoid Repopulating Ability. *Blood* **85**, 2269–2275 (1995).
108. Friel, J., Heberlein, C., Itoh, K. & Ostertag, W. Role of the stem cell factor (SCF) receptor and the alternative forms of its ligand (SCF) in the induction of long-term growth by stroma cells. *Leukemia* **11 Suppl 3**, 493–495 (1997).
109. Zabel, B. A. *et al.* Elucidation of CXCR7-mediated signaling events and inhibition of CXCR4-mediated tumor cell transendothelial migration by CXCR7 ligands. *J. Immunol.* **183**, 3204–3211 (2009).
110. Bui, T. M., Wiesolek, H. L. & Sumagin, R. ICAM-1: A master regulator of cellular responses in inflammation, injury resolution, and tumorigenesis. *J. Leukoc. Biol.* **108**, 787–799 (2020).
111. Zhu, Y. *et al.* Interplay between Extracellular Matrix and Neutrophils in Diseases. *J. Immunol. Res.* **2021**, 8243378 (2021).
112. Biedzinski, S. *et al.* Microtubules control nuclear shape and gene expression during early stages of hematopoietic differentiation. *EMBO J.* **39**, e103957 (2020).
113. Winkler, I. G., Hendy, J., Coughlin, P., Horvath, A. & Lévesque, J.-P. Serine protease inhibitors serpina1 and serpina3 are down-regulated in bone marrow during hematopoietic progenitor mobilization. *J. Exp. Med.* **201**, 1077–1088 (2005).
114. Lévesque, J.-P. *et al.* Mobilization by either cyclophosphamide or granulocyte colony-stimulating factor transforms the bone marrow into a highly proteolytic environment. *Exp. Hematol.* **30**, 440–449 (2002).
115. Singh, P., Mohammad, K. S. & Pelus, L. M. CXCR4 expression in the bone marrow microenvironment is required for hematopoietic stem and progenitor cell maintenance and early hematopoietic regeneration after myeloablation. *Stem Cells Dayt. Ohio* **38**, 849–859 (2020).
116. Ma, Q., Jones, D. & Springer, T. A. The chemokine receptor CXCR4 is required for the retention of B lineage and granulocytic precursors within the bone marrow microenvironment. *Immunity* **10**, 463–471 (1999).
117. Grabovsky, V. *et al.* Subsecond Induction of α4 Integrin Clustering by Immobilized Chemokines Stimulates Leukocyte Tethering and Rolling on Endothelial Vascular Cell Adhesion Molecule 1 under Flow Conditions. *J. Exp. Med.* **192**, 495–506 (2000).
118. Seo, Y. D. *et al.* Mobilization of CD8+ T cells via CXCR4 blockade facilitates PD-1 checkpoint therapy in human pancreatic cancer. *Clin. Cancer Res. Off. J. Am. Assoc. Cancer Res.* **25**, 3934–3945 (2019).
119. Peled, A. *et al.* The chemokine SDF-1 stimulates integrin-mediated arrest of $CD34^+$ cells on vascular endothelium under shear flow. *J. Clin. Invest.* **104**, 1199–1211 (1999).
120. Mendt, M. & Cardier, J. E. Role of SDF-1 (CXCL12) in regulating hematopoietic stem and progenitor cells traffic into the liver during extramedullary hematopoiesis induced by G-CSF, AMD3100 and PHZ. *Cytokine* **76**, 214–221 (2015).

121. Shen, X., Cao, K., Jiang, J., Guan, W. & Du, J. Neutrophil dysregulation during sepsis: an overview and update. *J. Cell. Mol. Med.* **21**, 1687–1697 (2017).
122. Bixel, M. G. *et al.* Flow Dynamics and HSPC Homing in Bone Marrow Microvessels. *Cell Rep.* **18**, 1804–1816 (2017).
123. Torisawa, Y. *et al.* Bone marrow–on–a–chip replicates hematopoietic niche physiology in vitro. *Nat. Methods* **11**, 663–669 (2014).
124. Srinivasan, G. *et al.* Lipocalin 2 Deficiency Dysregulates Iron Homeostasis and Exacerbates Endotoxin-Induced Sepsis. *J. Immunol. Baltim. Md 1950* **189**, 1911–1919 (2012).
125. Dambuza, I. M. *et al.* Clec7a-mediated regulation of Killer-like Lectin Receptor expression controls T cell immunity. 2025.12.04.692469 Preprint at https://doi.org/10.64898/2025.12.04.692469 (2025).
126. Verhelst, J., Parthoens, E., Schepens, B., Fiers, W. & Saelens, X. Interferon-Inducible Protein Mx1 Inhibits Influenza Virus by Interfering with Functional Viral Ribonucleoprotein Complex Assembly. *J. Virol.* **86**, 13445–13455 (2012).
127. STERZIK, B. & FEHRENBACH*, F. J. Reaction Components Influencing CAMP Factor Induced Lysis. *Microbiology* **131**, 817–820 (1985).